

IMPURITY PROFILING AND DEGRADATION STUDY OF EDARAVONE

4.1. SELECTION OF DRUG

The antioxidant property of phenolic compounds that shows keto-enol tautomerism were tested for free radical scavenging and lipid peroxidation inhibitory activity *in vitro* and for protection against brain damage caused by ischemia reperfusion in animal models *in vivo*, since 1984 (1, 2). This includes 2-pyrazolin-5-ones derivatives. Edaravone, EDA (MCI-186, Radicut) is 2-pyrazolin-5-ones derivative that shows a strong novel free radical scavenger activity. It was developed by Mitsubishi Tanabe Pharma Corporation, Osaka, Japan. Since April 2001, it has been widely used in treatment of acute ischemic stroke (AIS), due to its neurovascular protective effects (3-6). Furthermore, EDA has anti-necrotic, anti-apoptotic and anti-inflammatory cytokine effects, as well as free radicals scavenging activity in cardiovascular diseases and stroke, which shows protective effects in the heart, vessel, and brain (7-9). Moreover, it has preventive effects on myocardial injury, following reperfusion and ischemia in patients with AMI (acute myocardial infarction) (10).

In the year 2015, EDA was approved in Japan and South Korea for (11, 12) treatment of ALS (Amyotrophic Lateral Sclerosis), using intravenous injections. In the same year, EDA got Orphan Drug designation from the FDA and European Commission (13). Recently, Mitsubishi tanabe pharma has submitted new drug application for EDA to treat ALS in the US (14).

Despite of tremendous cardioprotective and neuroprotective effects of EDA to the best of our knowledge there is no report on the degradation study and characterization of degradation products of EDA, although one report discusses the impurity profile of EDA injection. Hence in the present study complete impurity profile and degradation study of EDA was carried out. The major unknown degradation related impurities were isolated and characterized. Also fragmentation pathways of unknown degradation products formed under different stress conditions were outlined.

4.2 DRUG PROFILE

General Properties

IUPAC Name: 1-Phenyl-3-methyl-2-pyrazolin-5-one; 3-Methyl-1-phenylpyrazolin-5(4H)one; 5-Methyl-2-phenyl-1-Hpyrazol-3-one.

Molecular Formula: C₁₀H₁₀N₂O

Molecular Weight: 174.2

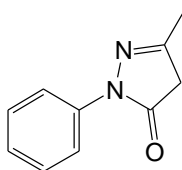


Figure 4.1: Structure of EDA

Chemical Structure:

Appearance: White to off-white powder or crystals

Melting point: 127-128 °C

pKa: 13.21

Solubility: Slightly soluble in water, freely soluble in methanol, ethanol and acetonitrile.

Drug Category: Neuroprotective agent as a potent antioxidant.

Mechanism of action: EDA is a free radical scavenger that exerts antioxidant effect by inhibiting hydroxyl radical dependent and independent lipid peroxidation (15, 16). The proposed mechanism of action may be protection against free radical related injuries following ischemic stroke (17). It also suppresses the increase in superoxide anion radical and hydroxyl radicals in several models associated with ischemic stroke (18, 19). Unlike other free radical scavengers, EDA readily crosses the blood–brain barrier (20).

Uses: Neuroprotective agent

Marketed Formulation:

- Radicut (Mitsubishi Tanabe Pharma Corporation)
- Aravon (Sun pharmaceutical industries Ltd)
- Advo (Unichem Laboratories Ltd)
- Fraseda (UCB India Ltd)
- Nuravon (Piramal healthcare)

4.3 LITERATURE REVIEW

Some methods have been reported for estimation and quantification of EDA. These includes UV spectrophotometric (21), fluorescent assay (22) , HPLC (21, 23, 24), HPTLC (25) and LC-MS/MS (26). The HPTLC method (25) was developed for *in vitro* estimation of EDA in Human Plasma. There is one published report for impurity profile of EDA (27) but degradation study and identification and characterization of degradation products was not reported. A report on analysis of related substances by LC-MS is available (28). Density Function Theory study (DFT) of Edaravone derivatives as an antioxidants has also been available in literature (29).

4.4 SECTION –A

DEVELOPMENT AND VALIDATION OF QbD BASED STABILITY INDICATING HPLC METHOD

4.4.1 EXPERIMENTAL

4.4.1.1 Chemicals and Reagents

The Edaravone bulk drug was purchased from Sigma Aldrich Co. St. Louis USA. Other chemicals and reagents were same as described in section 3.4.1.1.

4.4.1.2 Equipments and Chromatographic Condition

The equipments utilized in present experiment were same as in section 3.4.1.2. For stability indicating assay method the separation was accomplished on a Thermo Scientific BDS Hypersil RP- C18 column (250 ×4.6 mm, 5 μm) at wavelength of 244 nm. The separation was carried out in gradient mode. The mobile phase A consisted of 10 mM ammonium acetate buffer (pH adjusted to 5.8 with glacial acetic acid) and mobile phase B, 90:10 mixture of ACN and MeOH. The gradient program of developed method is presented in table 4.1. The analysis was performed at 34⁰C using column oven with injection volume of 20 μL and a flow-rate of 0.8 ml/min.

Table 4.1: Gradient program for developed method of EDA

Time (min)	Buffer (%)	Organic (%)	Elution
0.01	95	05	Linear gradient
04	85	15	Linear gradient
10	75	25	Linear gradient
12	55	45	Linear gradient
14	75	25	Linear gradient
16	85	15	Linear gradient
17	95	05	Re-equilibrium
20	95	05	Re-equilibrium

4.4.1.3 Preparation of Stock, Sample and Buffer solutions

Stock solutions of EDA were prepared in ACN having concentration of 1 mg/ml. The working standards were prepared in mobile phase to produce 10 – 300 µg/ml of EDA. To analyze the stressed samples suitable dilutions were made in mobile phase to obtain the final concentration of 100 µg/ml with respect to EDA. Same aliquots i.e. 10 – 300 µg/ml of EDA were prepared for recovery studies and assay of marketed formulation (Aravon I.V. infusion, 1.5 mg/ml, manufactured by Sun Pharmaceuticals Ind. Ltd, Halol, Gujarat, India).

Ammonium acetate buffer (20mM) was prepared by dissolving 0.70gm of anhydrous ammonium acetate in 500 mL of double distilled water and adjusted to pH 5.8 using glacial acetic acid which was finally filtered with 0.2µm Nylon membrane filter and degassed by ultra-sonication for 5 minutes.

4.4.1.4 Preparation of Degradation Products (DPs)

For the stress degradation studies, different stress conditions were used for bulk drug. Placebo samples (without drug) were also prepared for comparison with the stress degradation samples.

Hydrolytic Degradation (Acid/Base/neutral hydrolysis):

1 mg/ml of EDA in freshly prepared 0.05 N HCl/ 0.2 N NaOH was prepared and were refluxed at 70⁰C in dark for 180 min for acid and base hydrolysis. Aliquot of 2 mL of these samples were withdrawn neutralized with NaOH/HCl and stored in freeze before analysis. For neutral hydrolysis sample was prepared in water and refluxed at 100⁰C in dark for 7 hrs.

Oxidative (Peroxide- induced) Degradation:

1 mg/ml of EDA was prepared in 6% H₂O₂ by ultra sonication and was kept at room temperature in dark for 45 min.

Photolytic Degradation:

For the photochemical stability, solution of 1 mg/ml of EDA in acetonitrile was exposed to 5382 LUX and 144 UW/cm² for 21 days.

Thermal (Dry heat induced) Degradation:

For preparing dry heat degradation product, solid drugs (API) was spread in 1mm thickness on a petridish and placed in oven at 80⁰C for 21 days under dry heat condition in the dark.

Thermal-Humidity induced Degradation:

Solid drug (API) was placed in stability chamber at 40⁰C±2⁰ C and 75±5 % RH for 21 days.

All the degradation samples were suitably diluted with mobile phase to make final concentration of 150 ppm with respect to EDA and filtered using 0.2μ nylon membrane syringe filter prior to injection.

4.4.1.5 Method Development

Analytical target profile (ATP)

The ATP for present method was defined and these are:

- 1) To develop stability indicating RP-HPLC method that shows well resolved, sharp and asymmetric peak of EDA.
- 2) The peak of drug should be separated with peaks of DPs.

3) The resolved peaks should be acquired in shorter run time.

The defined ATP will lay down the basis for determining CQAs.

Preliminary investigations

Isocratic elution: Various combinations of mobile phase were tried in isocratic mode with MeOH and ACN as organic phase to obtain resolved chromatogram of EDA and its DPs. MeOH alone increases tailing, retention time (Rt) and also gives very broad peak. ACN alone was good in terms of peak symmetry and Rt. Higher percentage of buffer broadens the peak of EDA, although it resolved some peaks of DPs, the elution of some DPs were not observed even after 30 min. EDA peak symmetry was good when higher ratio of ACN was used but most of the peaks of DPs were co-eluted. Various C-8 and C-18 columns were also tried and it was observed that C-18 column was good in terms of resolution. BDS Hypersil RP- C18 column (250 ×4.6 mm, 5 μm) by Thermo Scientific gave best result hence was used for further optimization.

Selection of optimum pH was also important. Too acidic pH distorted peak shape of EDA and causes tailing while some DPs were not eluted beyond pH 6.5. Hence the method should be optimized in the pH range of 3.5 to 6.0. The column temperature has moderate impact on Rt, peak symmetry and resolution of EDA and DPs.

Gradient elution: In order to obtain peak symmetry, resolution and moderate Rt, gradient mode has to be optimized. LC-MS compatible ammonium acetate buffer of different pH range were tried. To resolve some DPs peaks isopropyl alcohol (IPA) was also tried as an organic modifiers. Some of the initially merged peaks were found to be resolved by IPA, but peak shape of EDA and some of its DPs were found to be distorted. Hence optimization had to be done using combination of ammonium acetate buffer and ACN. Various ratio of MeOH were also tried along with ACN to resolve some degradant peaks and it was observed that MeOH increases resolution but higher ratio causes peak broadening. Also higher buffer ratio was required to resolve peaks of polar DPs, so the gradient can be started with higher ratio of buffer. Hence, the aims defined in ATP were achieved by employing DoE approach. The gradient program as optimized by DoE is shown in table 4.1.

Design of Experiments (DoE)

Plackett Burman screening design (PBD): The PBD with 15 runs was initially used to estimate the main effects of six factors selected after preliminary investigation. These are pH of mobile phase, flow rate of mobile phase (FR), column oven temperature (Temp), buffer strength (BS), hold time-1 (HT-1), hold time-2 (HT-2) and % of methanol in mobile phase (% MeOH). Four center points were also added in the PB design that provides measure of inherent variability and process stability.

Box Behenken response surface design (BBD): The BBD design with 29 runs including four center points was used to evaluate the main and interaction effects of the significant variables or factors selected after PBD screening design to further optimize the HPLC analysis conditions.

4.4.1.6 Method Validation using ICH Q2(R1) guideline

The method was validated using ICH, Q2(R1) guideline for Linearity and range, precision, accuracy, limit of detection and Limit of quantification (LOD and LOQ) and robustness.

4.4.1.7 Application of developed HPLC method

The developed SIAM was applied to analysis of EDA in commercial formulation. Stress degradation was carried out in formulation and % degradation was calculated.

4.4.2 RESULTS AND DISCUSSION

4.4.2.1 Determination of suitable wavelength

The UV spectrum of EDA recorded in the range 200-400 nm is presented in figure 4.2. The spectrum indicates that λ_{\max} of EDA is 240.9 nm.

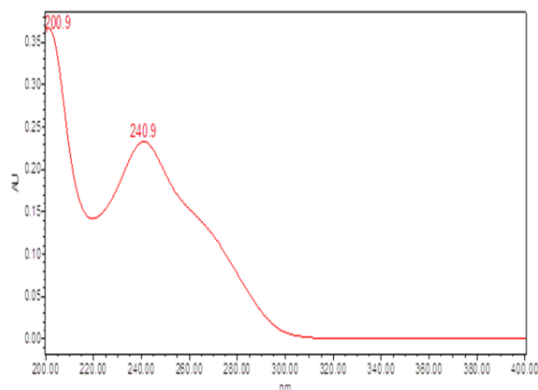


Figure 4.2: UV Spectra of EDA

The UV spectrum of EDA and its DPs were extracted in PDA detector from 200-400 nm and are illustrated in figure 4.3. The spectrum indicates that 244 nm gives a sufficient absorbance for the DPs and EDA hence chromatograms were recorded at this wavelength.

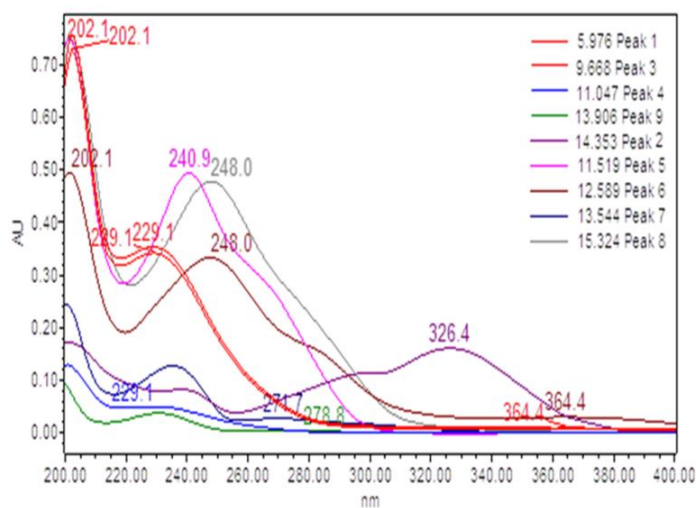


Figure 4.3: UV spectra of EDA and DPs extracted from PDA

4.4.2.2 Method optimization and development by QbD approach

To optimize the present stability indicating assay method, DPs formed under all stress conditions were mixed and final dilution was made to 150 ppm with respect to EDA, to obtain resolved chromatogram of EDA and DPs.

PBD screening design

The matrix of PBD screening is presented in table 4.2 and some of the chromatographic trials of PBD screening are shown in figure 4.4. The half normal plot and pareto plot (figure 4.5) showed that HT-2 was significant factor effecting RS1. For RS2 the significant factors were HT-1, FR, BS and Temperature. For RS3 Temperature was significant factor. HT-2 was significant factor for RS4. HT-1 and FR were significant factor effecting response Rt while none of the factors were effecting response As, as none of them were significant. Hence based on outcome of PBD screening HT-1, HT-2, FR and Temperature were chosen for response surface optimization by BBD. Although BS affects significantly response RS2, it was kept constant 20 mM based on preliminary trials and previous experience. Other factor viz % of methanol and pH were kept constant at 10% and 5.8 based on preliminary trials and previous experience.

Table 4.2: Matrix of PBD screening with their measured responses.

Run	Independent Variable							Dependent Variable					
	pH	FR	Temp.	BS	HT-1	HT-2	% MeOH	Rs1	Rs2	Rs3	Rs4	Rt	As
1.	3.80	0.8	25.0	10	2	2	0	1.34	2.26	0.00	3.04	11.58	0.98
2.	3.80	0.8	25.0	50	6	6	0	1.66	3.55	3.17	3.74	19.49	1.62
3.	5.05	1.0	32.5	30	4	4	15	0.00	0.00	10.72	6.70	15.48	0.92
4.	6.30	0.8	40.0	50	2	6	0	0.00	2.02	3.27	2.96	12.42	1.65
5.	3.80	1.2	40.0	50	2	6	30	0.00	1.01	4.88	3.04	12.36	1.72
6.	6.30	0.8	25.0	10	6	6	30	2.60	4.37	2.33	2.01	18.64	1.47
7.	3.80	1.2	40.0	10	6	2	0	1.58	1.11	6.25	3.21	14.90	1.37
8.	3.80	1.2	25.0	10	2	6	30	0.95	0.00	1.53	4.37	2.96	1.48
9.	5.05	1.0	32.5	30	4	4	15	0.00	0.00	10.72	6.70	15.48	0.92
10.	6.30	0.8	40.0	10	2	2	30	2.20	0.00	5.59	4.30	11.68	0.74
11.	6.30	1.2	25.0	50	2	2	0	1.36	1.30	2.03	3.66	9.20	0.95

12.	6.30	1.2	25.0	50	6	2	30	1.49	3.54	1.68	4.82	13.79	2.90
13.	5.05	1.0	32.5	30	4	4	15	0.00	0.00	10.72	6.70	15.48	0.92
14.	3.80	0.8	40.0	50	6	2	30	1.83	3.88	3.13	8.41	31.20	1.31
15.	6.30	1.2	40.0	10	6	6	0	0.00	0.00	2.23	1.20	15.96	1.15

pH= pH of mobile phase, FR= Flow rate of mobile phase, Temp.= Temperature, BS= Buffer strength, HT-1= Hold time 1, HT-2= Hold time 2, % MeOH= % of MeOH in mobile phase, RS1= Resolution between peak pair 1, RS2= RS1= Resolution between peak pair 1, RS3= Resolution between peak pair 3, RS4= Resolution between peak pair 4, Rt= Retention time, As= Asymmetry

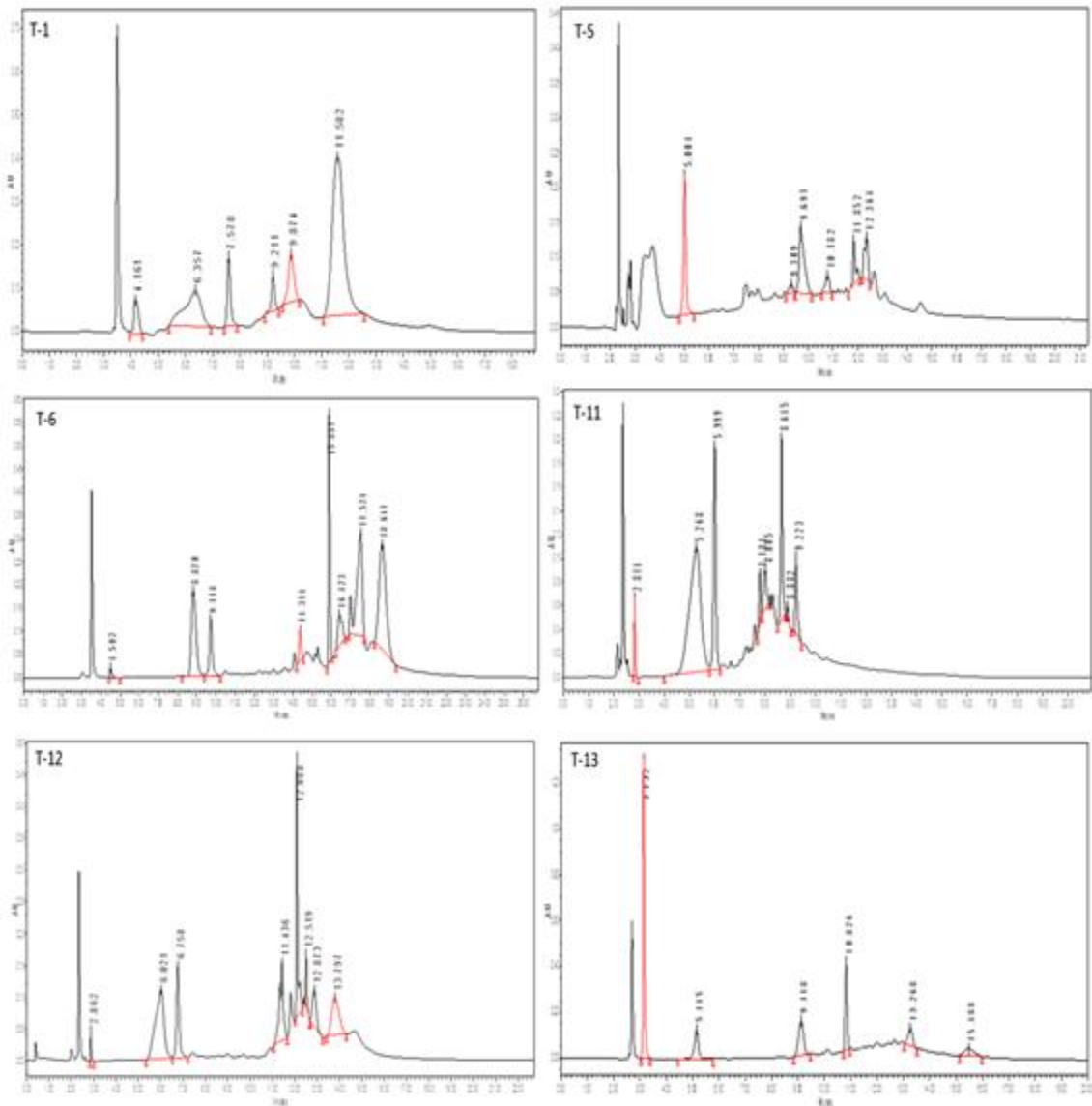
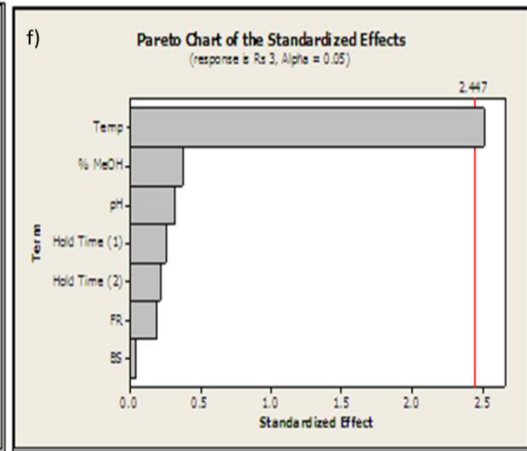
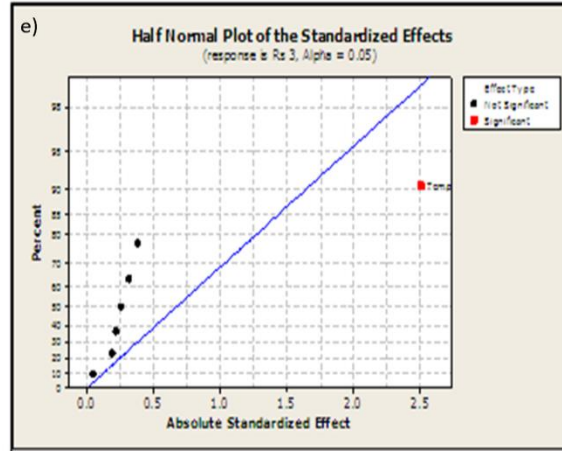
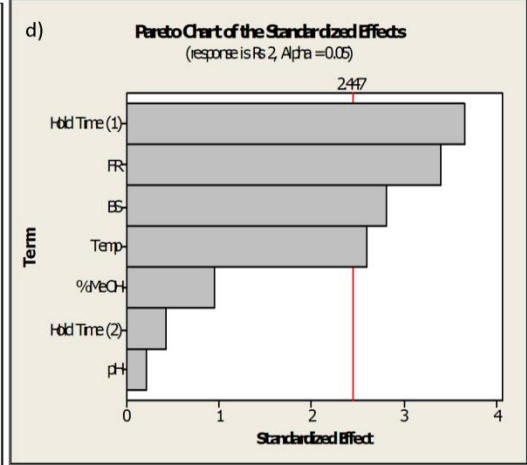
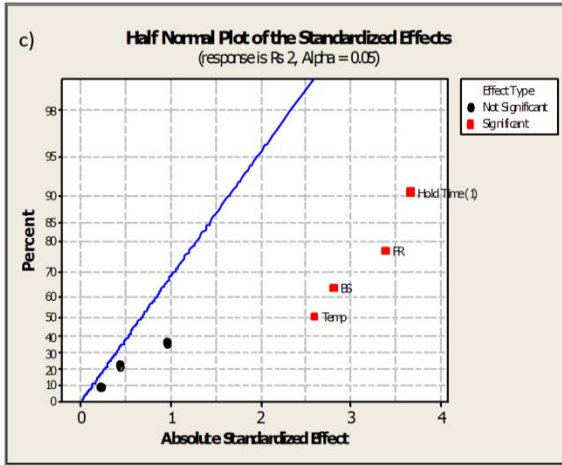
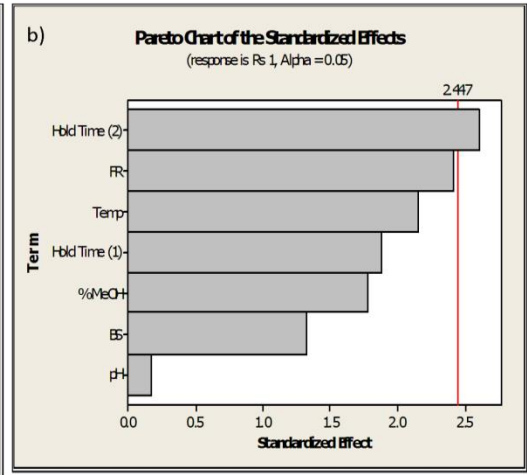
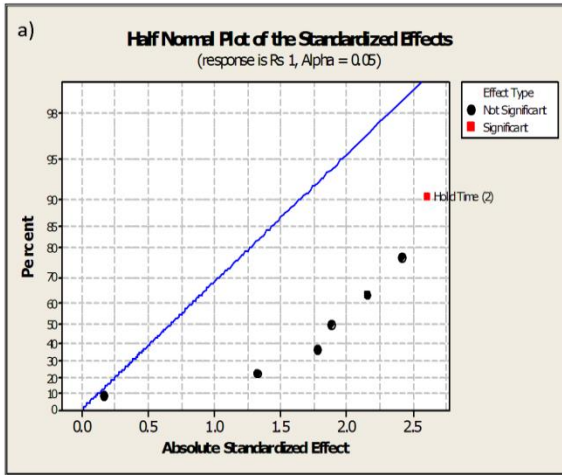


Figure 4.4: Some chromatographic trials of PBD screening



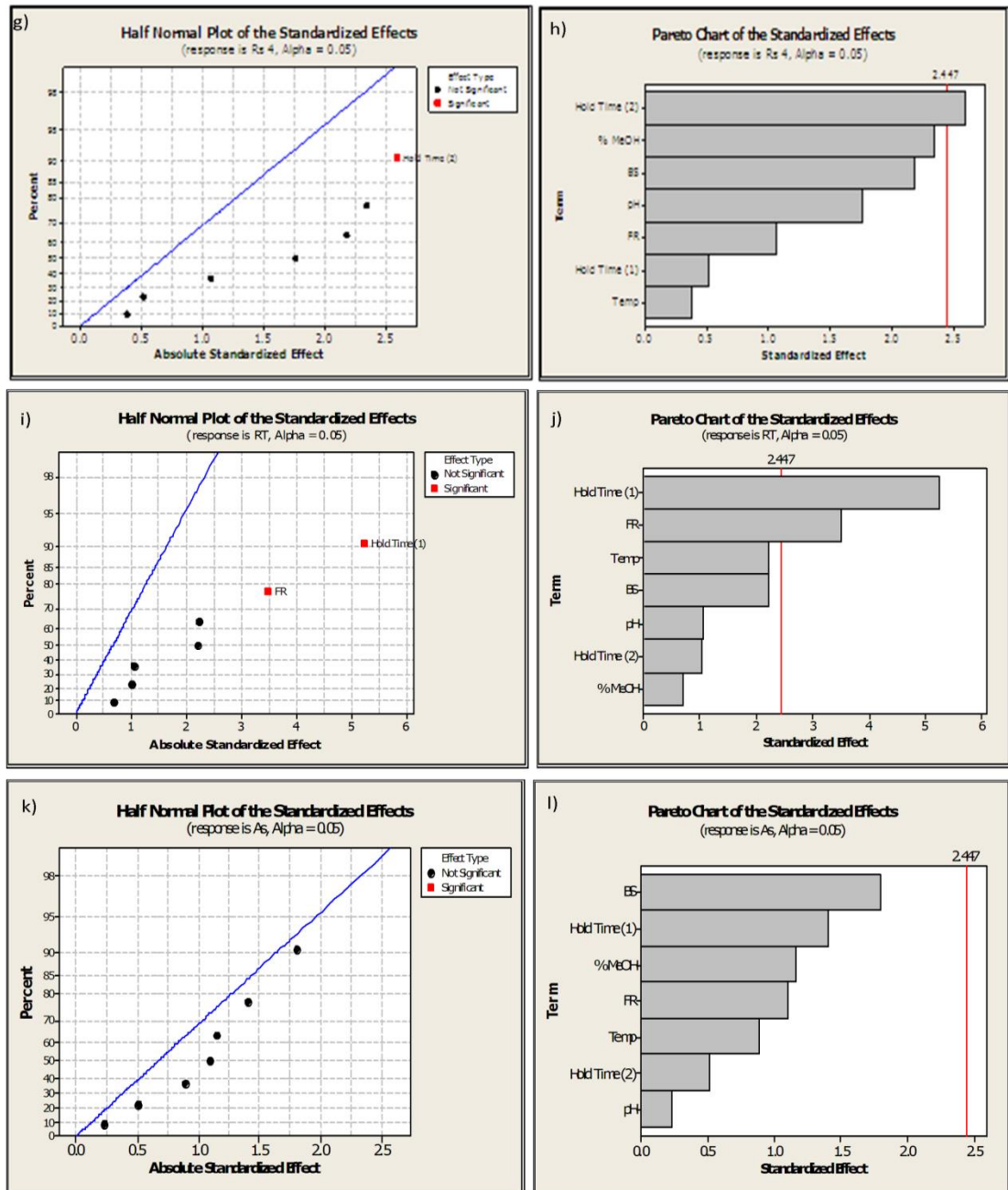


Figure 4.5: a) Half Normal plot for response RS1, b) pareto plot for response RS1, c) Half Normal plot for response RS2, d) pareto plot for response RS2, e) Half Normal plot for response RS3, f) pareto plot for response RS3, g) Half Normal plot for response RS4, h) pareto plot for response RS4, i) Half Normal plot for response Rt, j) pareto plot for response Rt, k) Half Normal plot for response As, l) pareto plot for response As

BBD response surface design

Factors and their levels for BBD are shown in table 4.3. As was not included as response in BBD since it was not affected by any of the factors described in PBD. The matrix of BBD with their measured responses is shown in table 4.4. Some chromatograms of BBD trials are shown in figure 4.6.

Table 4.3: Variables and their levels for BBD

Factors	Coded Levels	Actual Levels
A: Hold Time-1 [HT-1] (min)	-1 1	02 06
B: Hold Time-2 [HT-2] (min)	-1 1	02 06
C: Flow Rate (ml/min)	-1 1	0.8 1.2
D: Temperature ($^{\circ}$ C)	-1 1	25 40
Responses		Constraints
R1: resolution between peak pair 1 (RS1) [between DP-2 and DP-3]		$1.5 \leq R1 \leq 2.5$
R2: : resolution between peak pair 1 (RS2) [between EDA and DP-4]		$1.5 \leq R2 \leq 2.5$
R3: : resolution between peak pair 1 (RS3) [between DP-4 and DP-5]		$4.0 \leq R3 \leq 8.0$
R4: : resolution between peak pair 1 (RS4) [between DP-5 and DP-6]		$2.0 \leq R4 \leq 4.0$
R5: Retention time of last eluting peak		$14 \leq R5 \leq 17$

Table 4.4: Matrix of experiments for BBD and results of their responses

Run	Independent Variable				Dependent Variable				
	HT-1 [A]	HI-2 [B]	FR [C]	Temp. [D]	RS1	RS2	RS3	RS4	Rt
1	6.00	4.00	0.80	32.50	2.77	2.22	7.66	4.2	17.36
2	2.00	4.00	1.00	25.00	0	1.55	5.5	2.59	11.88
3	4.00	2.00	1.00	40.00	1.16	1.17	4.31	2.45	12.87
4	4.00	6.00	1.20	32.50	1.43	2.83	7.11	3.72	14.21

5	4.00	6.00	1.00	25.00	1.62	2.94	7.99	4.16	16.98
6	2.00	4.00	1.20	32.50	0	1.23	4.13	2.36	10.2
7	4.00	4.00	1.20	25.00	1.3	2	6.45	3.45	14.19
8	2.00	6.00	1.00	32.50	0.35	1.16	6.95	3.71	13.71
9	4.00	4.00	1.00	32.50	2.14	2.37	6.63	3.9	16.09
10	2.00	2.00	1.00	32.50	0	0.25	2.11	1.15	8.79
11	4.00	4.00	1.00	32.50	2.14	2.37	6.63	3.9	16.09
12	2.00	4.00	0.80	32.50	0.45	1.5	4.74	2.99	13.64
13	4.00	2.00	1.00	25.00	1.66	0.66	4.35	2.13	12.58
14	4.00	4.00	0.80	25.00	2.77	3.19	6.85	4.25	15.57
15	4.00	4.00	1.00	32.50	2.14	2.37	6.63	3.9	16.09
16	4.00	4.00	1.20	40.00	2.28	2.1	6.11	2.4	14.58
17	2.00	4.00	1.00	40.00	0.45	1.1	5.33	2.6	11.71
18	6.00	6.00	1.00	32.50	2.67	3.2	8.1	4.88	19.38
19	4.00	4.00	1.00	32.50	2.14	2.37	6.63	3.9	16.09
20	6.00	4.00	1.00	40.00	2.43	2.14	7.26	4.21	16.45
21	6.00	4.00	1.00	25.00	2.55	2	7.41	4.35	16.99
22	6.00	2.00	1.00	32.50	1.59	0.9	4.43	2.29	11.5
23	6.00	4.00	1.20	32.50	2.34	2.56	7.31	4.05	16.19
24	4.00	4.00	1.00	32.50	2.14	2.37	6.63	3.9	16.09
25	4.00	2.00	1.20	32.50	1.22	1	5.33	2	10.58
26	4.00	6.00	0.80	32.50	2.1	2.9	7.21	3.16	16.61
27	4.00	6.00	1.00	40.00	1.72	2.9	7.01	3.91	17.14
28	4.00	4.00	0.80	40.00	2.24	2.19	6.61	4.36	15.17
29	4.00	2.00	0.80	32.50	1.36	0.9	5.12	1.45	11.58

HT-1= Hold time 1, HT-2= Hold time 2, FR= Flow Rate, Temp.= temperature, RS1= resolution between peak pair 1, RS2= resolution between peak pair 2, RS3= resolution between peak pair 3, RS4=resolution between peak pair 4, Rt= Retention time of last eluting peak.

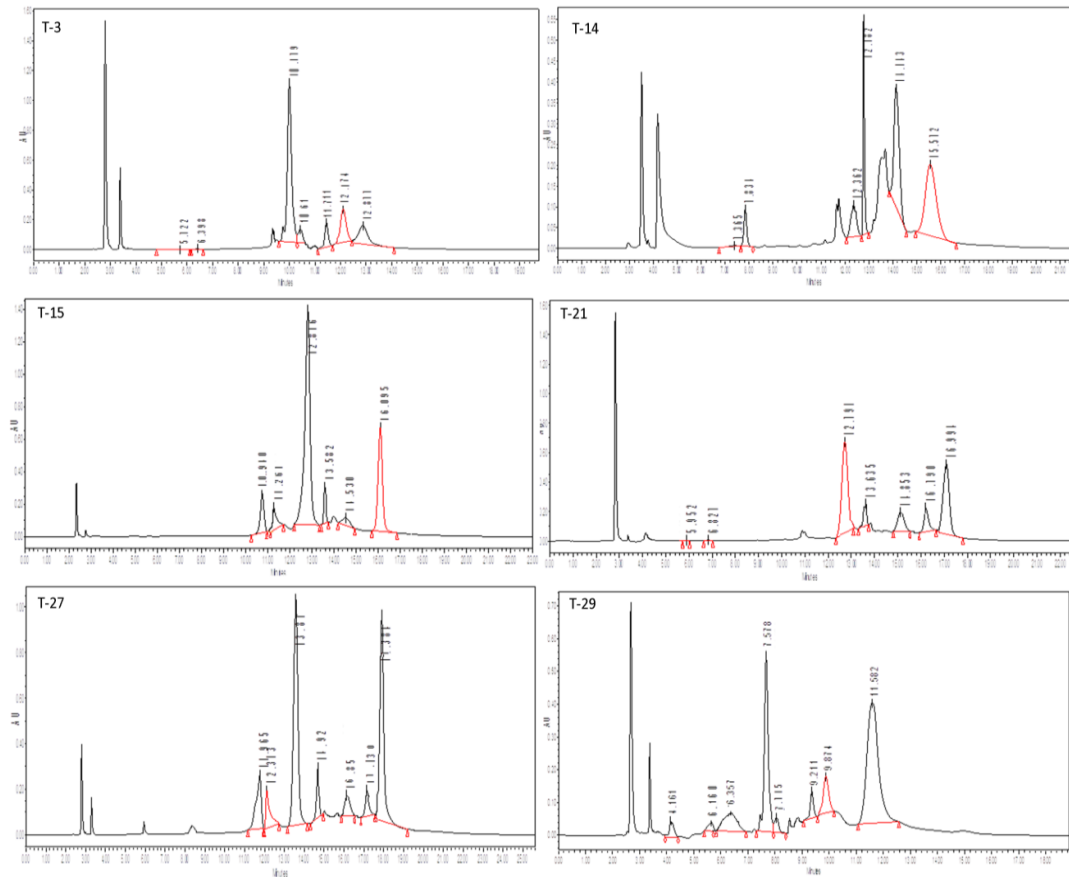


Figure 4.6: Some chromatograms of BBD Trials

Effect of factors on responses

RS1

From regression analysis (table 4.5) of full quadratic model it can be concluded that for RS1, HT-1 is most influencing factor affecting positively. HT-2 is contributing significantly and positively. The flow rate of mobile phase is also contributing negatively while temperature is not contributing significantly. The significant interaction terms are CD, A^2 and B^2 . The same can be inferred from main and interaction effect plot for RS1 (figure 4.7) and contour and 3D plots (figure 4.12). Other factors are not contributing significantly as the associated p-value are more than 0.05, but some of these terms are included in model to support hierarchy.

The quadratic equation in terms of coded factors for full model is as follows:

$$RS1 = +2.14+1.09* A+0.24* B-0.26* C+0.032* D+0.18* AB+5.000E-003* AC-0.14* AD-0.13* BC+0.15* BD+0.38* CD-0.64 *A^2-0.48*B^2-0.057*C^2-0.067*D^2$$

Table 4.5: Regression analysis results

Factors	RS1 coefficient	P value (prob >F)	RS2 coefficient	P value (prob >F)	RS3 coefficient	P value (prob >F)	RS4 coefficient	P value (prob >F)	Rt coefficient	P value (prob >F)
Intercept	2.14	< 0.0001	2.36	< 0.0001	6.16	< 0.0001	3.87	< 0.0001	15.97	< 0.0001
A	1.09	< 0.0001*	0.52	< 0.0001*	1.12	< 0.0001*	0.71	< 0.0001*	2.33	< 0.0001*
B	0.24	0.0009*	0.92	< 0.0001*	1.56	< 0.0001*	1.01	< 0.0001*	2.51	< 0.0001*
C	-0.26	0.0005*	-0.098	0.1991	-0.15	0.4189	-0.20	0.1047	-0.83	0.0002*
D	0.032	0.5903	--	--	-0.16	0.3758	--	--	--	--
AB	0.18	0.0881	0.35	0.0133*	--	--	--	--	0.74	0.0314*
AC	5.000E-003	0.9606	0.15	0.2484	--	--	0.12	0.5679	0.57	0.0908
AD	-0.14	0.1742	--	--	--	--	--	--	--	--
BC	-0.13	0.2044	--	--	--	--	--	--	-0.35	0.2856
BD	0.15	0.1540	--	--	--	--	--	--	--	--
CD	0.38	0.0020*	--	--	--	--	--	--	--	--
A ²	-0.64	< 0.0001*	-0.56	< 0.0001*	--	--	-0.22	0.1820	-1.19	0.0001*
B ²	-0.48	< 0.0001*	-0.44	0.0002*	--	--	-0.77	< 0.0001*	-1.43	< 0.0001*

C ²	-0.057	0.4804	--	--	--	--	-0.34	0.0428 *	-0.93	0.0012 *
D ²	-0.067	0.4081	--	--	--	--	--	--	--	--

Regression coefficients are in coded values, *Statistically significant (p<0.05)

Table 4.6: ANOVA results showing the effect of independent variables on the responses

Response	Model	SS	DF	MS	F-value	p-value	PRESS	r ²	Adj-r ²	Pred-r ²	AP
RS1	FQM	20.45	14	1.46	36.85	< 0.0001	3.20	0.974	0.947	0.848	20.39
RS2	RQM	17.22	7	2.46	37.27	< 0.0001	2.87	0.925	0.901	0.846	21.34
RS3	RLM	44.75	4	11.19	29.66	< 0.0001	13.63	0.832	0.804	0.747	20.99
RS4	RQM	23.15	7	3.31	19.33	< 0.0001	6.76	0.866	0.821	0.747	15.84
Rt	RQM	175.48	9	19.50	48.04	< 0.0001	30.04	0.958	0.938	0.836	25.87

RQM=reduced quadratic model, FQM= full quadratic model, RLM= reduced linear model, SS= Sum of Squares, DF= Degrees of freedom, PRESS= prediction error sum of squares, Pred- r²= Predicted r², Adj- r²= Adjusted r², AP= Adequate Precision.

RS2

From table 4.5, figure 4.8 and 4.13, it can be concluded that HT-1 and HT-2 are most influencing factor affecting positively with same magnitude response RS2 as both have similar p-value (<0.0001). Significant interaction terms are AB, A² and B². The quadratic equation in terms of coded factors for reduced model is as follows:

$$RS2 = +2.36 + 0.52 * A + 0.92 * B - 0.098 * C + 0.35 * AB + 0.15 * AC - 0.56 * A^2 - 0.44 * B^2$$

RS3

From table 4.5, figure 4.9 and 4.14, it can be concluded that HT-1 and HT-2 are most influencing factor affecting positively with same magnitude response RS3 as both have similar p-value (<0.0001). Flow rate and temperature are not contributing significantly. No interaction effects among factors were found. The linear equation in terms of coded factors for reduced model is as follows:

$$RS3 = +6.16 + 1.12 * A + 1.56 * B - 0.15 * C - 0.16 * D$$

RS4

From table 4.5, figure 4.10 and 4.15, it can be concluded that HT-1 and HT-2 are most influencing factor affecting positively with same magnitude response RS4 as both have similar p-value (<0.0001). The significant interaction terms are B² and C². The quadratic equation in terms of coded factors for reduced model is as follows:

$$RS4 = +3.87 + 0.71 * A + 1.01 * B - 0.20 * C + 0.12 * AC - 0.22 * A^2 - 0.77 * B^2 - 0.34 * C^2$$

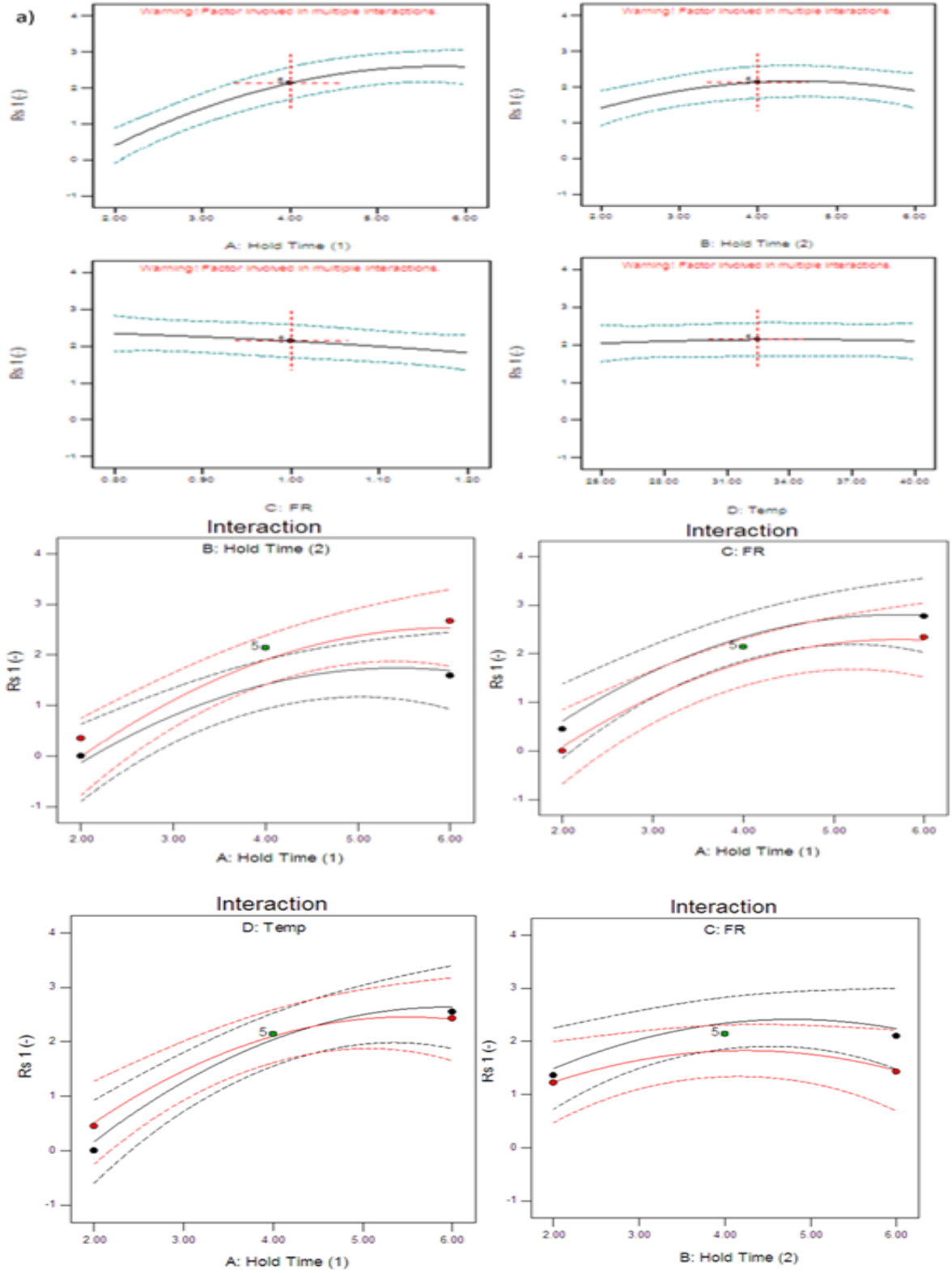
Rt

As shown in table 4.5, figure 4.11 and 4.16, it can be concluded that HT-1 and HT-2 are most influencing factor affecting positively with same magnitude response Rt as both have similar p-value (<0.0001). The flow rate of mobile phase is also contributing negatively while temperature is not contributing significantly. The significant interaction terms are AB, A², B² and C². The quadratic equation in terms of coded factors for reduced model is as follows:

$$Rt = +15.97 + 2.33 * A + 2.51 * B - 0.83 * C + 0.74 * AB + 0.57 * AC - 0.35 * BC - 1.19 * A^2 - 1.43 * B^2 - 0.93 * C^2$$

Model Fitting and Statistics

Regression coefficients of responses and ANOVA results are presented in table 4.5 and 4.6. The model F-values and values of "Prob > F" less than 0.05 indicate model terms are significant for all responses. Statistically, high values of the r² for all dependent variables indicate a good model fit. There was also reasonable good agreement between Adjusted-r² and Predicted-r² values that signifies good model fit (table 4.6). For some responses (RS2, RS3, RS4 and Rt) better Predicted-r² obtained for reduced model might be due to elimination of insignificant terms. Further the models, indicates the adequate precision (AP) value greater than 4, signifying adequate model discrimination. Hence the selected models can be utilized to navigate the design space for present method.



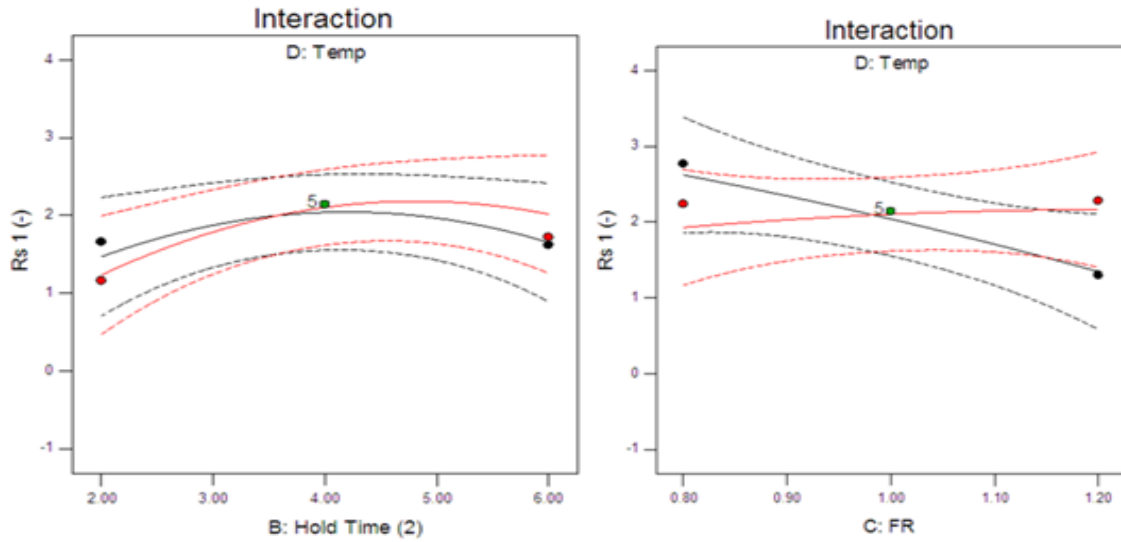
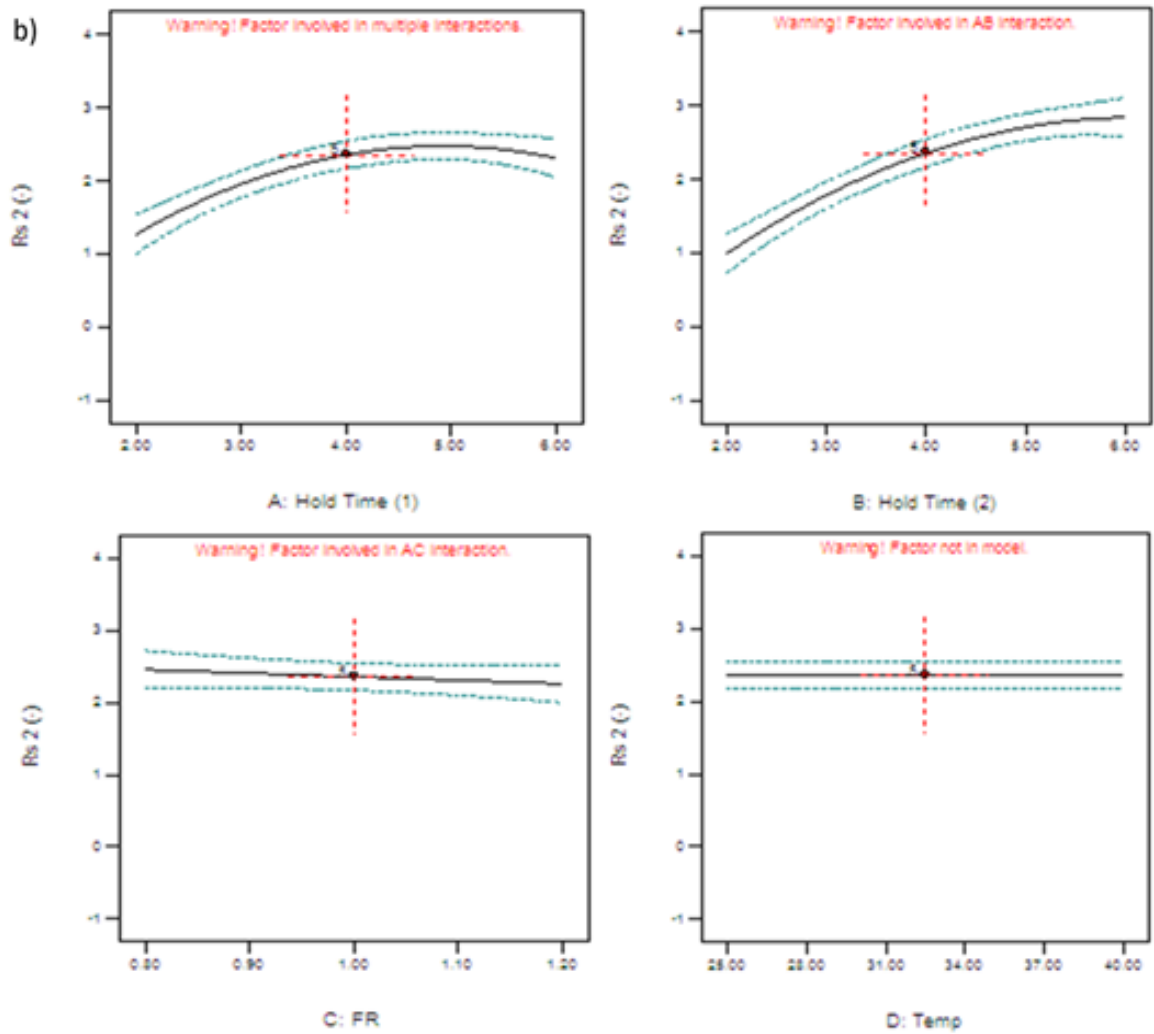


Figure 4.7: Main and interaction effect plots for RS1



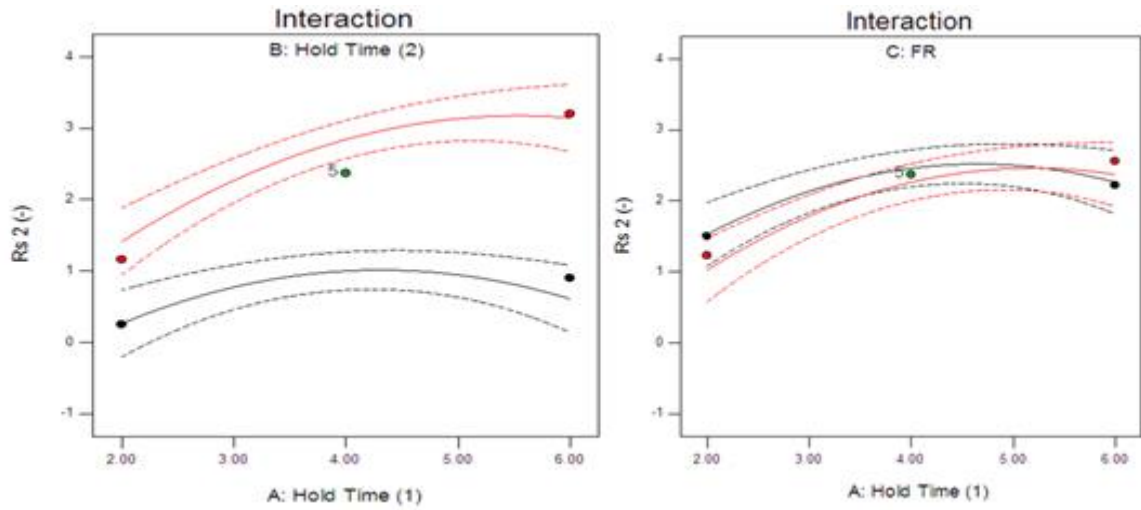


Figure 4.8: Main and interaction effect plots for RS2

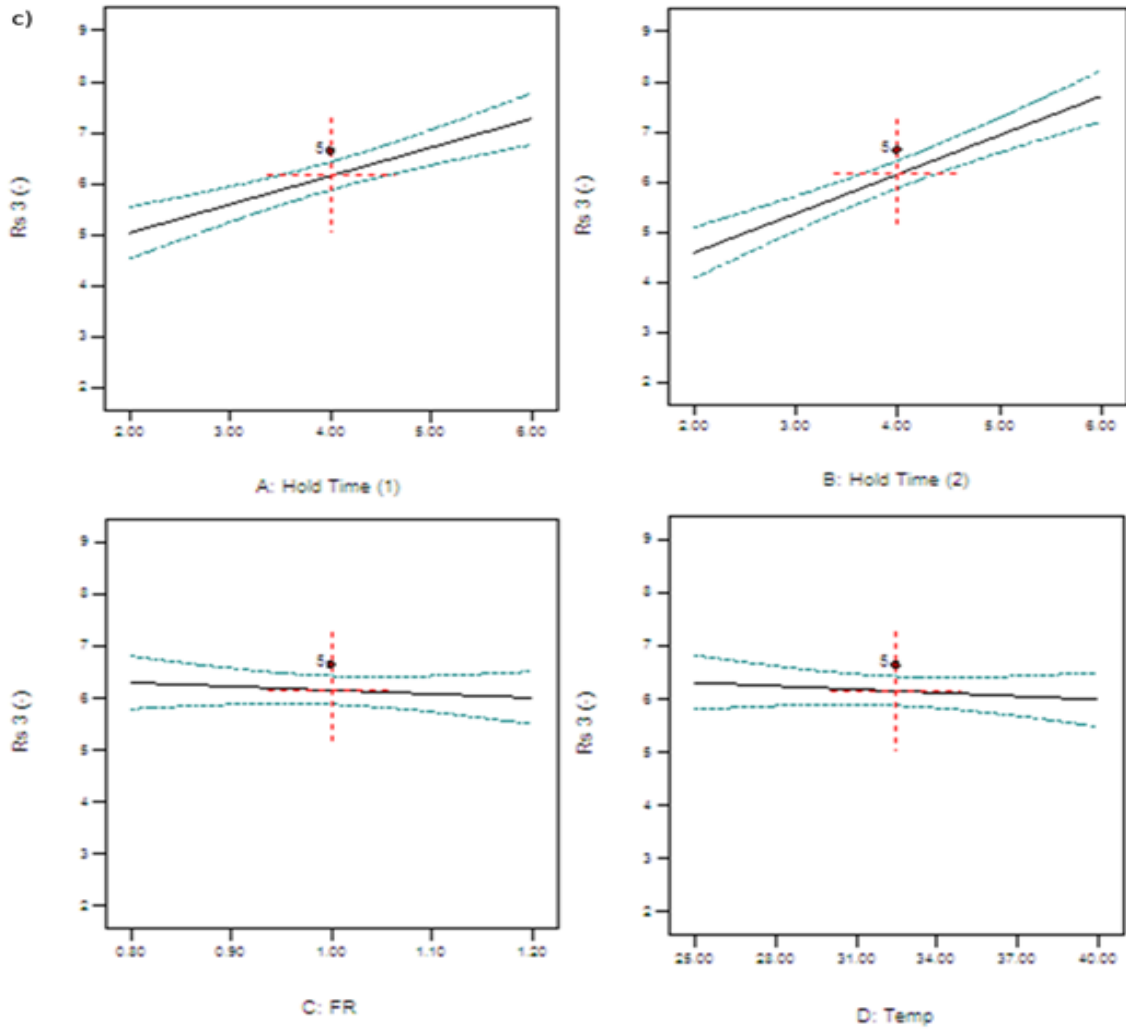


Figure 4.9: Main and interaction effect plots for RS3

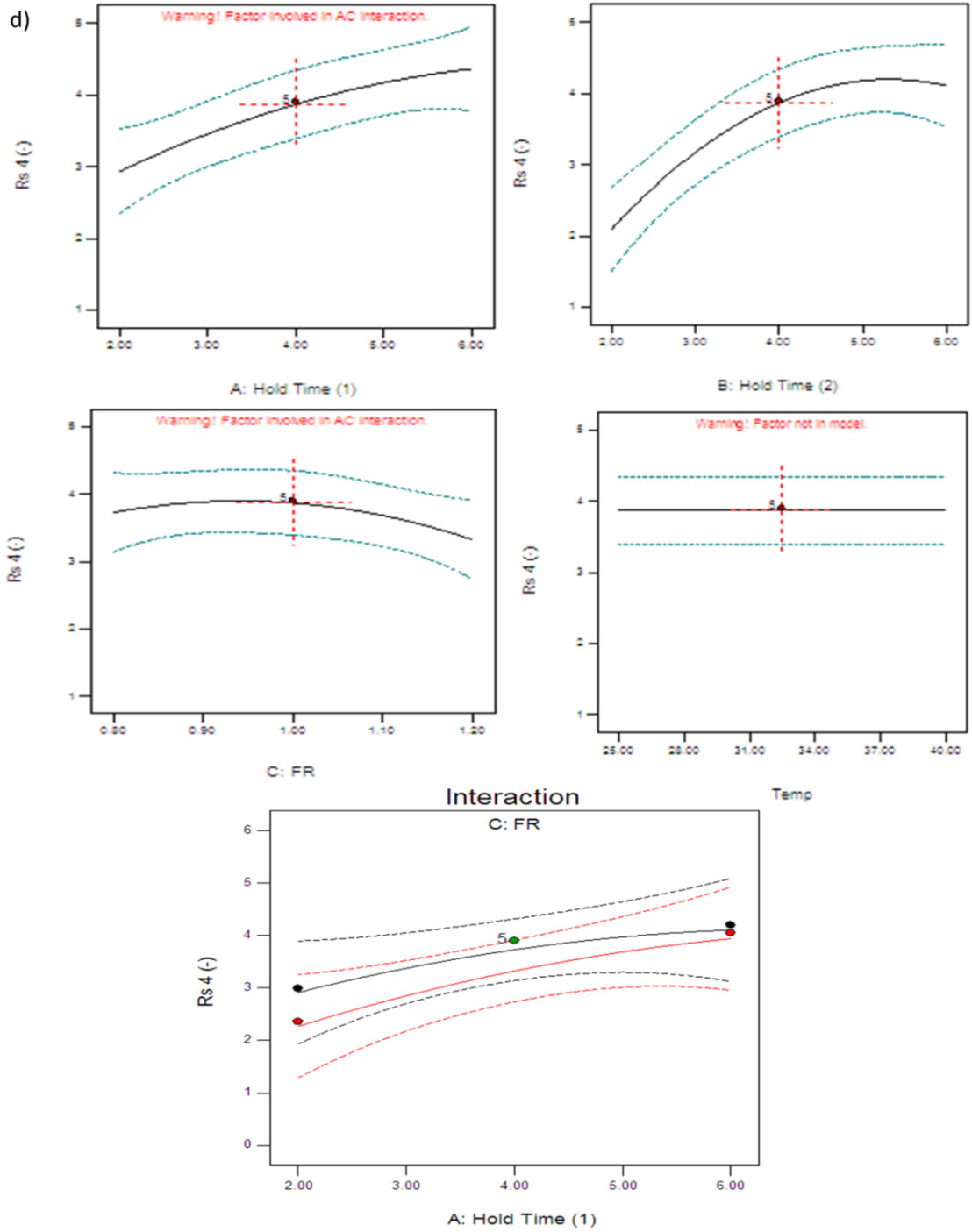


Figure 4.10: Main and interaction effect plots for RS4

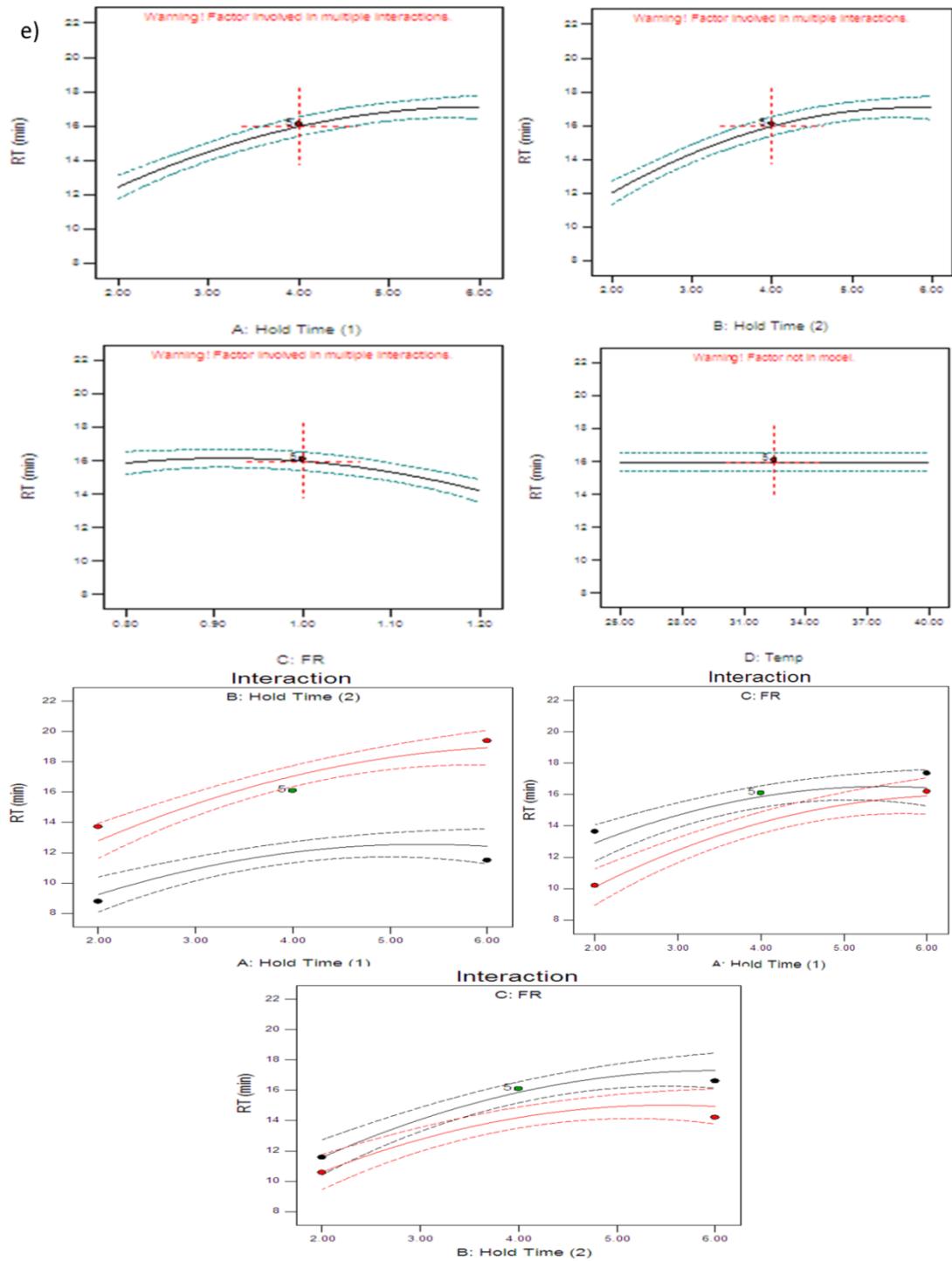


Figure 4.11: Main and interaction effect plots for Rt

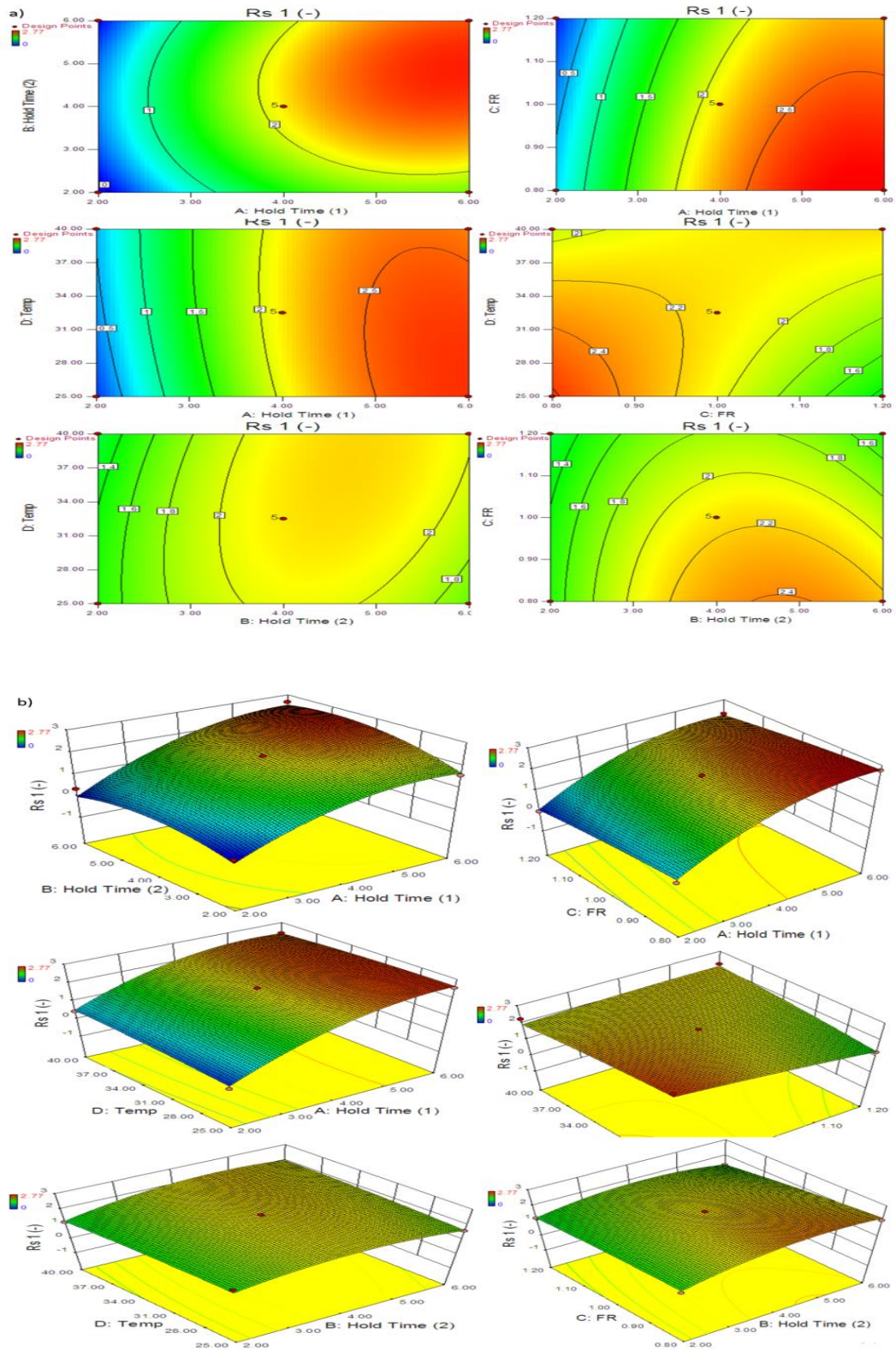


Figure 4.12: a) Contour Plots for RS1 and b) 3D Plots for RS1 (value increases from blue to red)

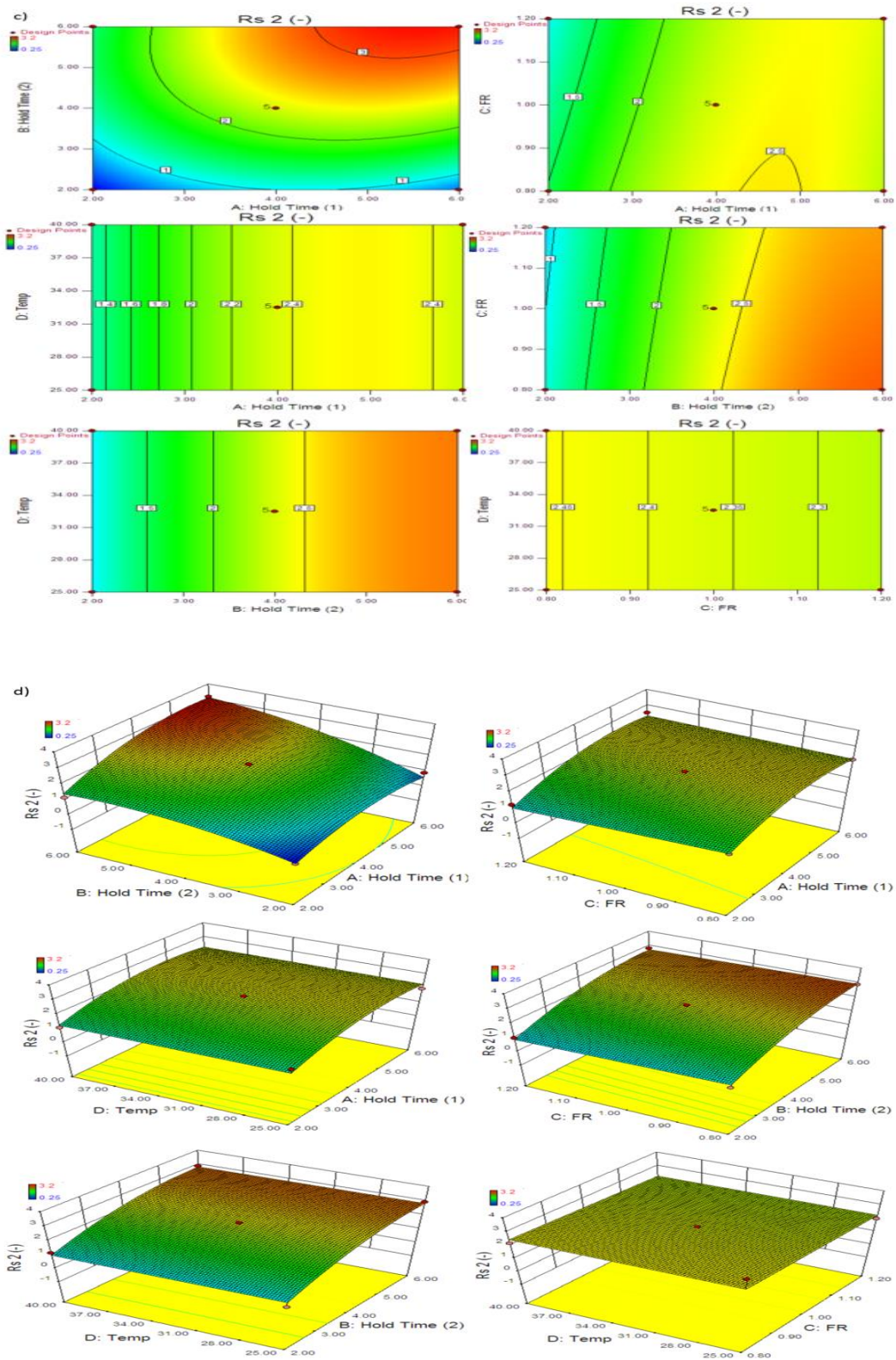


Figure 4.13: c) Contour Plots for RS2 and d) 3D Plots for RS2 (value increases from blue to red)

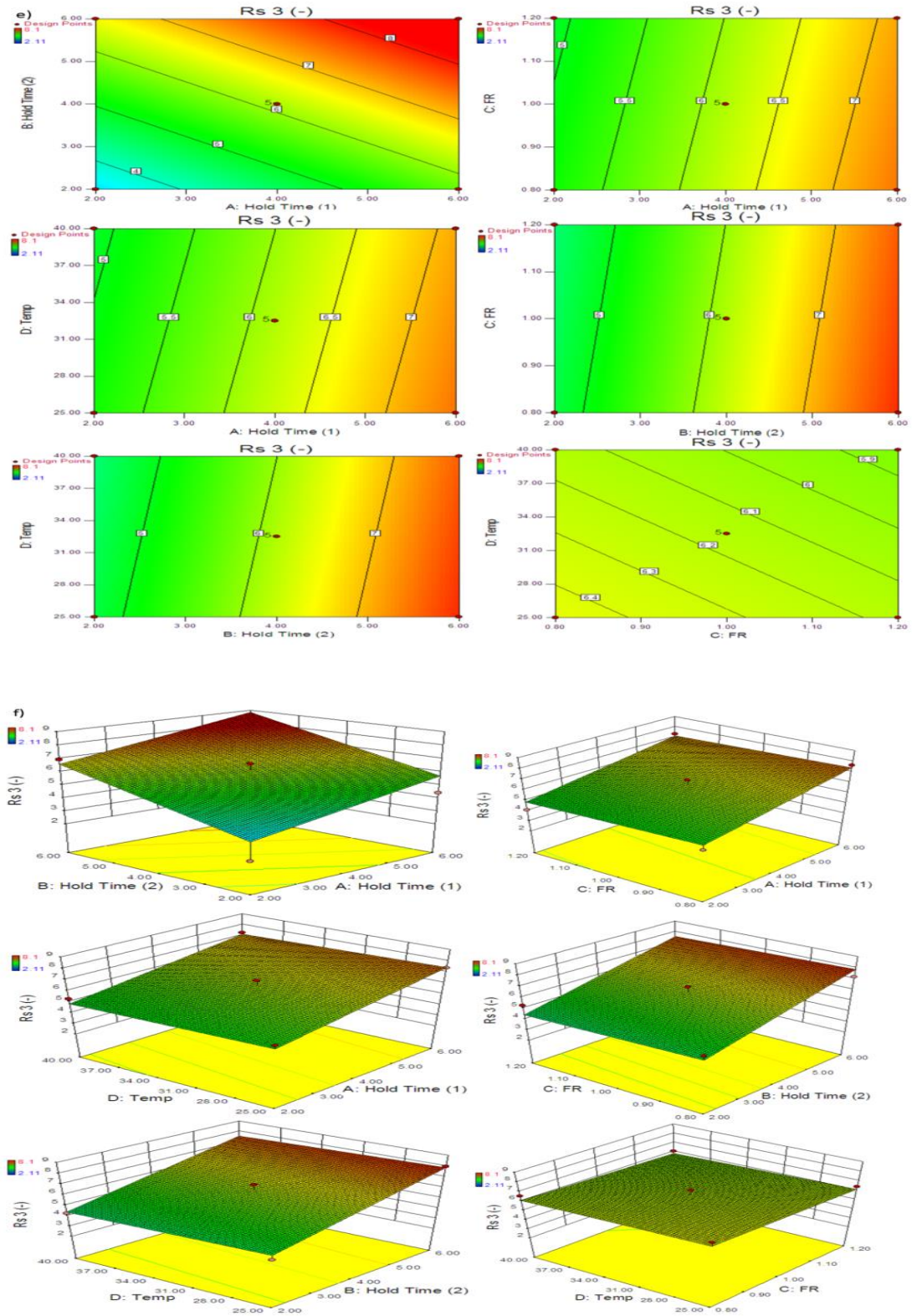


Figure 4.14: e) Contour Plots for RS3 and f) 3D Plots for RS3 (value increases from blue to red)

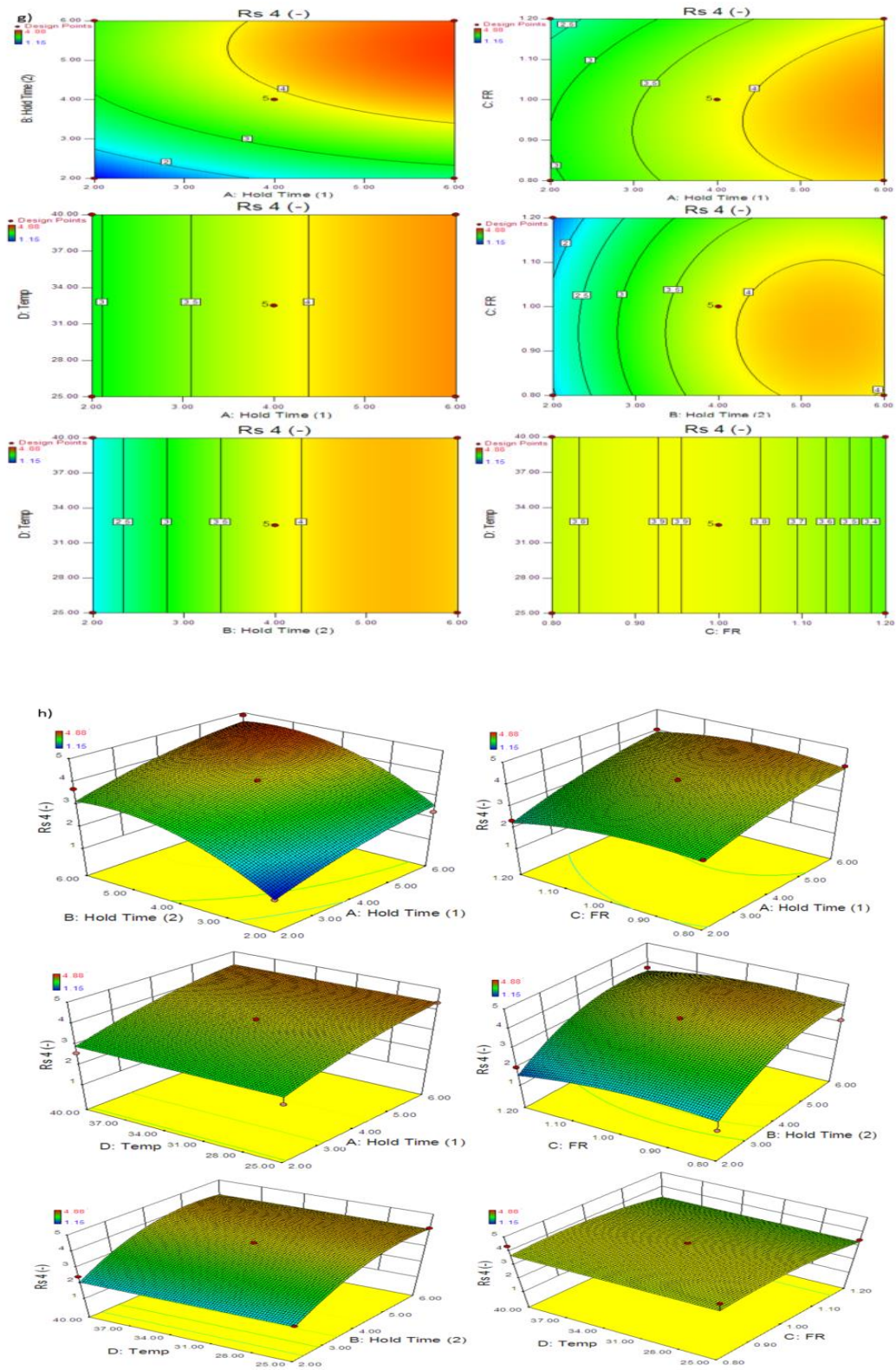


Figure 4.15: g) Contour Plots for RS4 and h) 3D Plots for RS4 (value increases from blue to red)

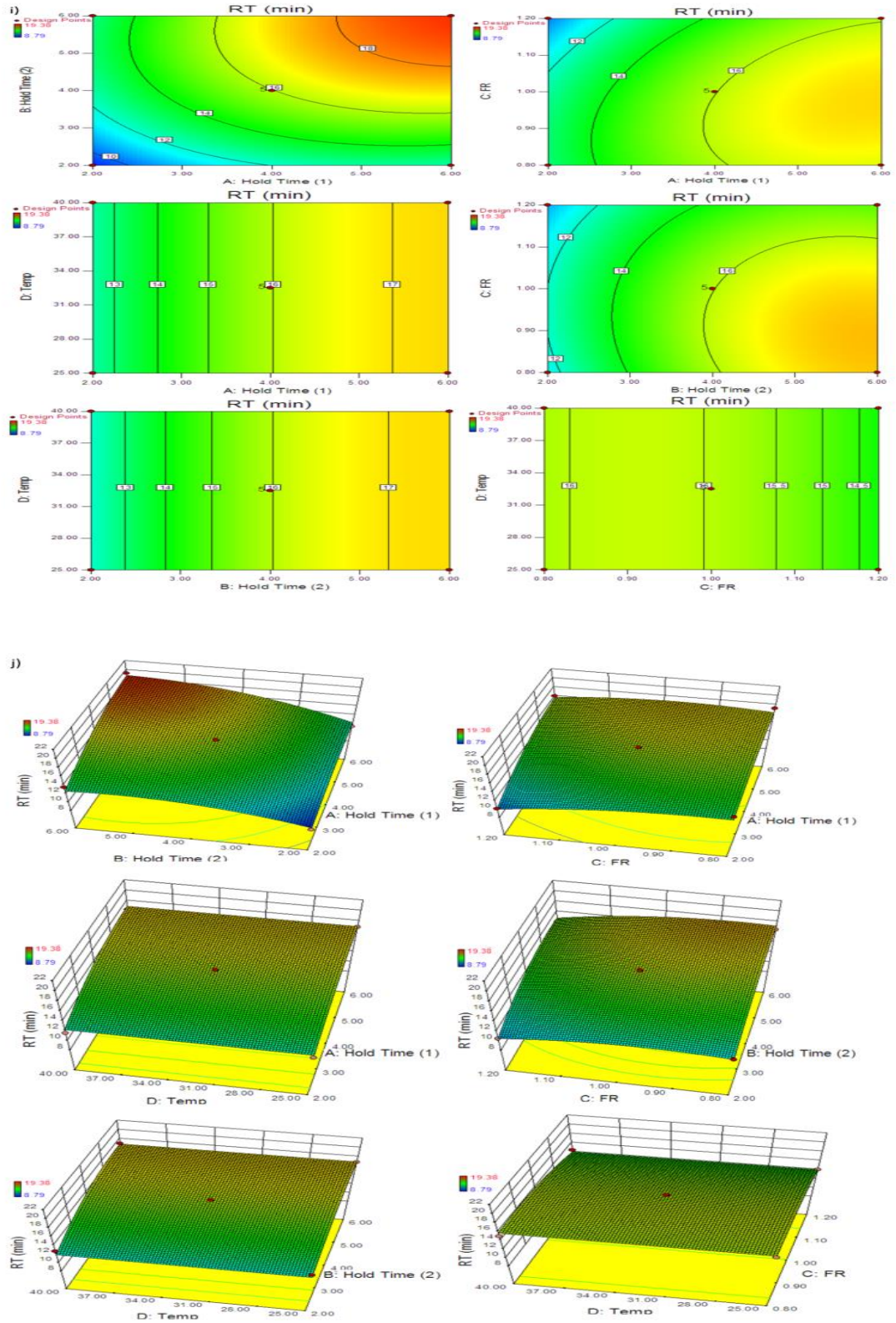
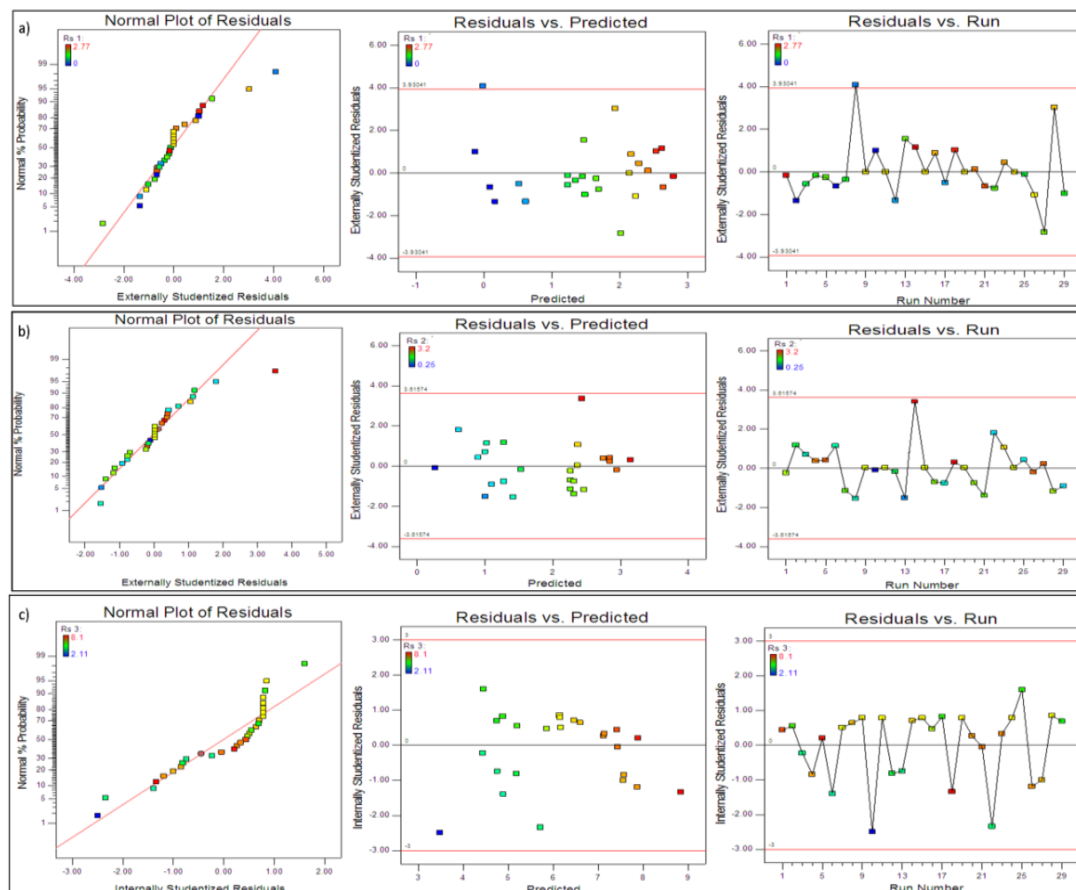


Figure 4.16: i) Contour Plots for Rt and j) 3D Plots for Rt (value increases from blue to red)

Interaction between the factors and residual plots

The ANOVA results (table 4.6) and figure 4.7-4.11 depicts the interaction effects amongst the factors. The p-value indicates that there is no interaction effects among the factors, for response RS3 as the associated p-value for interactions are more than 0.05. For RS1, CD, A^2 and B^2 , for RS2, AB, A^2 and B^2 , for RS4 B^2 and C^2 and for response Rt, AB, A^2 , B^2 and C^2 were showing significant interaction effects. The residual plots viz., normal probability plot of residuals and residual vs run for all responses are depicted in figure 4.17. The normal probability plot of residuals for all responses indicates that the residuals appear to follow almost straight line and thus non-normality, outliers, skewness or unidentified variables does not exist in the selected model. From the plot of residual vs fit of all responses, it can be seen that residuals appear to be randomly scattered about zero hence existence of missing terms, nonconstant variance, outliers can be omitted.



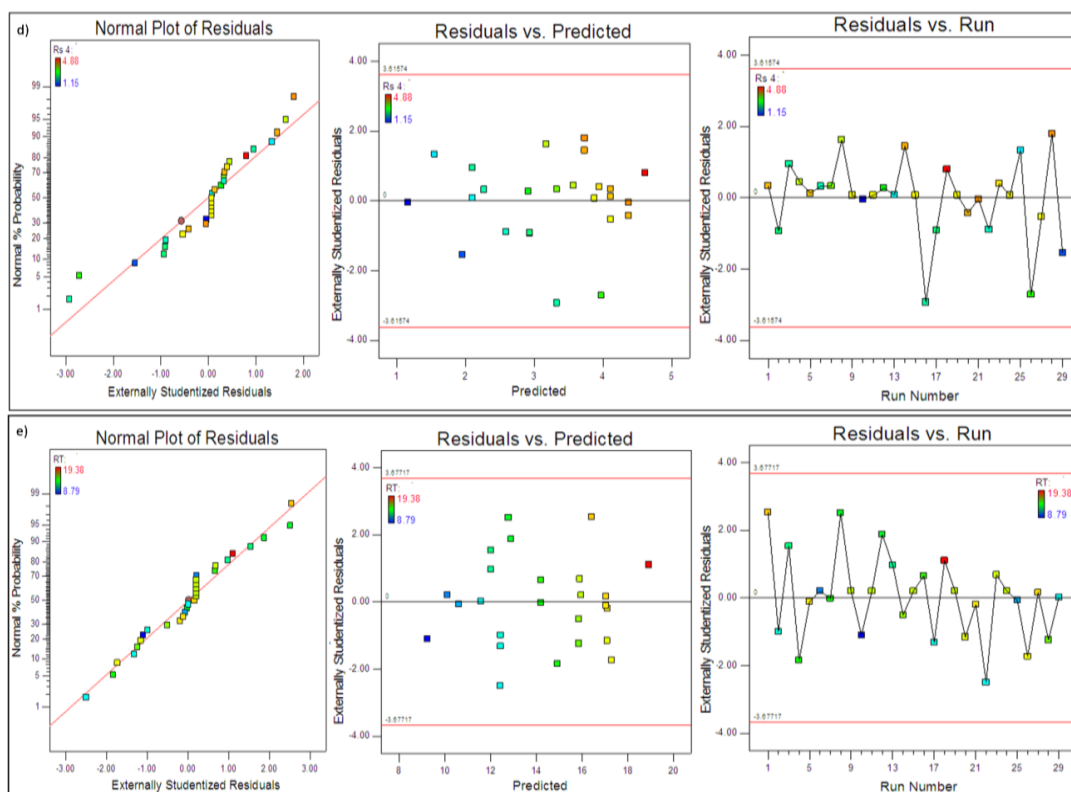


Figure 4.17: Residual plots for a) RS1, b) RS2, c) RS3, d) RS4 and e) Rt

Evaluation of model using cross-validation

Five experiments were conducted to evaluate the reliability of the model, by varying the variables at values other than that of the model. Low values of % bias or % relative error indicate the validity of selected model. Table 4.7 shows the predicted, experimental values and % bias for responses.

The % Bias between predicted and experimental values for responses were calculated by following equation:

$$\text{Bias} = \frac{(\text{Predicted Value} - \text{Experimental Value})}{\text{Predicted value}}$$

Table 4.7: % Bias of responses for the cross validation set

Response s	Test	Factors/Levels				Predicted values	Experimental Values	Bias (%)
		A	B	C	D			
RS1	1	5.55 (6)	3.32 (3)	0.83 (0.8)	34.04 (35)	2.457	2.76	-0.1233
	2	5.28 (5)	4.05 (4)	1.16 (1.2)	27.66 (28)	2.146	2	0.0680
	3	3.95 (4)	3.26 (3)	0.9	37.76 (38)	1.874	2.1	-0.1206
	4	5.223 (5)	2.84 (3)	0.950 (1)	33.43 (33)	2.213	2.43	-0.0981
	5	5.72 (6)	3.09 (3)	0.94 (0.9)	38.43 (38)	2.124	2.35	-0.1064
RS2	1	5.55 (6)	3.32 (3)	0.83 (0.8)	34.04 (35)	1.95	2.17	-0.1128
	2	5.28 (5)	4.05 (4)	1.16 (1.2)	27.66 (28)	2.49	2.27	0.0883
	3	3.95 (4)	3.26 (3)	0.9	37.76 (38)	2	2.35	-0.175
	4	5.223 (5)	2.84 (3)	0.950 (1)	33.43 (33)	1.66	1.89	-0.1385
	5	5.72 (6)	3.09 (3)	0.94 (0.9)	38.43 (38)	1.74	1.95	-0.1207
RS3	1	5.55 (6)	3.32 (3)	0.83 (0.8)	34.04 (35)	6.58	6.79	-0.0319
	2	5.28 (5)	4.05 (4)	1.16 (1.2)	27.66 (28)	6.89	6.67	0.0319
	3	3.95 (4)	3.26 (3)	0.9	37.76 (38)	5.51	5.78	-0.0490
	4	5.223 (5)	2.84 (3)	0.950 (1)	33.43 (33)	5.95	6.3	-0.0588
	5	5.72 (5)	3.09 (3)	0.94 (0.9)	38.43 (38)	6.33	6.57	-0.0379
RS4	1	5.55 (6)	3.32 (3)	0.83 (0.8)	34.04 (35)	3.7	4	-0.0811
	2	5.28 (5)	4.05 (4)	1.16 (1.2)	27.66 (28)	3.93	4	-0.0178

	3	3.95 (4)	3.26 (3)	0.9	37.76 (38)	3.4	3.71	-0.0912
	4	5.223 (5)	2.84 (3)	0.950 (1)	33.43 (33)	3.39	3.55	-0.0472
	5	5.72 (5)	3.09 (3)	0.94 (0.9)	38.43 (38)	3.71	4.11	-0.1078
	1	5.55 (6)	3.32 (3)	0.83 (0.8)	34.04 (35)	15.37	16.3	-0.0605
	2	5.28 (5)	4.05 (4)	1.16 (1.2)	27.66 (28)	16.026	15.47	0.0347
Rt	3	3.95 (4)	3.26 (3)	0.9	37.76 (38)	14.92	15.12	-0.0134
	4	5.223 (5)	2.84 (3)	0.950 (1)	33.43 (33)	14.75	15.19	-0.0298
	5	5.72 (5)	3.09 (3)	0.94 (0.9)	38.43 (38)	15.34	15.66	-0.0209

Note: values in bracket indicates actual values taken for experiment

Optimization using desirability function

The optimized methods with acceptable ranges for responses were determined by setting the goals of the critical responses. Response RS1 was selected to be in between 1.5-2.5, response RS2 was set to be in between 1.5-2.5, response RS3 was set to be in between 4-8, response RS4 was set to be in between 2-4, the Rt was set to be minimum in order to reduce the total run time of method.

Desirability function was calculated for the responses. Several optimized solutions for the specified criteria were generated by the software; out of which 4 solutions were used for checkpoint analysis (n=4) as shown in table 4.8. One of the solutions with HT-1 3.7, HT-2 5.8, FR 0.81 and Temperature 34 was chosen as the optimized working point as it gives acceptable resolution with reasonably symmetric peak shape and peak purity. DP-10 did not showed peak purity, the reason for which is explained in section 4.9.

The desirability (contour and 3D plot) and overlay plot for optimized working point is shown in figure 4.18 and 4.19. The observed responses values (table 4.9) of optimized working point lie within 95% confidence interval of the predicted response values. The final optimized chromatogram obtained with the selected working point is depicted in figure 4.20 that comprises of well resolved peaks of EDA and DPs. DP-9 and DP-10 were

eluted as extra peaks while resolving DP-4 and DP-5. The peak purity studies of resolved peaks are presented in table 4.10 and figure 4.21.

Table 4.8: Point Verification and working point selection

Optimized solution	Pred	Obs	Pred	Obs	Pred	Obs	Pred	Obs	Pred	Obs
	RS1	RS1	RS2	RS2	RS3	RS3	RS4	RS4	Rt	Rt
HT-1 5.57 (6),HT-2 3.33 (3), FR 1.03 (1), Temp. 38.48 (38)	2.29	2.36	1.98	2.1	6.36	6.14	3.85	3.75	15.80	15.63
HT-1 3.38 (3),HT-2 5.19 (5), FR 0.9, Temp. 33.16 (33)	1.83	1.72	2.54	2.44	6.79	6.46	3.99	3.72	16.35	16.11
HT-1 5.66 (6),HT-2 2.95 (3), FR 1.02 (1), Temp. 27.96 (28)	2.29	2.4	1.65	1.85	6.34	6.55	3.55	3.36	14.99	15.45
HT-1 3.70 (4),HT-2 5.77 (6), FR 0.81 (0.8), Temp. 34.14 (34)	2.04	2.07	2.81	2.95	7.47	7.26	3.97	3.64	16.95	16.36

Note: the values given in bracket were actual experimental values; Pred=predicted, Obs=observed

Table 4.9: Observed vs. Predicted responses for optimized working point

Response	Prediction	Observed	SE Mean	95% CI low	95% CI high
RS1	2.041	2.07	0.308371	1.38	2.70278
RS2	2.809	2.95	0.139429	2.51874	3.09865
RS3	7.467	7.26	0.299616	6.84847	8.08522
RS4	3.968	3.64	0.303373	4.59923	1.28027
Rt	16.946	16.36	0.463172	15.9761	17.915

SE=standard error, CI=confidence interval

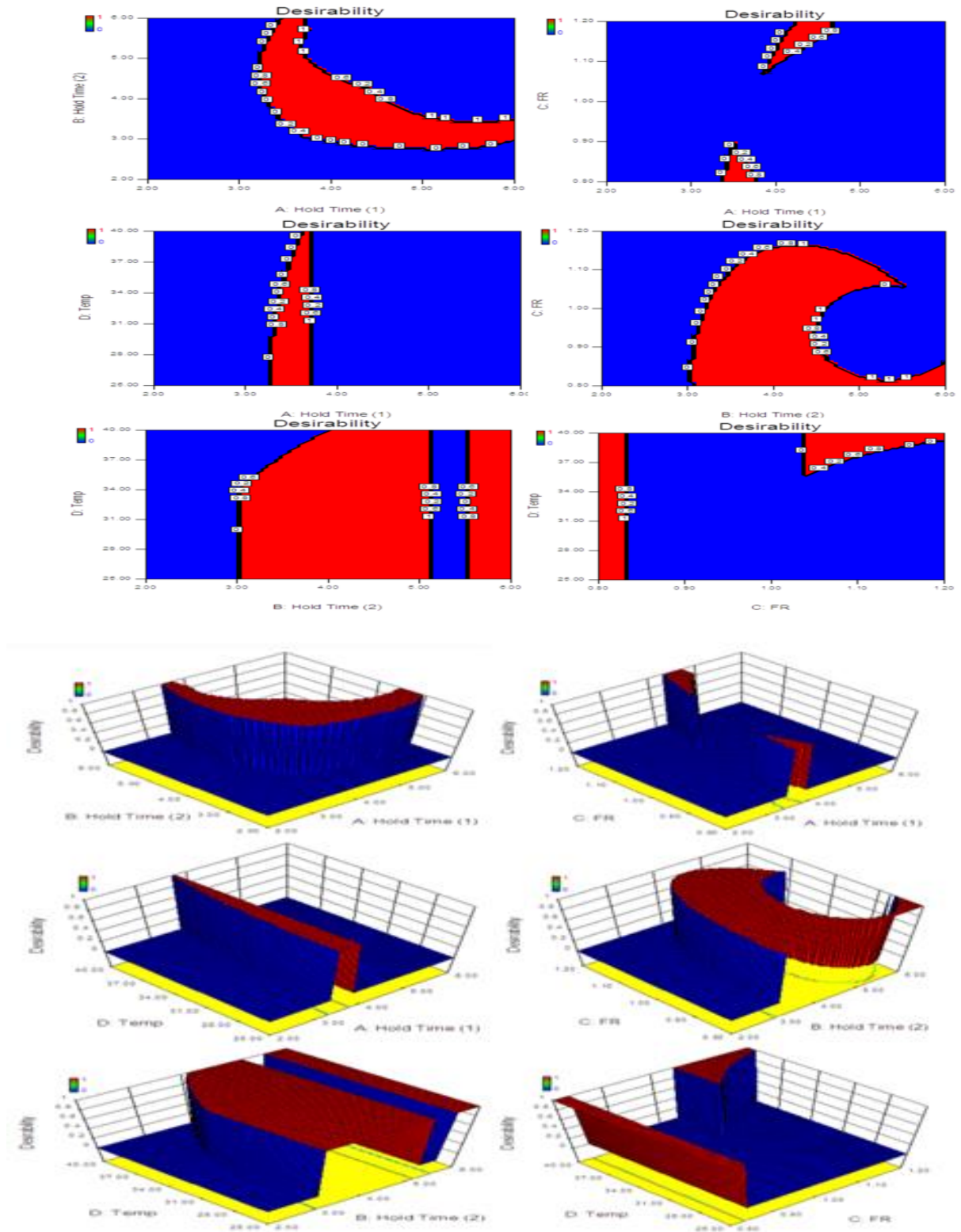


Figure 4.18: Contour and 3D Desirability plots for optimized chromatogram (desirability increases from blue to red region; blue region indicates 0 and red region indicates 1 desirability)

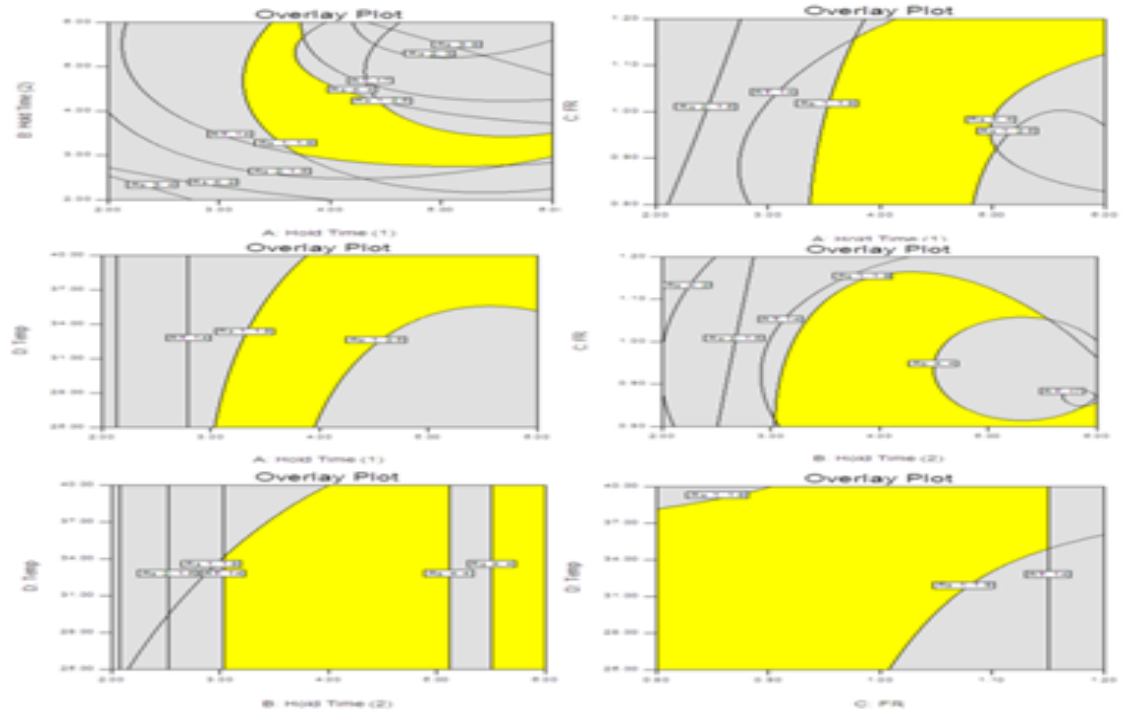


Figure 4.19: Overlay plots for optimized chromatogram (yellow region: design space, gray region: undesirable region)

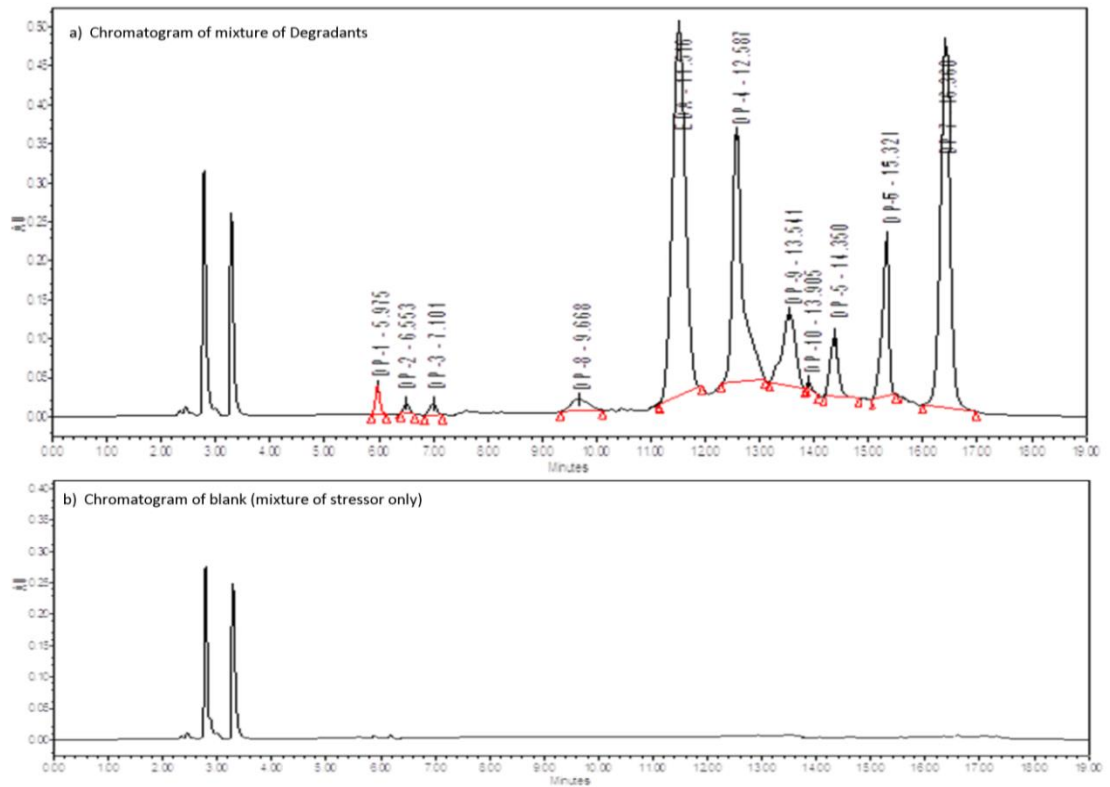
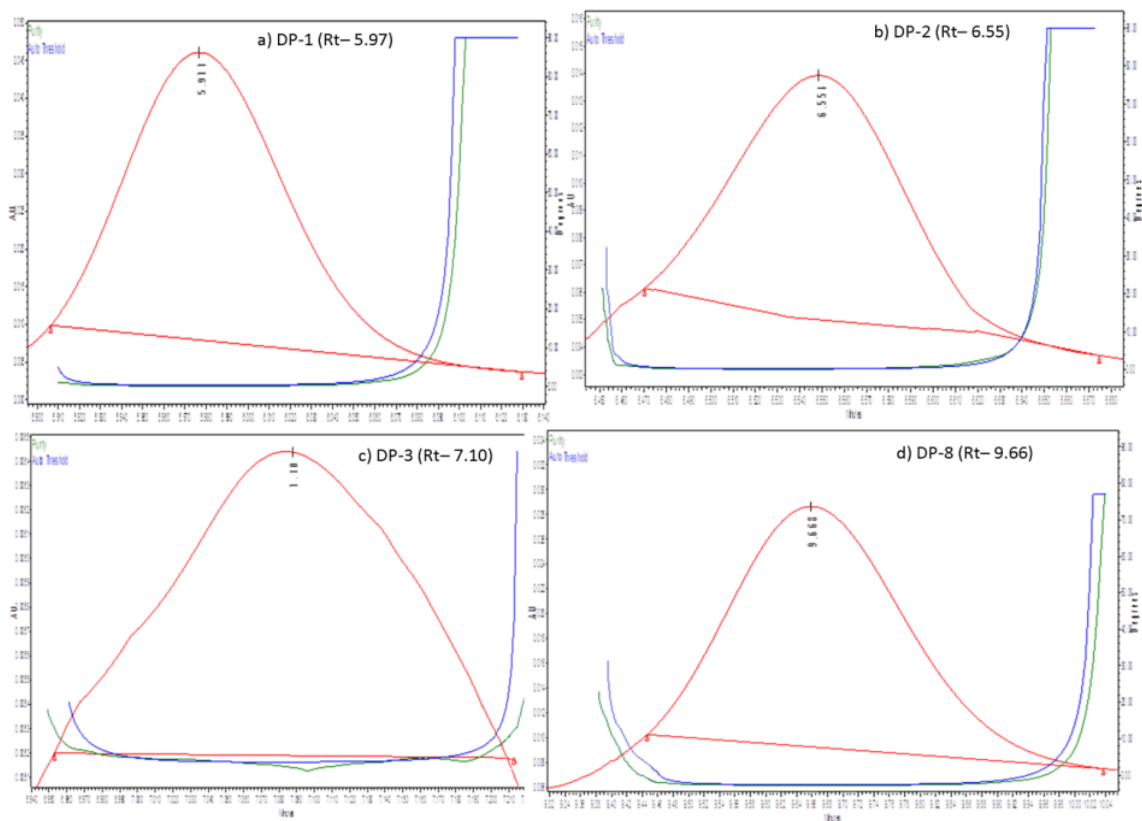


Figure 4.20: Chromatogram showing resolved peaks in mixture of degradants

Table 4.10: Peak purity studies in mixture of degradants

Degradant	Rt	Peak purity Angle	Peak purity Threshold
DP-1	5.975	0.225	0.286
DP-2	6.553	0.187	0.449
DP-3	7.101	1.046	1.101
DP-8	9.668	0.277	0.506
EDA	11.516	0.407	0.489
DP-4	12.587	0.114	0.221
DP-9	13.541	0.219	0.264
DP-10	13.905*	5.882	0.253
DP-5	14.350	0.291	0.312
DP-6	15.321	0.129	0.264
DP-7	16.360	0.105	0.226

Note*indicates peaks are not pure; peaks at Rt 13.90 showed different masses in LC-MS for base neutral and dry heat induced degradation.



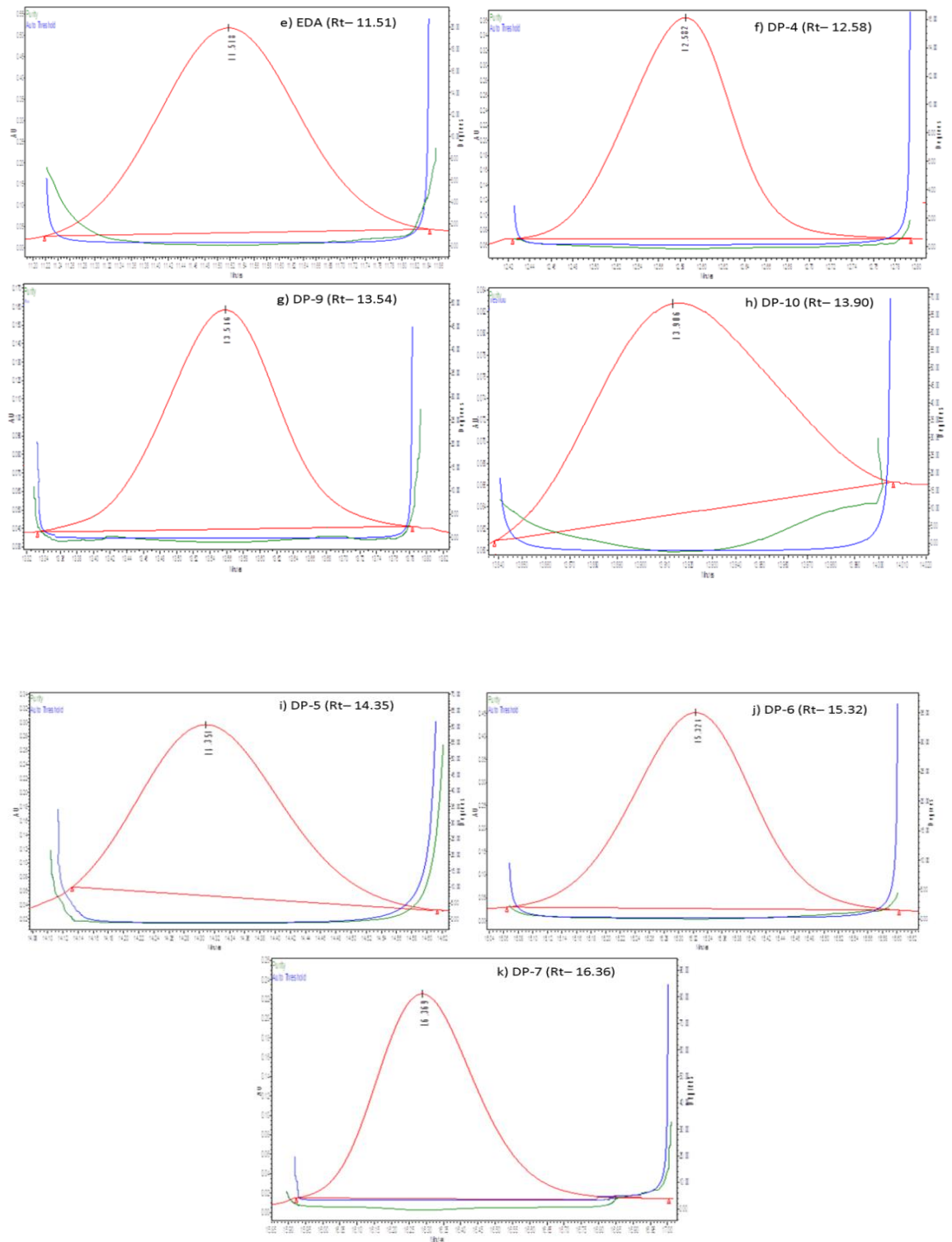


Figure 4.21: Peak purity plots for optimized chromatographic conditions

4.4.2.3 Method Validation using ICH Q2(R1) guideline

4.4.2.3.1 Linearity and Range

The calibration curve was constructed for EDA and was found to be linear over the concentration range of 10-300 µg/ml. The correlation co-efficient was 0.9992 with regression equation $y = 79799x + 27554$. The overlain chromatogram and calibration curve is shown in figure 4.22. The linearity data is shown in table 4.11.

Table 4.11: Linearity data of developed method

S.No.	Edaravone	
	Conc.(µg/ml)	Peak Area (mV.s) (Mean±%RSD)
1	10	778289±0.5311
	50	3963866±0.1625
2	100	8138624±0.5795
3	150	12082694±0.0802
4	200	16187304±0.0550
5	250	19497930±0.1512
6	300	24264573±0.2851

* Average of three determinants

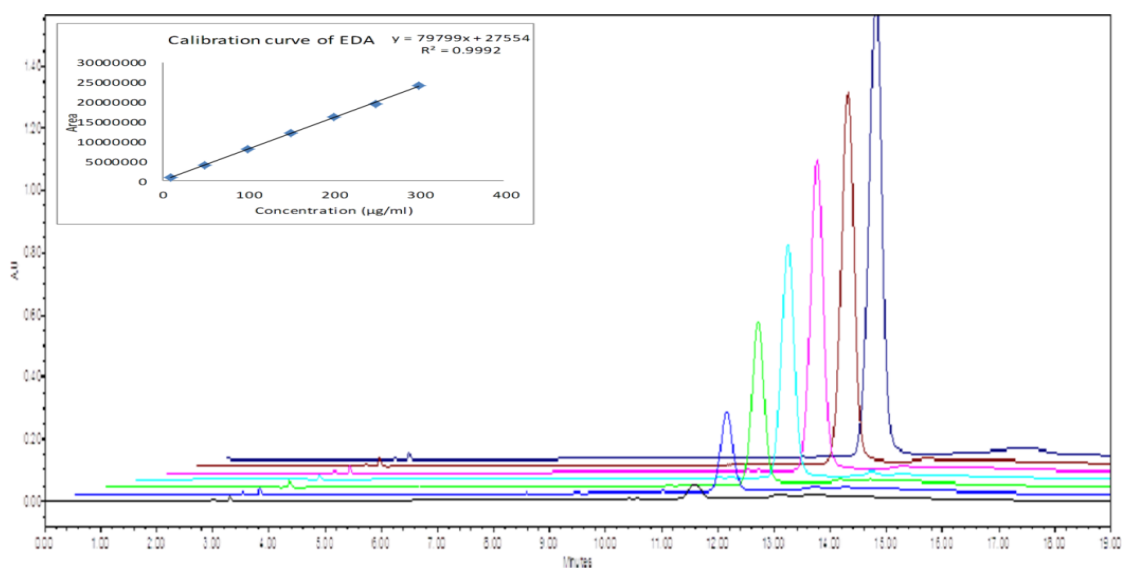


Figure 4.22: Overlay chromatogram showing linearity and calibration curve of developed method

4.4.2.3.2 Precision

For intra-day precision (table 4.12) the experiment was repeated 3 times in a day and for inter-day (table 4.13) precision on 3 different days. The average % RSD of intra-day and inter-day measurements were found to be 0.2011 and 0.3035 respectively. The low value of %RSD obtained confirms the precision of the developed method.

Table 4.12: Intra-day precision for estimation of EDA

S. No (µg/ml)	Peak Area (mV.s)			MEAN	%RSD
	Set 1	Set 2	Set 3		
10	781978	783827	781079	782294.7	0.1791
50	3959897	3963285	3953126	3958769	0.1306
100	8113058	8089206	8128061	8110108	0.2416
150	12072519	12106705	12069063	12082762	0.1722
200	16177504	16109954	16094490	16127316	0.2737
250	19489729	19450839	19500121	19480230	0.1333
300	24184995	24232750	24100392	24172712	0.2772
Average %RSD					0.2011

Table 4.13: Inter-day precision for estimation of EDA

S. No (µg/ml)	Peak Area(mV.s)			MEAN	%RSD
	Set 1	Set 2	Set 3		
10	781179	782979	780017	781391.67	0.1909
50	3958126	3961172	3942011	3953769.7	0.2604
100	8180066	8101305	8109658	8130343	0.5321
150	12035920	12098751	12089959	12074877	0.2817
200	16039322	16176983	16089750	16102018	0.4325

250	19547102	19480772	19490025	19505966	0.1841
300	24179091	24089499	24199978	24156189	0.2429
Average %RSD					0.3035

4.4.2.3.3 Accuracy

Accuracy of the developed method was confirmed by recovery study from marketed formulation of EDA at 3 level of standard addition (80 %, 100% and 120 %). The results are shown in table 4.14. Recovery greater than 99 % with low standard deviation (SD) justifies the accuracy of the developed method.

Table 4.14: Recovery study from formulation (Aravon IV infusion)

Excess drug added to analyte (%)	Theoretical Content ($\mu\text{g/ml}$)	*Amount Found ($\mu\text{g/ml}$)	Recovery (%) \pm S.D.
0	100	100.4535	100.4535 \pm 0.499
80	180	99.3073	99.3073 \pm 0.0490
100	200	99.9495	99.9495 \pm 0.0933
120	220	99.8888	99.8888 \pm 0.2150

*Average of three determinants.

4.4.2.3.4 Limit of detection and quantification

The LOD and LOQ of present method were found to be 0.5341 and 1.6186

4.4.2.3.5 Robustness studies

For robustness study few parameters were varied, these are variation of hold time-1, hold time-2, flow rate, column temperature, mobile phase composition and pH of buffer. The low average value (less than 2 %) of % RSD for determination of EDA revealed the robustness of the developed method (table 4.15)

Table 4.15: Robustness of developed HPLC method

Factor	Level	Retention	Area	Theoretical plate	Tailing
Hold Time-1					
3.5	-0.1	10.86	12070991	11656	1
4.0	0	11.54	12072519	11727	1.09
4.5	0.1	12.16	12068539	11701	0.99
Mean ± % RSD		11.52±0.056	12070683±0.00016	11694.67±0.0030	1.02±0.053
Hold Time-2					
5.5	-0.1	11.04	12071519	11679	0.98
6.0	0	11.54	12072519	11727	1.09
6.5	0.1	11.93	12068277	11720	1
Mean ± % RSD		11.50±0.038	12070772±0.00018	11708.67±0.0022	1.02±0.057
Flow Rate					
0.7	-0.1	11.99	12071540	11696	1.28
0.8	0	11.54	12072519	11727	1.09
0.9	0.1	11.4	12068261	11729	0.97
Mean ± % RSD		11.64±0.026	12070773±0.000184	11717.333±0.0015	1.11±0.140
Temperature					
30	-0.1	11.75	12072063	11677	1.2
34	0	11.54	12072519	11727	1.09
38	0.1	11.48	12069217	11739	1
Mean ± % RSD		11.59±0.012	12071266±0.000148	11714.33±0.0028	1.09±0.091
Mobile phase composition (ratio of buffer at the start of gradient)					
94	-0.1	11.98	12074821	11717	1.28
95	0	11.54	12072519	11727	1.09
96	0.1	11.4	12059824	11730	0.9
Mean ± % RSD		11.64±0.026	12069055±0.00066	11724.67±0.0005	1.09±0.174

pH					
5.6	-0.2	11.79	12063901	11615	1.51
5.8	0	11.54	12072519	11727	1.09
6.0	0.2	11.46	12075024	11739	1.1
Mean \pm % RSD		11.59 \pm 0.014	12070481 \pm 0.00048	11693.67 \pm 0.0058	1.23 \pm 0.194

4.4.2.3.6 Selectivity

The results of stress degradation studies indicated a high degree of selectivity of developed method for EDA.

4.4.2.3.7 Specificity

As illustrated in figure 4.20 the developed method is specific since complete separation of EDA and other DPs were observed. The peaks of EDA and DPs were well resolved. The resolution factor for the separating peaks were greater than 1.5 from the nearest resolving peak. Also it was justified by peak purity plots as shown in figure 4.21. The peak purity studies of resolved peaks are presented in table 4.10.

4.4.2.3.8 Stability in sample solutions

Solutions containing different concentrations of EDA and stressed samples were prepared from standard stock solution and then stored at room temperature for 24 hrs. No additional peaks were found in chromatogram indicating the stability of EDA the sample solution.

4.4.2.3.9 System Suitability Parameters (SST)

System suitability testing was carried out on freshly prepared standard solutions, n=6, containing EDA. SST parameters obtained with 20 μ L injection volumes are summarized in table 4.16.

Table 4.16: System Suitability Parameters for EDA

Parameter	Data Obtained
Retention time (min) \pm SD	11.535 \pm 0.078
Theoretical plate \pm SD	11721.67 \pm 8.091

Tailing factor \pm SD	1.00 \pm 0.055
Resolution \pm SD	RS1: 2.04 \pm 0.050, RS2: 2.95 \pm 0.084, RS3: 7.22 \pm 0.069, RS4: 3.63 \pm 0.040

*Data shown is the average of six replicates. SD= Standard Deviation

4.4.2.4 Stress Degradation studies

As presented in figure 4.20 ten DPs were formed under stress conditions when mixture of degradants was analysed in LC-PDA. The summary of forced degradation condition with % degradation (% Deg) in various conditions is presented in table 4.17. % Deg was calculated by formula:

$$\% \text{ Deg} = \frac{\left[\begin{array}{l} \text{(Initial area of untreated stock solution} \\ \text{- reduced area of treated stock solution)} \end{array} \right]}{\text{Actual initial area of untreated stock solution}} \times 100$$

EDA was most sensitive towards oxidative degradation. It undergoes significant degradation under acid, base and dry heat induced degradation. Slight degradation was observed under neutral, photolytic and thermal-humidity degradation condition. The chromatograms of stressed samples are shown in figure 4.23. Also peak purity plot for individual stress degradation condition (for DP at Rt 13.8-13.9 which was not pure in mixture of degradants) of acid, base, neutral, oxidative, photolytic degradation and thermal-humidity induced degradation are shown in figure 4.24 alongwith their peak purity studies in table 4.18.

Table 4.17: Summary of stress degradation of EDA API and formulation

Stressor Type	Stressor Conc.	Time	DPs Formed with Rt	%Degradation (API)	%Degradation (Formulation)
Acid	0.05N HCl	180	DP-3(7.19),		69.99

degradation	at 70 ⁰ C	min	DP-5(14.25), DP-6(15.35), DP-7(15.96)	70.87	
Base degradation	0.2N NaOH at 70 ⁰ C	180 min	DP-1(6.09), DP-9(13.29), DP-10(13.94), DP-6(15.38), DP-7(16.24)	63.51	63.00
Neutral degradation	100 ⁰ C	7 hr	DP-8(9.66), DP-6(15.36), DP-7(16.16) DP-10(13.89),	46.54	45.31
Oxidative degradation	6% H ₂ O ₂ at RT	45 min	DP-2(6.55), DP-5(14.35), DP-10(13.90)	52.07	51.80
Photolytic degradation	5382 LUX and 144UW/cm ₂	21 days	DP-6(15.34), DP-7(16.16)	44.27	44.01
Dry Heat induced degradation	80 ^o C	21 days	DP-4(12.57), DP-10(13.90), DP-5(14.35) DP-6(15.32), DP-7(16.36)	67.42	20.41 (for 72 Hr)
Thermal-Humidity induced degradation	40 ^o C 70 ± 5% RH	21 days	DP-8(9.54), DP-4(12.59) DP-6(15.42), DP-7(16.18)	37.59	37.04

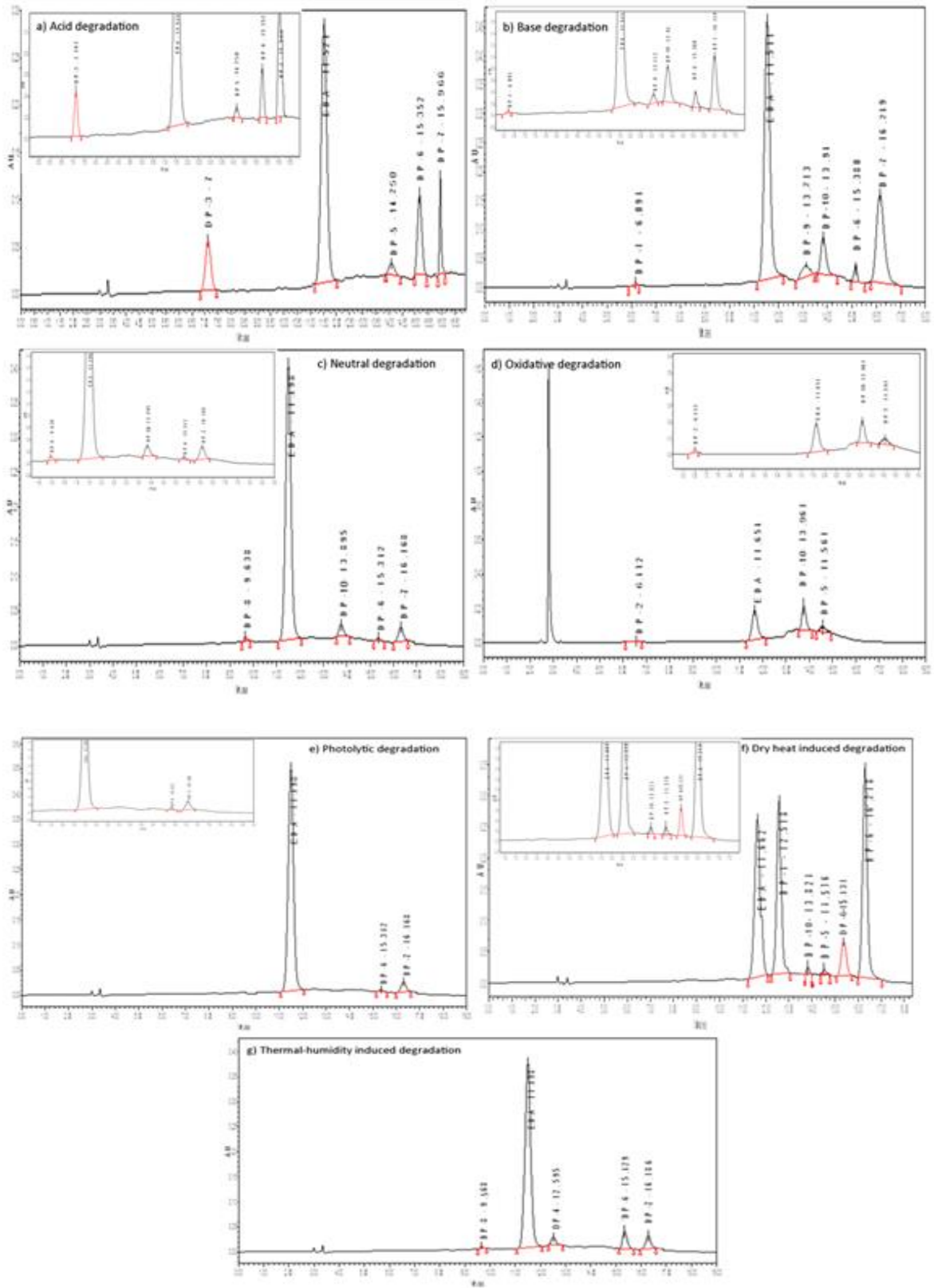


Figure 4.23: Chromatograms of a) Acid degradation, b) Base degradation, c) Neutral degradation, d) Oxidative degradation e) Photolytic degradation, f) Dry heat induced degradation and d) Thermal-humidity induced degradation

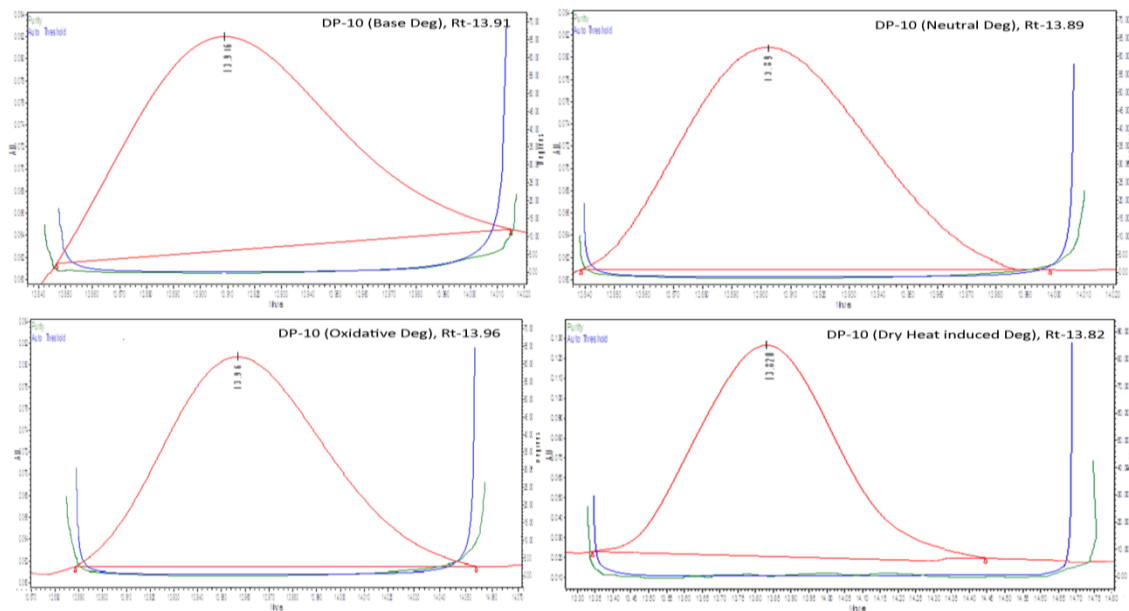


Figure 4.24: Peak purity plots for DPs formed at Rt 13.8-13.9

Table 4.18: Peak purity studies for DPs formed at Rt 13.8- 13.9

S. No.	Degradation condition	Rt	Peak purity angle	Peak purity threshold
1.	Base	13.91	0.246	0.281
2.	Neutral	13.89	0.407	0.489
3.	Oxidation	13.96	0.291	0.312
4.	Dry heat induced	13.82	0.347	0.357

4.4.2.5 Applicability of developed stability indicating assay method for analysis formulation

The developed method was successfully applied for the estimation of EDA in its marketed formulation (Edaravone Injection, Aravon, 1.5 mg/ml by Sun Pharmaceutical Ind. Ltd.). The % assay was found to be 99.96 ± 0.355 (EDA \pm SD), the label claim was 1.5 mg/ml.

The developed method was also used to analyze stress degraded samples of a formulation containing EDA. Stress degradation were carried out under same condition as specified for API and analyzed in the same way using same chromatographic conditions. The DPs were discernible and well separated. As presented in table 4.18 minor variation was observed in degradation of API and formulation.

4.5 SECTION-B

DEGRADATION KINETIC STUDY OF EDARAVONE BY HPLC METHOD

The degradation kinetic was studied for acid, base, neutral, oxidative and photolytic degradation.

4.5.1 EXPERIMENTAL

4.5.1.1 Chemicals and Reagents

Chemicals and reagents utilized in present section were same as described in section 3.4.1.1.

4.5.1.2 Equipments and chromatographic conditions

The equipments utilized were same as described in section 3.4.1.2 and chromatographic conditions were same as described in section 4.4.1.2 for degradation kinetic study.

4.5.1.3 Preparation of Stock, Samples and Buffer solutions

Standard and stock solutions were prepared in same solvent with same dilutions as described in section 4.4.1.3. For preparation of sample solutions 10 mg of EDA was dissolved in variable strength of HCl, NaOH and H₂O₂ for Hydrolysis and oxidative degradation. For neutral degradation drug was dissolved in double distilled water by ultrasonication as it is slightly soluble in water and soluble in boiling water. These solutions were transferred into another clean and dry round bottom flask and refluxed in a thermostatically controlled oil bath at specified temperature. Aliquots of 0.5 mL of samples were collected and placed into a 10 mL volumetric flask at different time intervals for specific time and temperature for specific degradation condition for kinetic study. In case of acid and base degradation solutions were neutralized with equivalent strength of NaOH/HCl. For photolytic degradation solution of EDA in ACN was kept in photostability chamber and 0.5 mL aliquots were withdrawn after specific time interval. The volume was completed with mobile phase and filtered through 0.2 mm membrane filter before HPLC analysis. Each experiment was repeated three times at each temperature and time interval and the mean concentration was taken.

The solutions (initial concentration $C_0 = 150 \mu\text{g/ml}$) were injected using the chromatographic conditions of the HPLC method described in section 4.4.1.2.

The % of drug degradation was calculated from the formula:

$$\% \text{ Deg} = \frac{\left[\begin{array}{l} \text{(Initial area of untreated stock solution} \\ \text{- reduced area of treated stock solution)} \end{array} \right]}{\text{Actual initial area of untreated stock solution}} \times 100$$

The buffer solution used for HPLC analysis was prepared in same way as described in section 4.4.1.3.

4.5.2 RESULTS AND DISCUSSION

The degradation rate kinetics was determined using linear and nonlinear regression analysis by plotting % of drug degradation (% Deg) versus time (for zero-order process), log of % Deg versus time (for first-order process) and 1/% Deg versus time (for second-order process). The rate constant (K_{obs}), half-life ($t_{1/2}$) and activation energy (E_a) were also calculated from the slope of lines at each temperature for acid, base, neutral and oxidative degradation. In the present study linear and nonlinear fit function from Graphpad Prism Software was used. Also, the arrhenius plots were constructed to study the effect of temperature on the rate of hydrolysis for acid, base and neutral degradation.

The linear regression analysis was performed for neutral, oxidative and photolytic degradation, while acid and base degradation followed nonlinear regression analysis at the selected temperature and concentration.

4.5.2.1 Kinetics of acid and base degradation

The % degradation of EDA during acid and base degradation was observed by HPLC. The r^2 values for linear and nonlinear regression for acid and base degradation are shown in table 4.19 and 4.21. For both acid and base hydrolysis nonlinear regression analysis (figure 4.25 and 4.27) was performed for pseudo first order reaction kinetics at selected temperature and concentration as non linear regression fits better and r^2 value is higher. The r^2 value was highest for second order process but since the volume of stressor is much higher as compared to drug and was constant all over the degradation, it could be considered to follow pseudo first order reaction kinetic. The estimates of K_{obs} , $t_{1/2}$ and activation energy (E_a) (table 4.20 and 4.22) can be obtained directly by plotting logarithm

of observed % Deg versus time data in nonlinear regression analysis using Graphpad Prism Software. The magnitude of rate constants indicates that rate of degradation was influenced not only by temperature but also by hydrogen and hydroxide ion concentration. The arrhenius plots along with residual plots for acid and base degradation are illustrated in figure 4.26 and 4.28.

Table 4.19: Linear and non linear regression equation and r^2 value for zero, first and second order reaction for acid degradation

S. No	Conc. (HCl)	Te mp.	r^2 value for LRA			r^2 value for NLRA		
			Zero Order	First Order	Second Order	Zero Order	First Order	Second Order
1	0.05 N	60	0.8287	0.7785	0.6908	0.9573	0.9864	0.9976
		70	0.9227	0.8653	0.757	0.9717	0.9924	0.9988
		80	0.7609	0.7356	0.6701	0.9325	0.9763	0.9947
2	0.1 N	60	0.8082	0.7687	0.688	0.9456	0.982	0.996
		70	0.6939	0.6933	0.6469	0.9013	0.9634	0.9909
		80	0.5203	0.5347	0.5273	0.9149	0.9612	0.9858
3	0.2 N	60	0.6709	0.6753	0.6397	0.8977	0.9589	0.9879
		70	0.4718	0.5015	0.5069	0.8931	0.95	0.981
		80	0.3305	0.3911	0.43	0.8121	0.8999	0.9549

LRA- linear regression analysis, NLRA- nonlinear regression analysis

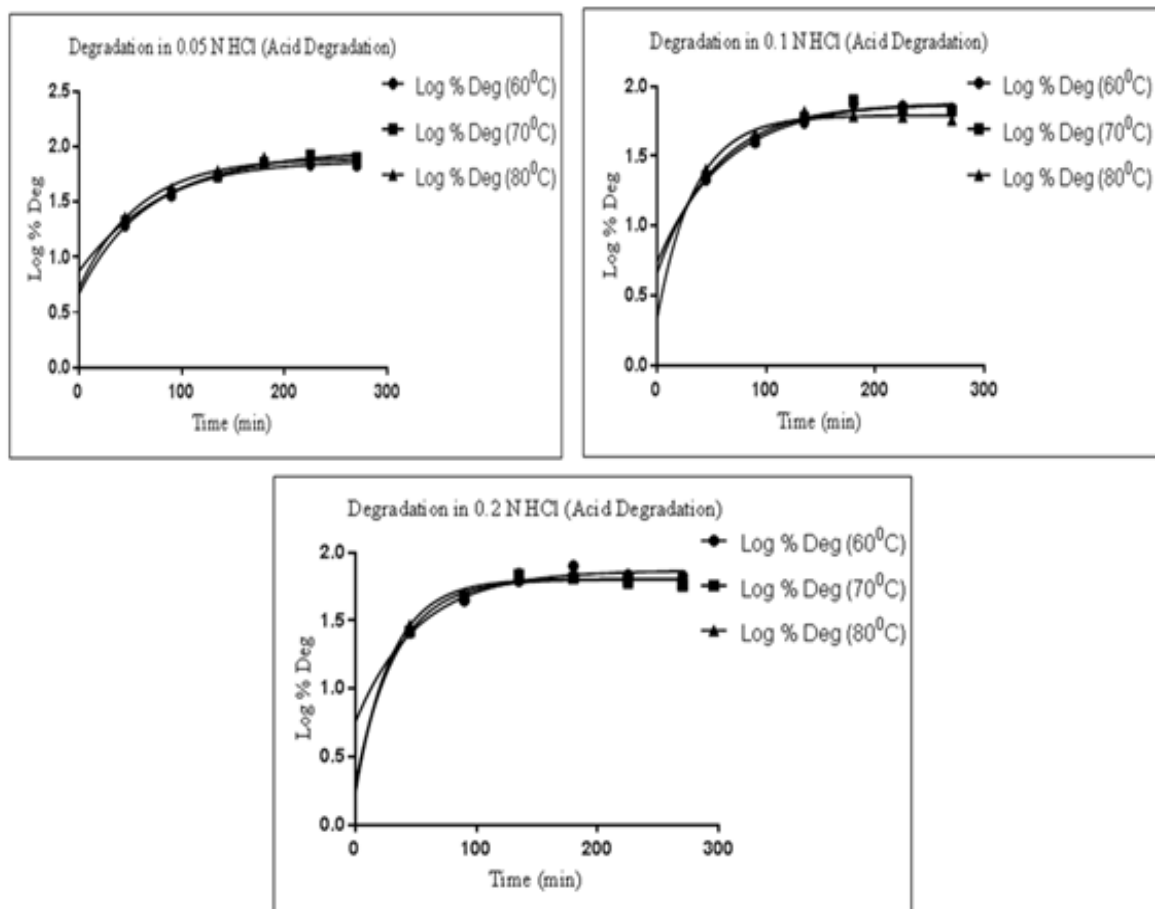


Figure 4.25: Non linear pseudo first order reaction kinetic plots for acid degradation

Table 4.20: Half- life ($t_{1/2}$) and activation energy (E_a) for pseudo first order reaction kinetic of acid degradation

S. No	Conc. (HCl)	Regression Equation	Temp.	$t_{1/2}$ (Hr.)	E_a (kJ/mol)
1	0.05 N	-205.6*X - 1.234	60	43.89	-1.7094
			70	59.66	
			80	40.22	
2	0.1 N	-1438*X + 2.628	60	35.64	-11.9562
			70	22.88	
			80	20.36	
3	0.2 N	-1536*X + 2.794	60	43.12	-12.771
			70	37.13	
			80	23.57	

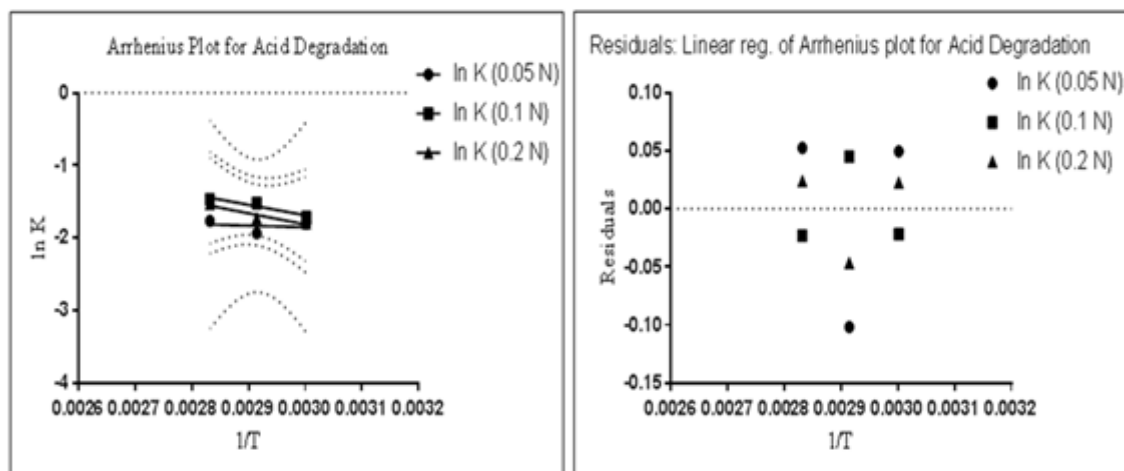


Figure 4.26: Arrhenius plot and residual plot for acid degradation

Table 4.21: Linear and non linear regression equation and r^2 value for zero, first and second order reaction for base degradation

S. No	Conc. (NaOH)	Temp.	r^2 value for LRA			r^2 value for NLRA		
			Zero Order	First Order	Second Order	Zero Order	First Order	Second Order
1	0.2 N	60	0.6598	0.6717	0.6822	0.8006	0.8194	0.8368
		70	0.8169	0.8131	0.7868	0.9215	0.9563	0.9794
		80	0.6074	0.6252	0.6237	0.8828	0.9332	0.966
2	0.5 N	60	0.6226	0.6267	0.6299	0.907	0.918	0.928
		70	0.748	0.7498	0.7305	0.9115	0.951	0.9765
		80	0.4484	0.491	0.5164	0.8133	0.8848	0.9356
3	0.8 N	60	0.5624	0.5683	0.5734	0.8784	0.8899	0.9007
		70	0.6646	0.6777	0.67	0.8909	0.9386	0.9696
		80	0.3783	0.4272	0.4614	0.7676	0.8509	0.9126

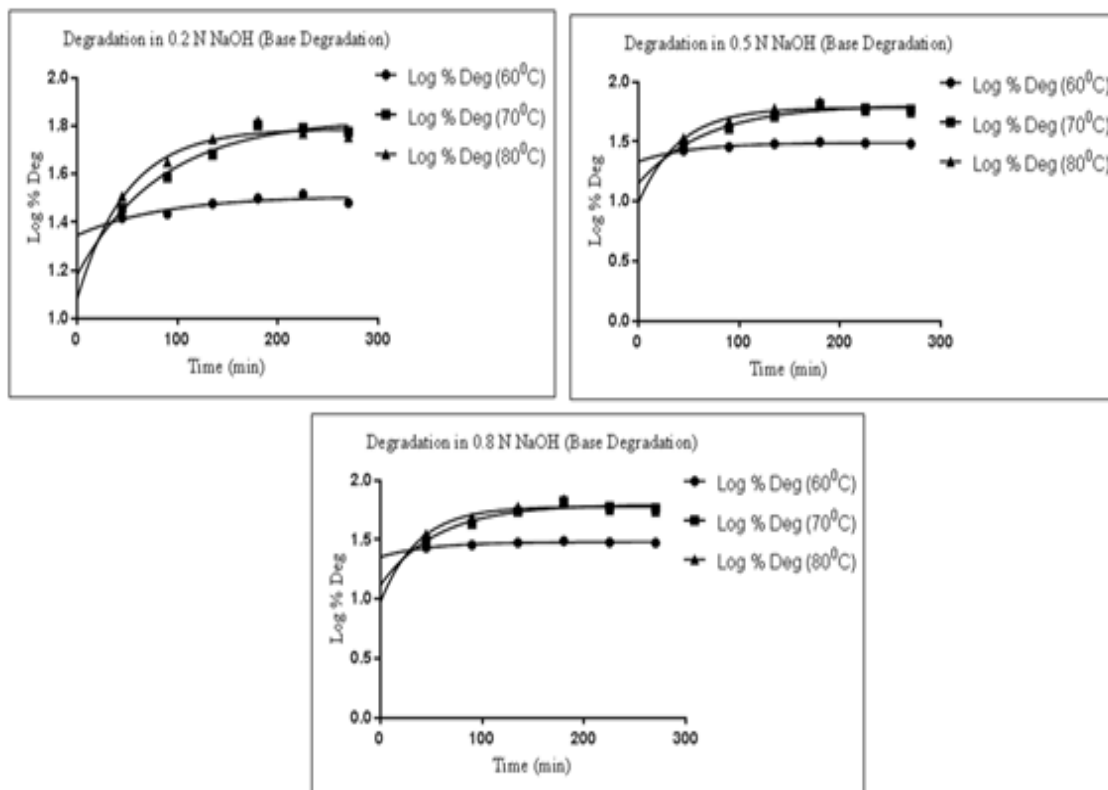


Figure 4.27: Non linear pseudo first order reaction kinetic plots for base degradation

Table 4.22: Half- life ($t_{1/2}$) and activation energy (e_a) for pseudo first order reaction kinetic of base Degradation

S. No	Conc. (HCl)	Regression Equation	Temp.	$t_{1/2}$ (Hr.)	Ea (kJ/mol)
1	0.2 N	-1415*X + 2.274	60	59.91	-11.765
			70	58.14	
			80	34.26	
2	0.8 N	-679.9*X + 0.2638	60	36.65	-5.6530
			70	46.71	
			80	27.88	
3	0.1 N	-708.7*X + 0.4	60	33.64	-5.89247
			70	38.96	
			80	25.35	

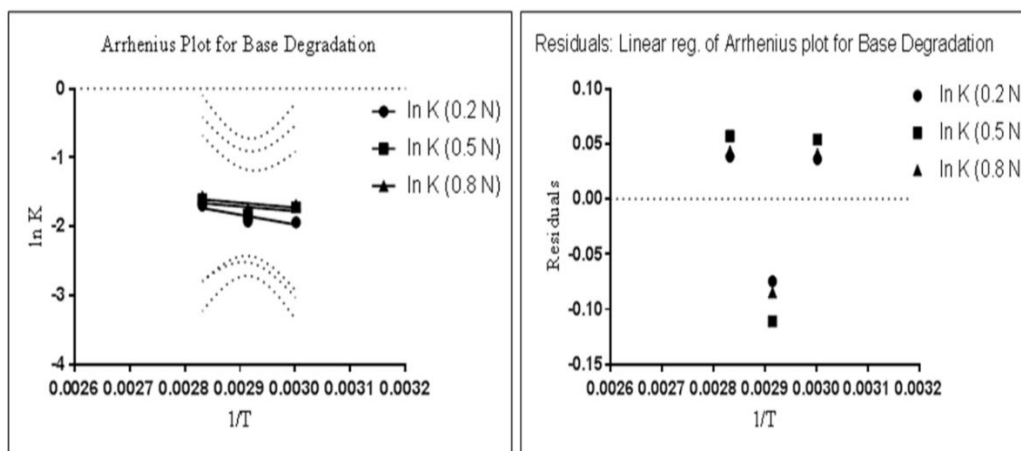


Figure 4.28: Arrhenius plot and residual plot for base degradation

4.5.2.2 Kinetics of Neutral, oxidative and photolytic degradation

The degradation rate kinetics for neutral, oxidative and photolytic degradation was determined using linear regression analysis. Highest r^2 value for zero order reaction indicates that the neutral, oxidative and photolytic degradation followed apparent zero order reaction kinetic (figure 4.29, 4.31, 4.32) at selected concentration and temperature. The calculated rate constants were given in table 4.23, 4.25 and 4.26 for neutral, oxidative and photolytic degradation respectively. The value of rate constant (estimated from slopes) was obtained from plot of % Deg versus time. The resulting K_{obs} values were plotted against temperature (in kelvin) to obtain arrhenius plot for neutral degradation which is presented in figure 4.30 and table 4.24.

Table 4.23: Regression equation and r^2 value for zero, first and second order reaction for neutral degradation calculated by linear regression analysis

S. No	Te mp.	r^2 Value			Regression Equation		
		Zero Order	First Order	Second Order	Zero Order	First Order	Second Order
1	80	0.9958	0.9948	0.9693	$3.884 * X + 16$	$0.0549 * X + 1.266$	$-0.004274 * X + 0.0509$
2	90	0.9946	0.9919	0.9645	$3.912 * X + 16.72$	$0.05394 * X + 1.281$	$-0.004094 * X + 0.04924$
3	100	0.9938	0.9905	0.9592	$3.917 * X + 18.13$	$0.05158 * X + 1.31$	$-0.003734 * X + 0.04625$

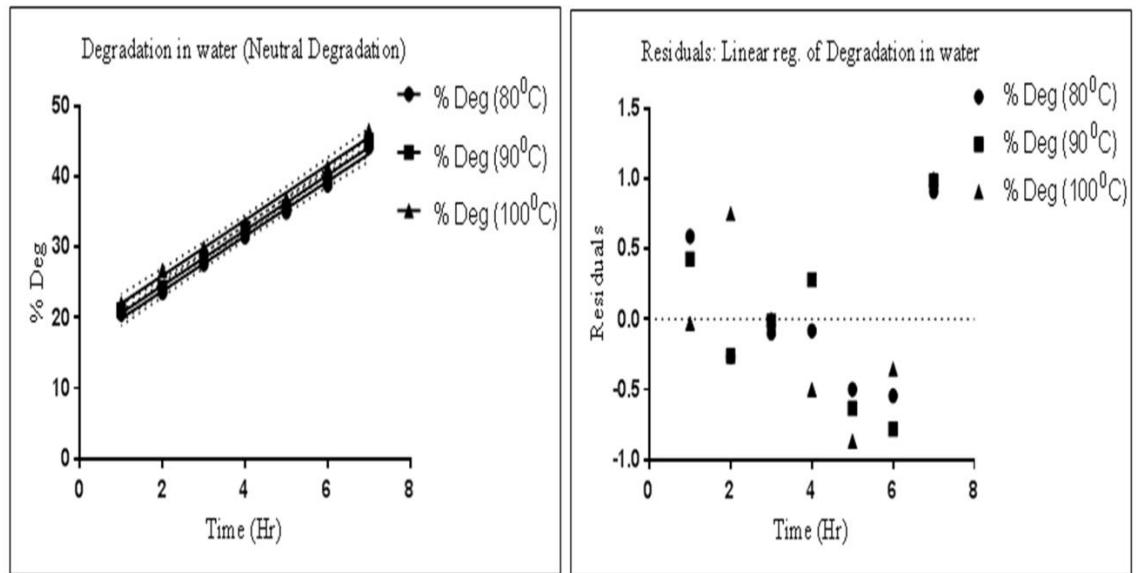


Figure 4.29: Zero order reaction kinetic and residual plots for neutral degradation

Table 4.24: Half- life ($t_{1/2}$) and activation energy (E_a) for zero order reaction kinetic of neutral Degradation

S. No	Stressor	Temp.	$t_{1/2}$ (Hr)	E_a (kJ/mol)
1	Neutral Degradation	80	194.18	0.2022
		90	195.56	
		100	195.83	

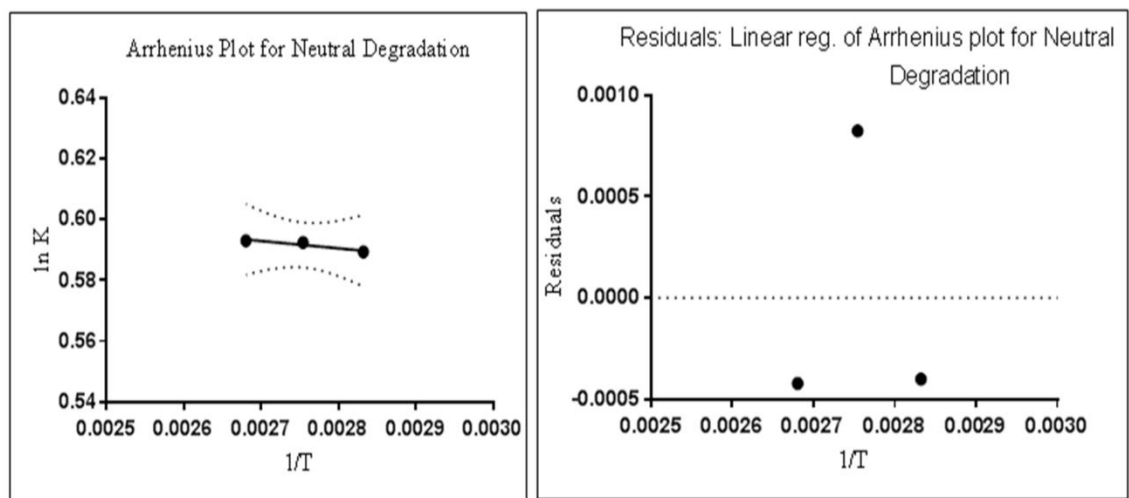


Figure 4.30: Arrhenius plot and residual plot for neutral degradation

Table 4.25: Regression equation and r^2 value for zero, first and second order reaction for oxidative degradation

S. No	Te mp.	r^2 Value			Regression Equation		
		Zero Order	First Order	Second Order	Zero Order	First Order	Second Order
1	6 %	0.993	0.9833	0.9444	$0.7521 * X + 20.24$	$0.00579 * X + 1.448$	$-0.0002519 * X + 0.03204$
2	3 %	0.9927	0.9887	0.9395	$0.7816 * X + 12.66$	$0.006739 * X + 1.343$	$-0.0003365 * X + 0.03946$

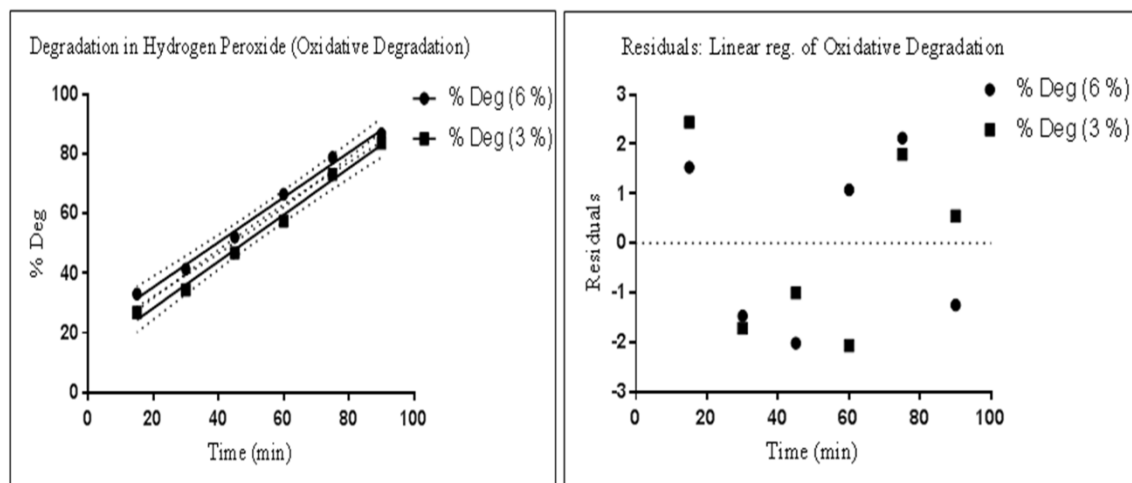


Figure 4.31: Zero order reaction kinetic and residual plots for oxidative degradation

Table 4.26: Regression equation and r^2 value for zero, first and second order reaction for photolytic degradation

S. No	r^2 Value			Regression Equation		
	Zero Order	First Order	Second Order	Zero Order	First Order	Second Order
1	0.9759	0.8823	0.7345	$3.127 * X - 5.591$	$0.04613 * X + 0.8806$	$-0.004417 * X + 0.09757$

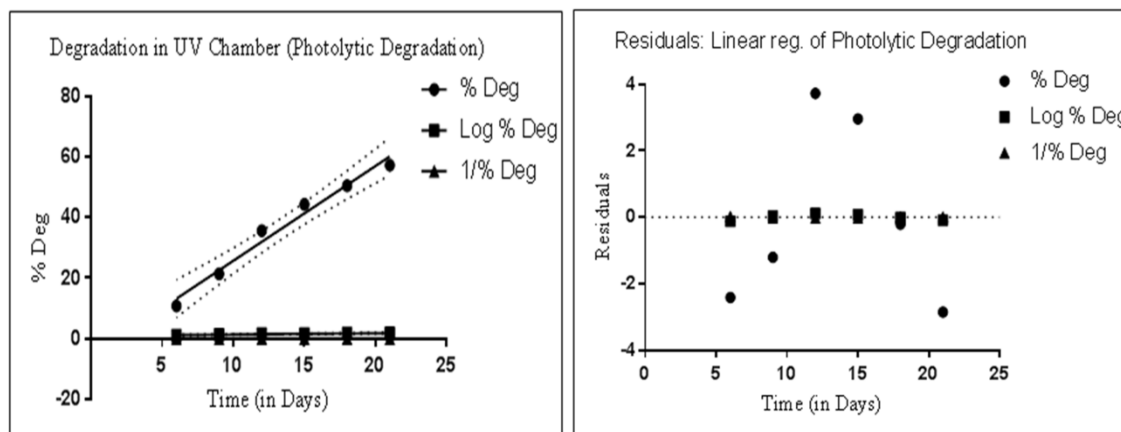


Figure 4.32: Zero order reaction kinetic and residual plots for photolytic degradation

4.6 SECTION –C

DEVELOPMENT AND VALIDATION OF QbD BASED STABILITY INDICATING HPTLC METHOD

4.6.1 EXPERIMENTAL

4.6.1.1 Chemicals and Reagents

The EDA bulk drug was purchased from Sigma Aldrich Co, St Louis, USA. EDA injection, ARAVON, containing 1.5 mg/ml of EDA was purchased from local pharmacy. AR grade petroleum ether (pet. ether), ethyl acetate, Glacial Acetic Acid and Methanol was procured from Spectrochem Pvt. Ltd., Mumbai. Precoated silica gel aluminum plate 60 F₂₅₄, (20 X 20 cm) were procured from Merck, Darmstadt, Germany.

4.6.1.2 Equipments and chromatographic conditions

Densitometry was carried out with a CAMAG TLC Scanner 3 fitted with win CATS 1.4.0 planar chromatography manager software and data analysis was performed with Design Expert 7.0 software. Precoated silica gel aluminum plate 60 F₂₅₄, (20 X 20 cm; Merck, Darmstadt, Germany) was used for chromatographic separation. The plates were washed with methanol and activated at 80⁰C for 20 min prior to chromatography. The samples were filtered through a 0.2 μm nylon membrane syringe filter before application. The application rate was maintained constantly at 150 nl/s. The spaces among the bands were maintained automatically by the software. Samples were applied to the HPTLC plates using the spray-on technique of CAMAG LINOMAT V under the flow of nitrogen gas,

and developed in a CAMAG (20cm X 20 cm) twin trough glass chambers, previously saturated with the mobile phase to a distance of 89 mm. The slit dimension was kept at 5 mm X 0.45 mm at 20 mm/s scanning speed. The mobile phase consisted of Petroleum ether- Ethyl acetate- Glacial acetic acid (GAA) in the ratio of 3:2:0.01. Subsequently after development, TLC plates were dried in a current of air and scanned on Camag TLC scanner 3 in the absorbance mode at 244 nm. Deuterium lamp was utilized as source of radiation emitting a continuous UV spectrum in the range of 200–400 nm. Evaluation was done using linear regression analysis by peak areas.

4.6.1.3 Preparation of Standard, Stock and Sample solutions

Stock solutions (1 mg/ml) were prepared in ACN for quantitation of the EDA in bulk and commercial dosage forms (Aravon injection, Sun Pharmaceuticals Ind. Ltd.). To analyze the stressed samples suitable dilutions were made in mobile phase to obtain the final concentration of 12 µg/band with respect to EDA. Same aliquots of EDA were prepared for recovery studies and assay of marketed formulation.

4.6.1.4 Preparation of Degradation Products (DPs)

For stress degradation study, stress conditions utilized for samples were same as described in section 4.4.1.4. Placebo samples were also prepared by same stress degradation condition for comparison.

4.6.1.5 Method optimization and development

Analytical target profile (ATP)

The ATP of the present work was to develop stability indicating HPTLC method that shows well resolved chromatogram of EDA and DPs with distinct R_f value.

Preliminary investigations

To get separation among EDA and DPs various non polar solvents were tried along with ethyl acetate because when ethyl acetate was used alone; all components were travelled along with mobile phase. Chloroform, hexane, pet. ether and toluene were tried among nonpolar phase. Pet. ether gives satisfactory result. To remove tailing and quenching of spot glacial acetic acid (GAA) was added as third component. It also increases the resolution of some DPs.

Risk assessment by cause- effect relationship and CNX approach

Risk assessment by Ishikawa or Fishbone diagram and Cause-Effect Risk Assessment Matrix with CNX approach was performed based on knowledge obtained from preliminary trials, to determine the relationship between input variables or factors and the method performance.

Design of Experiments (DoE)

Significant factors selected after CNX risk assessment were subjected to Box-Behnken response surface design (BBD) by Design Expert (Version 7.0) Software. The BBD design matrix with 17 runs including five center points was used to evaluate the main and interaction effects of the factors.

4.6.1.6 Method validation using Q2(R1) ICH guideline

The present method was validated according to the ICH guideline.

4.6.1.7 Application of developed HPLC method

The marketed formulation was analyzed for drug content to determine the possibility of excipient interference. The analysis was repeated in triplicate. Stress degradation was carried out in the same way as described for API and % degradation was calculated.

4.6.2 RESULTS AND DISCUSSION**4.6.2.1 Method development and optimization by QbD approach****4.6.2.1.1 CNX Risk Assessment**

The ishikawa diagram is shown in figure 4.33 that shows the variables that may affect the present method performance characteristics. The Cause-Effect Risk Assessment Matrix with CNX approach was utilized (table 4.27) to identify critical method variables (CMVs) based on scores. The variables with higher score (> 150) were selected for BBD optimization.

4.6.2.1.2 BBD response surface design

Based on CNX risk assessment three variables, mobile phase composition (MPC), chamber saturation time (CST) and migration distances (MD), were further subjected to BBD optimization to identify method conditions. The wavelength and ratio of GAA were fixed

at 244 and 10 μL based on preliminary trials and previous experience. Table 4.28 shows the factors with their levels and selected responses used for BBD. The matrixes of BBD with their measured responses are shown in table 4.29.

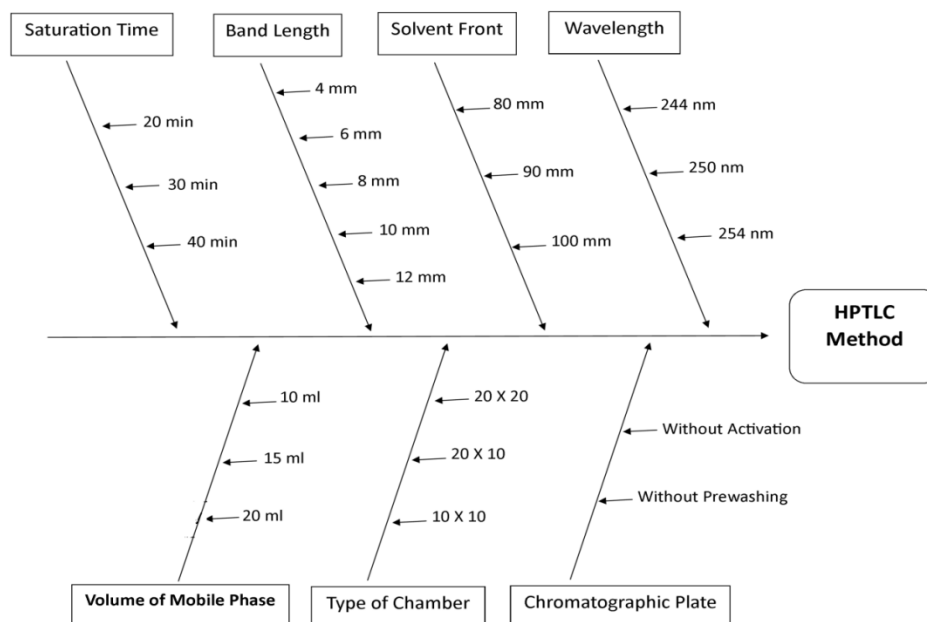


Figure 4.33: Ishikawa or cause effect diagram

Table 4.27: CNX risk assessment for chromatographic separation

Method parameter	Cause	Component attributes		Total score*	C, N, X	Strategy
		Resolution	Area			
	Attribute Score	10	10			
Silica Plate	prewashing	5	5	100	C	Washed with methanol
Silica Plate	activation	5	5	100	C	Activated at 80 ⁰ C for 30 min
Mobile Phase	Ratio of pet ether/ ethyl acetate	10	10	200	X	DoE
Mobile Phase	Ratio of GAA	10	10	200	C	Fixed to 10 μl
Chamber	Saturation	10	5	150	X	DoE

Equilibrium	time					
Silica Plate	Migration Distance	10	5	150	X	DoE
Sample Application	Band length	0	0	00	C	Applied above level of mobile phase
Mobile Phase	Volume	0	0	00	C	As per chamber size
Silica Plate	Size	5	0	50	C	Used 10X10 or 20X20
Wavelength	Wavelength	10	5	150	C	Set at 244

C= Control, N= Noise, E= Experimental, DoE= design of Experiment

*Total Score = (Risk level of First component attribute \times 10) + (Risk level of Second component attribute \times 10) where, Score: 1-Negligible risk, 5-Low risk, 10-High risk

Table 4.28: Variables and their levels for box behenken design

Factors	Coded Levels	Actual Levels
A: Chamber Saturation time (min)	-1 1	20 40
B: Migration distance (mm)	-1 1	80 100
C: Mobile phase composition (Ratio of Petroleum Ether)	-1 1	4 8
Responses	Constraints	
R1: Resolution between DP-1 and DP-2 (RS1)	$0.08 \leq R1 \leq 0.1$	
R2: Resolution between DP-2 and DP-3 (RS2)	$\leq R2 \geq 0.1$	
R3: Retardation Factor of EDA (Rf)	$R3 \geq 0.5$	

Table 4.29: Matrix of experiments for BBD and results of their measured responses

Run	Independent variable			Dependent variable		
	CST (A)	MD (B)	MPC (C)	RS1	RS2	Rf
1	30.00	90.00	6.00	0.12	0.1	0.44
2	20.00	90.00	4.00	0.006	0.12	0.9

3	40.00	90.00	4.00	0	0.12	0.92
4	30.00	90.00	6.00	0.12	0.1	0.44
5	20.00	90.00	8.00	0.12	0.012	0.34
6	20.00	100.00	6.00	0.08	0.077	0.33
7	30.00	90.00	6.00	0.12	0.1	0.44
8	40.00	80.00	6.00	0.085	0.11	0.31
9	40.00	100.00	6.00	0.11	0.12	0.53
10	30.00	80.00	4.00	0.006	0.11	0.72
11	30.00	90.00	6.00	0.12	0.1	0.44
12	30.00	90.00	6.00	0.12	0.1	0.44
13	20.00	80.00	6.00	0.11	0.07	0.4
14	40.00	90.00	8.00	0.076	0.05	0.35
15	30.00	80.00	8.00	0.12	0	0.16
16	30.00	100.00	8.00	0.13	0.05	0.46
17	30.00	100.00	4.00	0	0.1	0.97

CST= Chamber Saturation Time, MD= Migration Distance, MPC= Mobile Phase Composition, RS1= resolution between DP-1 and DP-2, RS2= resolution between DP-2 and DP-3, Rf= Retardation Factor of EDA

Statistical Analysis and Inferences

A quadratic experimental domain was adopted by the software. The ANOVA (table 4.30) results showed highly statistical significant difference between the model terms ($p < 0.05$), high R^2 value, insignificant lack of fit and lower values of PRESS. The significant factors were selected from half normal probability plot. Further, the polynomial regression equations generated for each of the studied responses RS1, RS2 and Rf were assessed for the model terms and interacting variables and were shown in figure 4.34. Coefficients for each model terms and each factor were analyzed to identify influence of each variable and

their interactions on magnitude of responses (table 4.31). Model equations for the studied response variables are given below:

$$RS1 = + 0.12 - 5.625E-003 * A + 0.054 * C - 9.500E - 003 * A * C - 0.019 * A^2 - 0.051 * C^2$$

$$RS2 = + 0.10 + 0.015 * A + 7.125E-003 * B - 0.042 * C + 9.500E-003 * A * C + 0.015 * B * C - 8.000E-003 * B^2 - 0.027 * C^2$$

$$Rf = + 0.44 + 0.087 * B - 0.28 * C - 0.049 * B^2 + 0.19 * C^2$$

Table 4.30: ANOVA results showing the effect of independent variables on the responses

Response	Model	SS	DF	MS	F-value	p-value	PRESS	r ²	Adj- r ²	Pred- r ²	AP
RS1	RQM	0.037	5	7.441E-003	48.61	< 0.0001	6.689E-003	0.9567	0.9370	0.8280	17.860
RS2	RQM	0.021	7	3.026E-003	70.59	< 0.0001	2.664E-003	0.9821	0.9682	0.8765	26.775
Rf	RQM	0.82	4	0.20	54.14	< 0.0001	0.11	0.9475	0.9300	0.8771	21.738

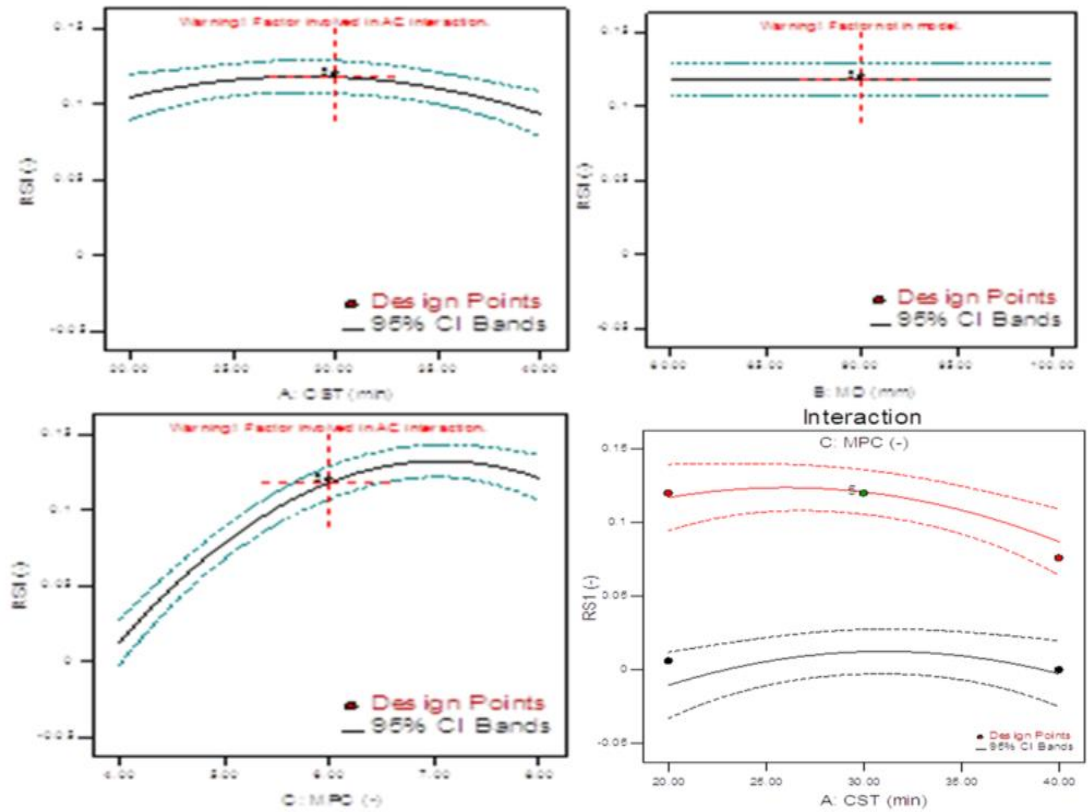
RQM=reduced quadratic model, SS= Sum of Squares, DF= Degrees of freedom, MS= Mean of square, PRESS= prediction error sum of squares, Adj- r²= Adjusted r², Pred- r²= Predicted r², AP= Adequate Precision.

Table 4.31: Regression analysis results

Factors	RS1 coefficient	p value (prob>F)	RS2 coefficient	p value (prob>F)	Rf coefficient	p value (prob>F)
Intercept	0.12	< 0.0001	0.10	< 0.0001	0.44	< 0.0001
A	-5.625E-003	0.2249	0.015	0.0001	--	--
B	--	--	7.125E-003	0.0132	0.087	0.0017
C	0.054	< 0.0001	-0.042	< 0.0001	-0.28	< 0.0001

AB	--	--	--	--	--	--
AC	-9.500E-003	0.4056	9.500E-003	0.0175	--	--
BC	--	--	0.015	0.0013	--	--
A ²	-0.019	0.0094	--	--	--	--
B ²	--	--	-8.000E-003	0.0333	-0.049	0.1298
C ²	-0.051	< 0.0001	-0.027	< 0.0001	0.19	< 0.0001

Regression coefficients are in coded values, Statistically significant (p<0.05); RS1= resolution between DP-1 and DP-2, RS2= resolution between DP-2 and DP-3, Rf= Retardation Factor of EDA



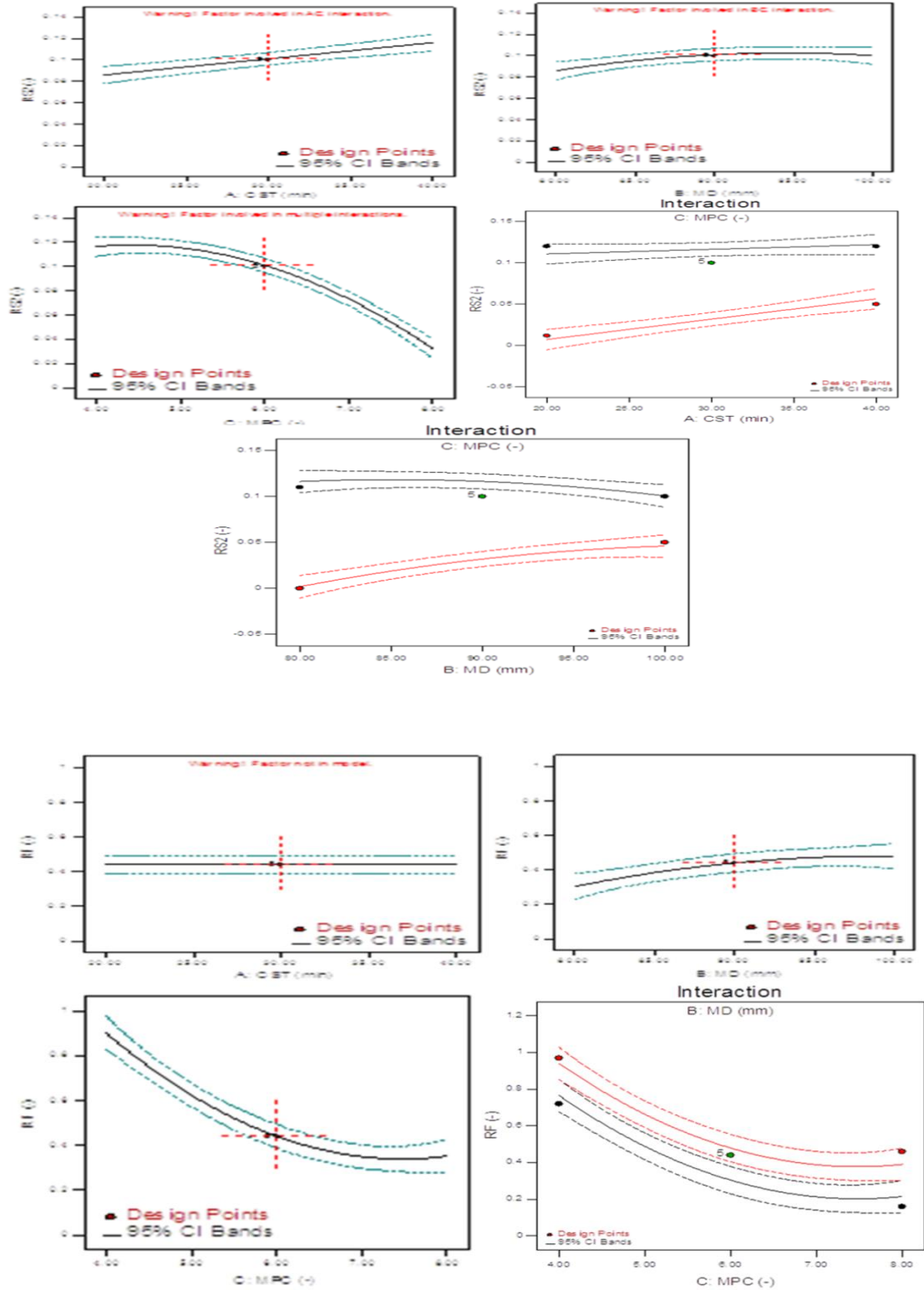


Figure 4.34: Main and interaction effect plots for RS1, RS2 and Rf

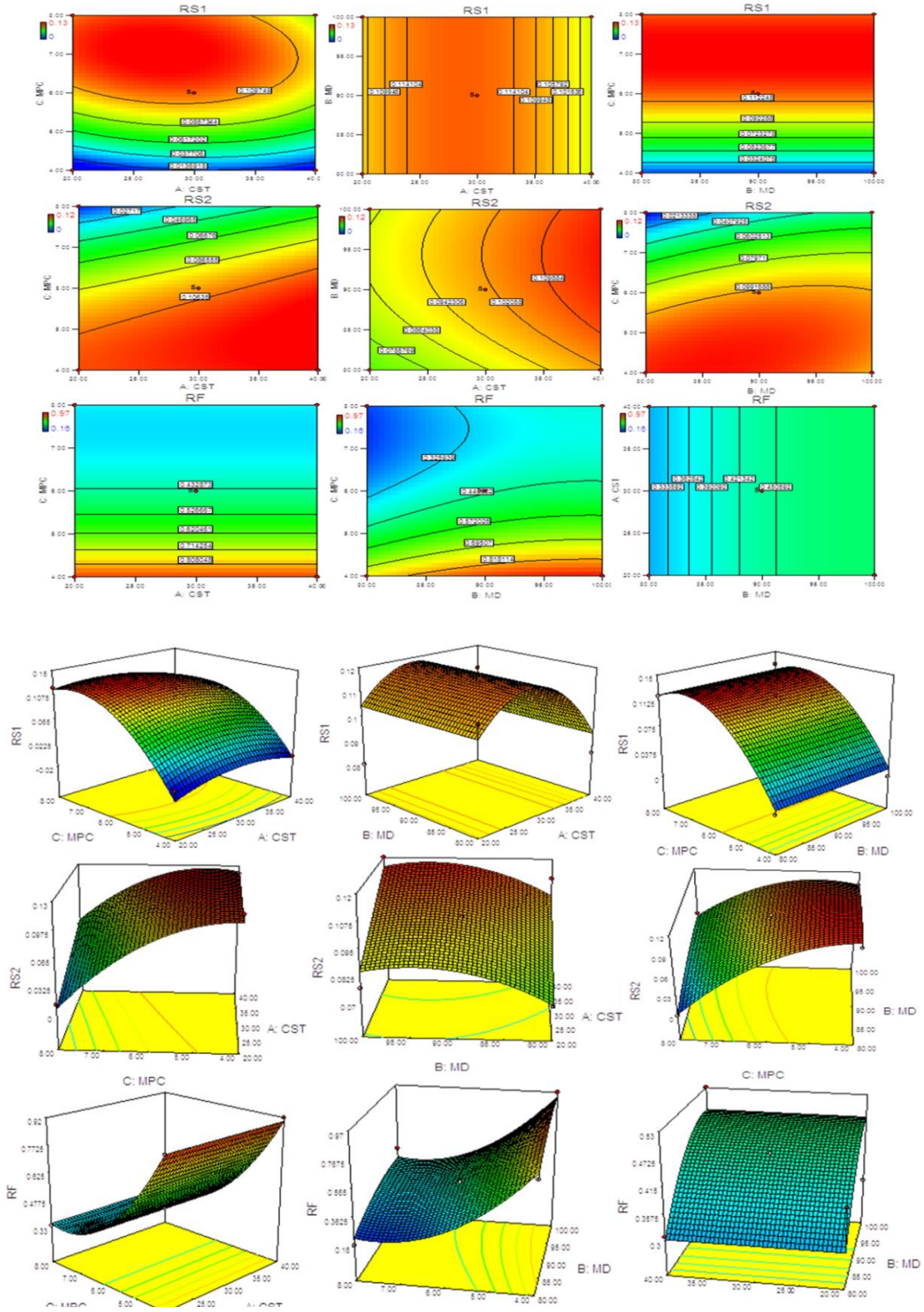


Figure 4.35: Contour and 3D Plots for RS1, RS2 and Rf (value increases from blue to red)

The magnitude of the coefficients in the equation and the p-value (< 0.001) indicated that the factors A and C significantly affected the response RS1. The significant interaction effect were A^2 and C^2 . For response RS2 all factors i. e. A, B, C affected significantly. The significant interaction effects were AC, BC, B^2 and C^2 . For response Rf, B and C significantly affected, and significant interaction effects observed was C^2 , as indicated by p-value. The model summary data indicated a reasonably good agreement between the adjusted and predicted r^2 value for all responses. The VIF value for all the models were 1, indicating coefficients are well estimated and there is no chance of multi-collinearity.

Response surface plots and corresponding contour plots were generated for each dependent variable after analysing the normal plots of the residuals. The response surface plots of the factors for responses RS1, RS2 and Rf are shown in figure 4.35. The normal probability plot of residuals for responses reveals that the residuals appear to follow almost straight line and thus existence of non-normality, outliers, skewness or unidentified variables can be ruled out (figure 4.36).

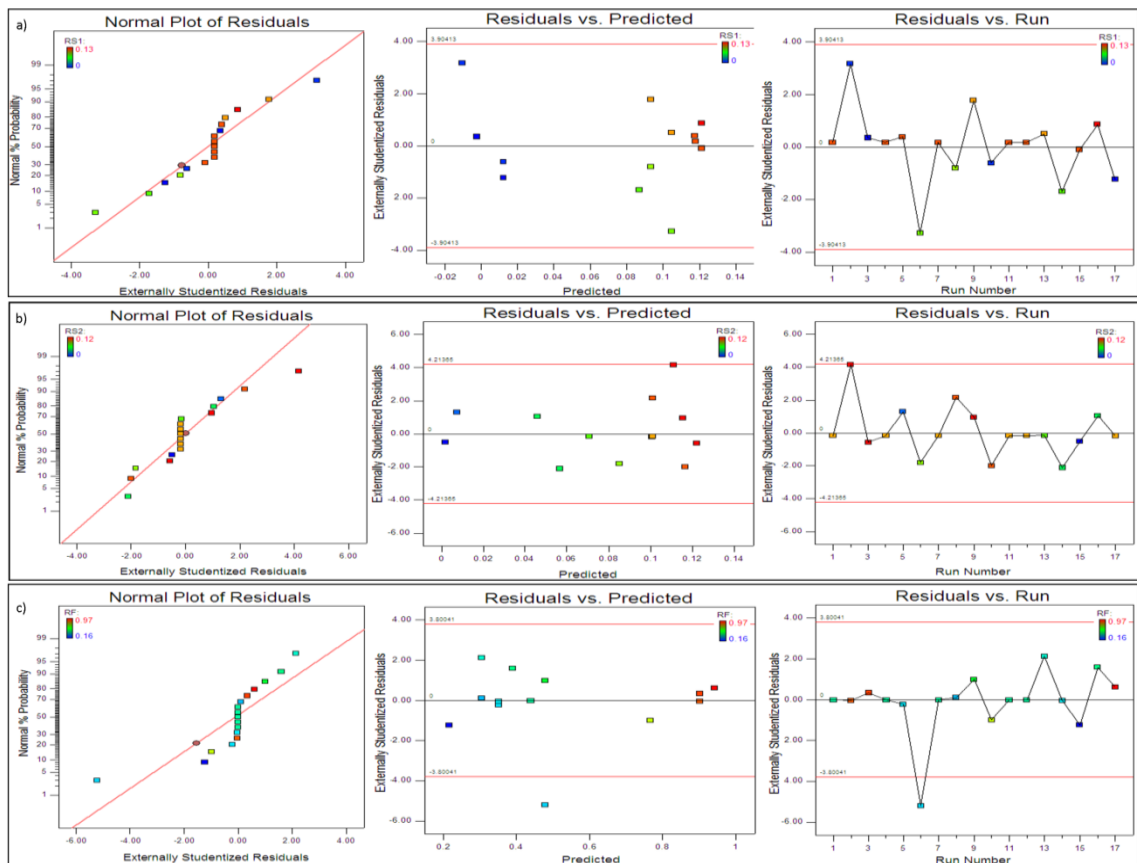


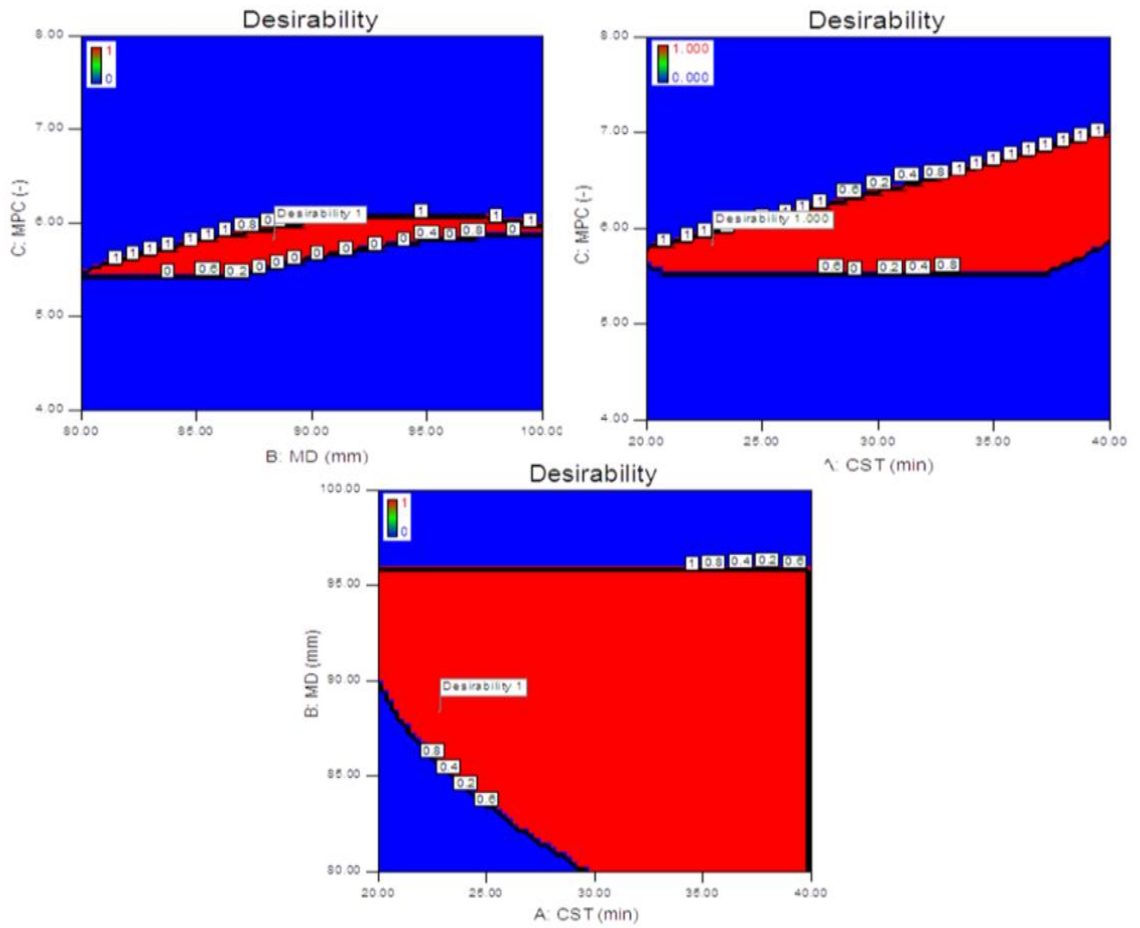
Figure 4.36: Residual plots for RS1, RS2 and Rf

The definite optimum conditions were calculated using numerical optimization. To obtain the composite desirability (di) the response criteria were set as, in range (0.08-0.1) for RS1 and RS2 and in range (0.3-0.5), for Rf. The aim of optimization was to find a good set of conditions that will meet all the set goals. Derringer's desirability was calculated and the final optimum solution (CST-22 min, MD- 89 mm, MPC-5.8) was selected. From the numerical optimization the predicted values response at 95% Confidence interval (CI) low and high, and 95% prediction interval (PI) low and high were obtained for selected optimized chromatographic condition. The experimental results along with CI and PI values for selected responses were shown in table 4.32. The experimental results represent fairly good agreement with the predicted results showing the robustness of the selected model. The desirability (contour and 3D) and overlay plots for optimized chromatographic condition are shown in figure 4.37 and 4.38.

Table 4.32: Point prediction and confirmation report for method optimization and development

Response	Predicted Mean	CI for Mean		PI for Mean		Actual Experimental Value
		95% low	95% high	95% low	95% high	
RS1	0.102703	0.090	0.11	0.073	0.13	0.1
RS2	0.0937361	0.086	0.10	0.077	0.11	0.09
Rf	0.468781	0.42	0.52	0.32	0.61	0.46

RS1= resolution between DP-1 and DP-2, RS2= resolution between DP-2 and DP-3, Rf= Retardation Factor of EDA, CI = Confidence interval, PI = prediction interval



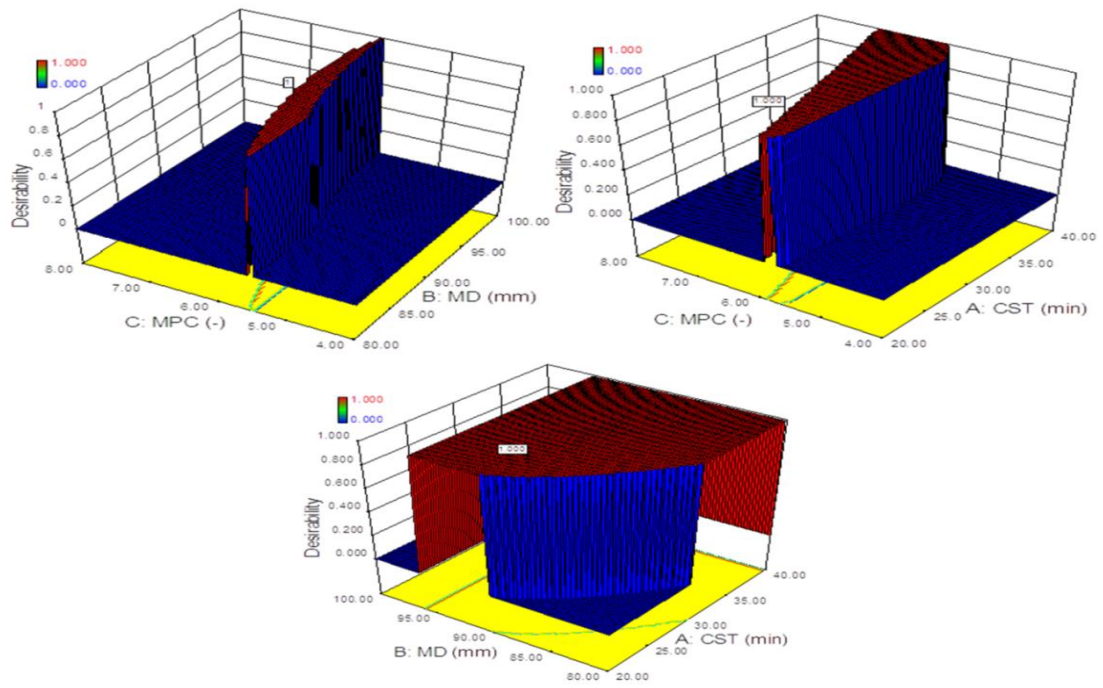


Figure 4.37: contour and 3D-Desirability plots for optimized chromatogram (desirability increases from blue to red region; blue region indicates 0 and red region indicates 1 desirability)

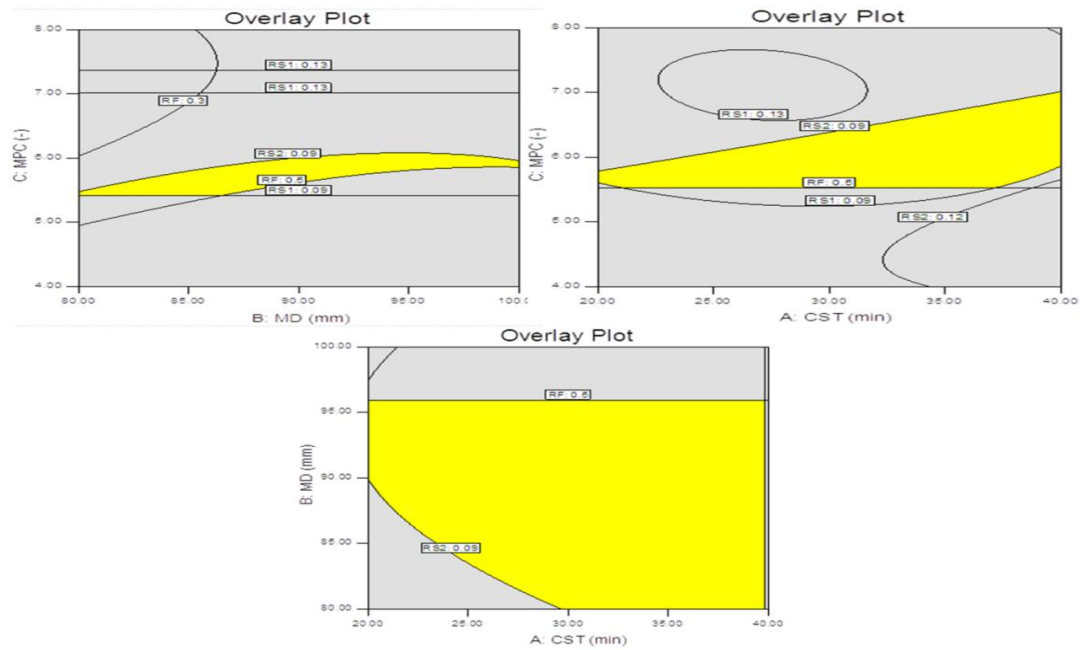


Figure 4.38: Overlay plot for optimized chromatogram (yellow region: design space, gray region: undesirable region)

Evaluation of model using cross-validation

Five experiments were conducted to evaluate the reliability of the model, by varying the variables at values other than that of the model. Table 4.33 shows the predicted, experimental values and % bias for responses. Low values of % bias indicate the validity of selected model. Percent relative error or Bias between predicted and experimental values for responses were calculated by the equation:

$$\text{Bias} = \frac{(\text{Predicted Value} - \text{Experimental Value})}{\text{Predicted value}}$$

Table 4.33: % Bias of responses for the cross validation set

Responses	Test	Factors/Levels			Predicted values	Experimental values	Bias (%)
		CST	MD	MPC			
RS1	1	29.39 (29)	83.65 (84)	5.73 (5.7)	0.10	0.11	-0.1
	2	36.49 (36)	97.94 (98)	6.77 (6.8)	0.11	0.10	0.0909
	3	22.24 (22)	84.56 (84)	5.58 (5.6)	0.09	0.089	0.0111
	4	31.35 (31)	80.76 (81)	5.81 (5.8)	0.11	0.12	-0.0909
	5	39.38 (39)	95.76 (96)	7.14 (7.1)	0.10	0.098	0.02
RS2	1	29.39 (29)	83.65 (84)	5.73 (5.7)	0.098	0.10	-0.0204
	2	36.49	97.94	6.77	0.098	0.091	0.0714

		(36)	(98)	(6.8)			
	3	22.24	84.56	5.58	0.093	0.09	0.0322
		(22)	(84)	(5.6)			
	4	31.35	80.76	5.81	0.094	0.10	-0.0638
		(31)	(81)	(5.8)			
	5	39.38	95.76	7.14	0.093	0.098	-0.0537
		(39)	(96)	(7.1)			
Rf	1	29.39	83.65	5.73	0.405	0.43	-0.0617
		(29)	(84)	(5.7)			
	2	36.49	97.94	6.77	0.400	0.38	0.05
		(36)	(98)	(6.8)			
	3	22.24	84.56	5.58	0.443	0.42	0.0519
		(22)	(84)	(5.6)			
	4	31.35	80.76	5.81	0.345	0.37	-0.0724
		(31)	(81)	(5.8)			
	5	39.38	95.76	7.14	0.378	0.40	-0.0582
		(39)	(96)	(7.1)			

Note: The values in bracket are actual values taken for experiment; CST= Chamber Saturation Time, MD= Migration Distance, MPC= Mobile Phase Composition, RS1= resolution between DP-1 and DP-2, RS2= resolution between DP-2 and DP-3, Rf= Retardation Factor of EDA

The optimized conditions obtained by using QbD was then used to obtain the final chromatograms, the chromatogram showed good resolution, selectivity, and symmetrical peaks and are shown in figure 4.39. The Rf values of EDA and DPs obtained by selected optimized chromatographic conditions are presented in table 4.34.

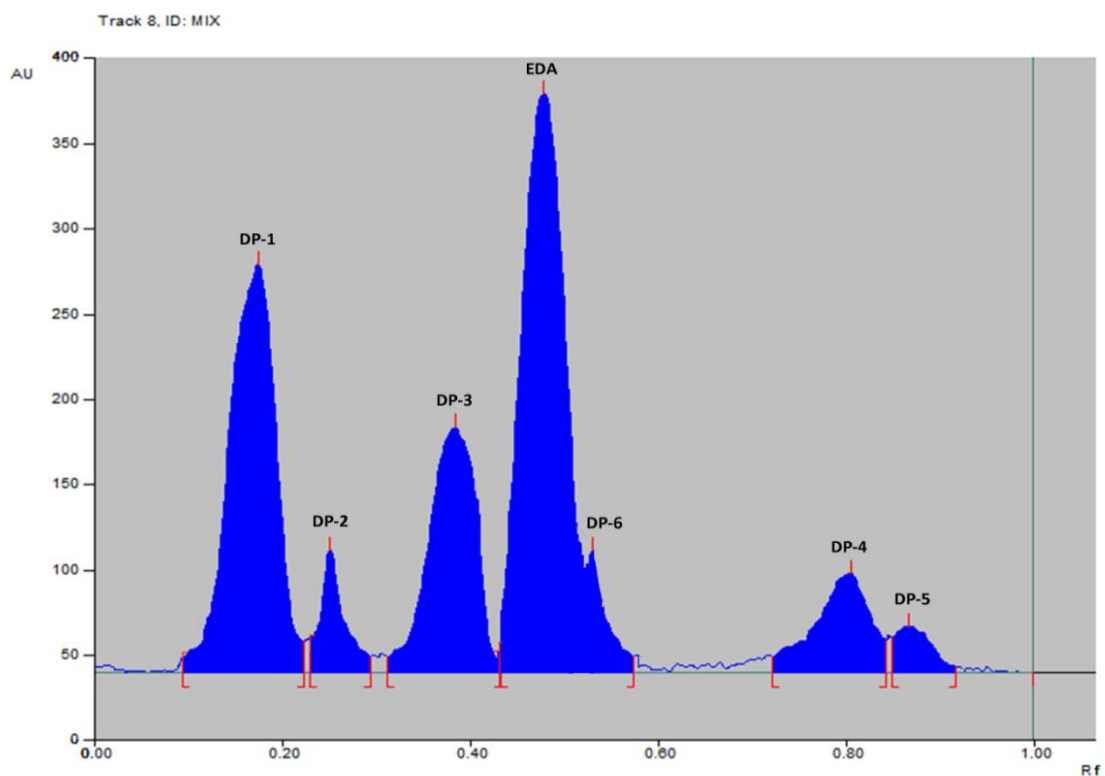


Figure 4.39: Chromatogram showing resolved peaks in mixture of degradants

Table 4.34: Rf values of EDA and DPs formed in mixture of degradants

S. No	DP formed	Rf value
1.	DP-1	0.213
2.	DP-2	0.314
3.	DP-3	0.413
4.	EDA	0.528
5.	DP-6	0.618
6.	DP-4	0.910
7.	DP-5	0.989

4.6.2.2 Method validation

4.6.2.2.1 Linearity and Range: To construct calibration curve concentrations of EDA were plotted against peak areas and regression equations were calculated. The linearity of the method was investigated in the concentration range of 2- 24 $\mu\text{g}/\text{spot}$. The correlation co-efficient was 0.9987 with regression equation $y = 1055.6x + 11280$. The overlay chromatogram and calibration curve is shown in figure 4.40. The linearity data is shown in table 4.35.

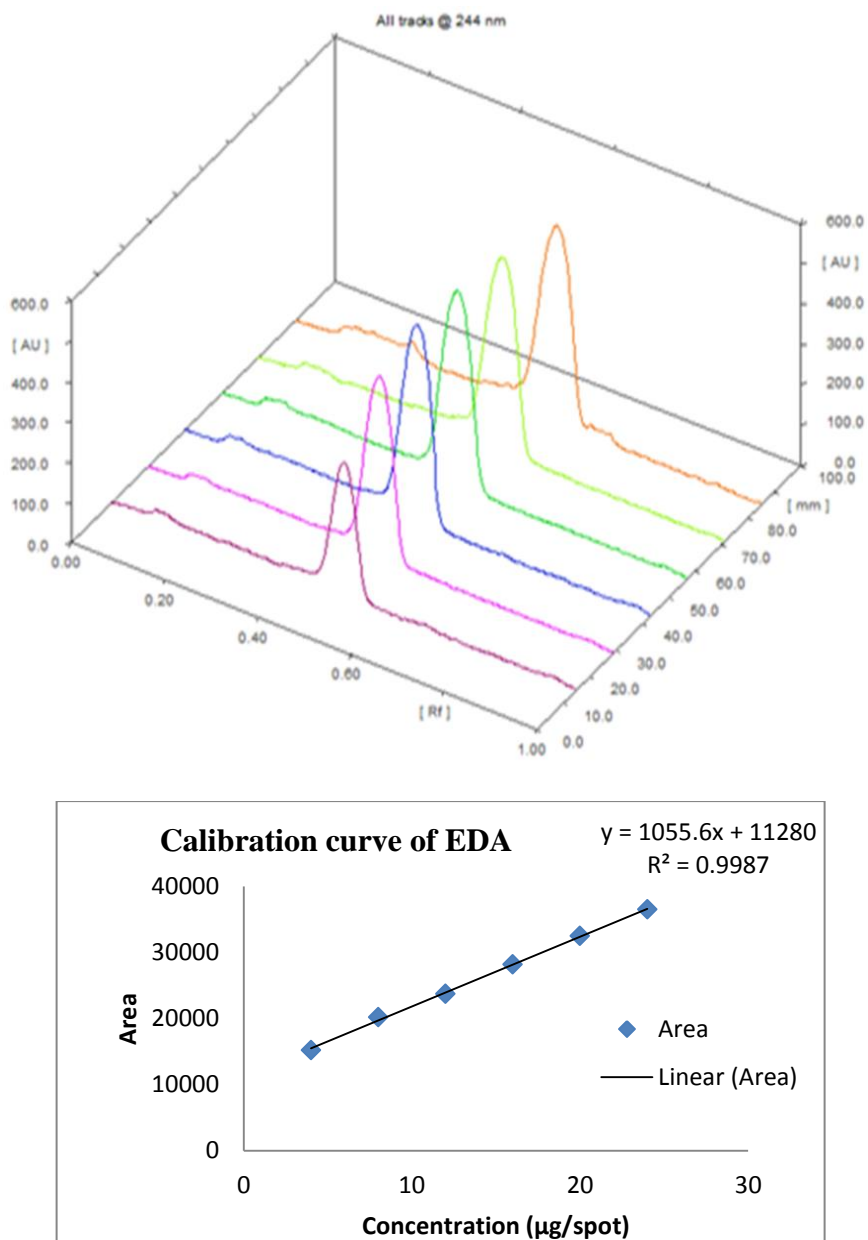


Figure 4.40: Overlay plot and calibration curve showing linearity of method

Table 4.35: Linearity data for EDA

S. No	Conc.($\mu\text{g}/\text{spot}$)	Peak area (Mean \pm %RSD)
1.	4	15145 \pm 0.0033
2.	8	20120 \pm 0.0046
3.	12	23949 \pm 0.0070
4.	16	28147 \pm 0.0014
5.	20	32554 \pm 0.0014
6.	24	36220 \pm 0.0076

4.6.2.2.2 Precision

The repeatability and reproducibility were expressed in terms of relative standard deviation (% RSD). The % RSD value less than 2 for intraday (table 4.36) and inter-day assay (table 4.37), denotes that the method is precise at the selected concentration levels.

Table 4.36: Intra-day precision for estimation of EDA

S. No ($\mu\text{g}/\text{spot}$)	Peak area			Mean	% RSD
	Set 1	Set 2	Set 3		
4	15149	15099	15280	15176	0.6159
8	20035	20113	19987	20045	0.3172
12	24089	23975	24104	24056	0.2932
16	28187	28015	28262	28154.67	0.4497
20	32573	32449	32160	32394	0.6542
24	35946	36011	35564	35840.33	0.6738
Average % RSD					0.5007

Table 4.37: Inter-day precision for estimation of EDA

S. No ($\mu\text{g}/\text{spot}$)	Peak area			Mean	% RSD
	Set 1	Set 2	Set 3		

4	15201	15192	15015	15136	0.6929
8	20197	20018	20184	20133	0.4957
12	24118	24331	23994	24147.67	0.7058
16	28243	28113	28391	28249	0.4923
20	32677	32781	32401	32619.67	0.6020
24	36006	36217	35905	36042.67	0.4416
Average % RSD					0.5717

4.6.2.2.3 Limit of detection and quantitation (LOD and LOQ)

The LOD and LOQ of present method were found to be 0.327 and 0.989 $\mu\text{g}/\text{spot}$ respectively.

4.6.2.2.4 Specificity: The chromatogram of blank solution, i. e. without EDA, did not show any spot, while the solution of EDA gives clear and compact chromatogram of drug. No other peaks were eluted, therefore the method is considered to be specific.

4.6.2.2.5 Recovery studies

Standard addition method (corresponding to 80%, 100%, and 120%) was utilized to determine recovery of EDA from formulation matrix. The values of recovery (%) and SD are shown in table 4.38.

Table 4.38: Recovery from marketed formulation

Excess drug added to analyte (%)	Theoretical Content ($\mu\text{g}/\text{spot}$)	*Amount Found ($\mu\text{g}/\text{spot}$)	Recovery (%) \pm S.D.
0	12	100.5	100.5 \pm 0.075
80	21.6	100.27	100.27 \pm 0.050
100	24	99.88	99.88 \pm 0.1123
120	26.4	99.93	99.93 \pm 0.1113

*Average of three determinants.

4.6.2.2.6 Robustness of the method

Robustness of the developed chromatographic method was determined by introducing small changes in the chamber saturation time, mobile phase composition, plate activation time, migration distance and volume of mobile phase. The effects on the results were examined that showed very slight changes in the peak areas and R_f values. The lower values of % RSD indicate the robustness of method as shown in table 4.39. Robustness of the method was carried out at concentration of 12 µg/spot.

Table 4.39: Results of robustness study

Parameter	% RSD (Area)	% RSD (R _f)
Chamber saturation time		
20 min	0.44	0.66
25 min	0.56	0.75
Mobile phase composition (Pet ether - Ethyl acetate - GAA)		
6.0:4.0:10µl, v/v/v/v	0.44	0.72
6.0:4.0:15µl, v/v/v/v	0.38	0.69
5.6:4.4:10µl, v/v/v/v	0.45	0.75
5.6:4.4:15µl, v/v/v/v	0.74	0.99
Plate activation		
15 min	0.45	0.66
25 min	0.50	0.57
Volume of mobile phase		
8 mL	0.24	0.54
12 mL	0.41	0.66
Migration distance		
88 mm	0.69	0.76
90 mm	0.51	0.77

4.6.2.3 Stress degradation study

Stress degradation was carried out with bulk drug. Six DPs were formed in mixture of degradants and are shown in figure 4.39. The drug was unstable and found to be degraded under all stress conditions. EDA was highly unstable when subjected to oxidation and almost 50% degradation was observed in 45 min. Acid and base degradation were fast as compared to neutral degradation. The degradation conditions, % of degradation along with number of DPs formed are presented in table 4.40. The chromatogram obtained from mixture of degradants are shown in figure 4.39 and chromatograms of individual stress degradation is shown in figure 4.41 .

Table 4.40: Summary of stress degradation of EDA API and formulation

Stressor type	Stressor Conc.	Time	% Deg (API)	% Deg (Formulation)	DPs formed with Rf value
Acid degradation	0.05N HCl at 70 ⁰ C	180 min	69.96	69.24	DP-1(0.20), DP-3(0.42), DP-4(0.89), DP-5(0.97)
Base degradation	0.2N NaOH at 70 ⁰ C	180 min	62.68	62.09	DP-1(0.21), DP-2(0.44), DP-4(0.91)
Neutral degradation	100 ⁰ C	7 hr	45.45	44.91	DP-1(0.19), DP-2(0.29), DP-4(0.88)
Oxidative degradation	6% H ₂ O ₂ at RT	45 min	51.97	50.80	DP-1(0.19), DP-3(0.41), DP-4(0.89)
Photolytic degradation	5382 LUX and 144UW/cm ²	21 days	40.54	40.23	DP-1(0.19), DP-3(0.42)
Dry Heat induced degradation	80° C	21 days	67.12	20.11 (for 72 Hr)	DP-1(0.19), DP-3(0.42), DP-4(0.88), DP-5(0.94)
Thermal-Humidity induced degradation	40 ° C 70 ± 5% RH	21 days	35.99	35.04	DP-1(0.18), DP-3(0.42), DP-4(0.88), DP-5(0.93)

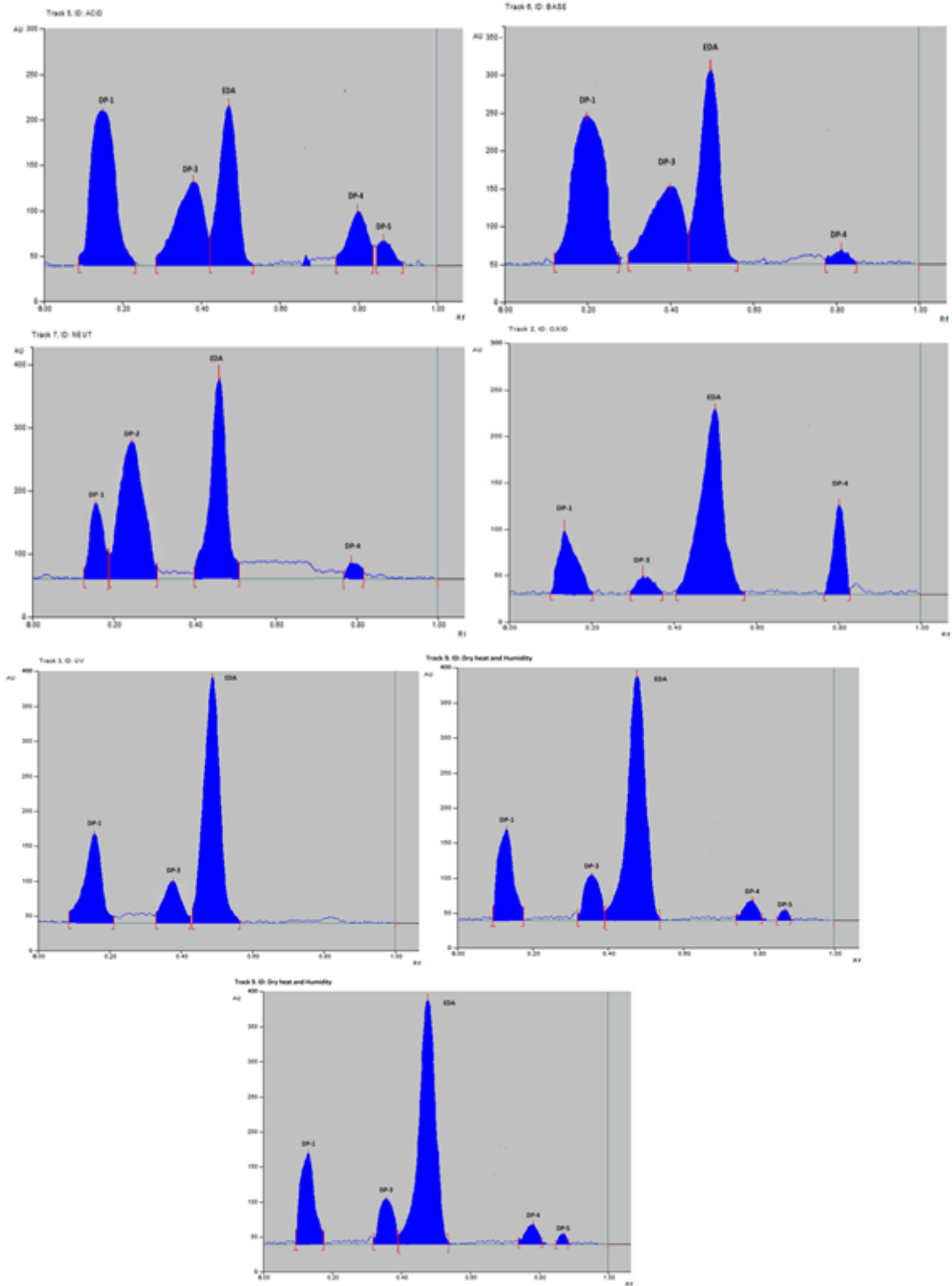


Figure 4.41: Chromatograms of a) Acid degradation, b) Base degradation, c) Neutral degradation, d) Oxidative degradation e) Photolytic degradation, f) Dry heat induced degradation and d) Thermal-humidity induced degradation

4.6.2.4 Application of developed HPTLC method

The proposed chromatographic method was used to estimate the content of EDA in commercially available formulation (Aravon I.V. infusion, 1.5 mg/ml, manufactured by Sun Pharmaceuticals Ind. Ltd, Halol, Gujarat, India). The % assay of EDA was found to be 99.88 ± 0.1553 (% \pm SD). The method was selective for analysis of EDA, as no interference from the excipients was shown in chromatogram.

The proposed chromatographic method was also utilized to analyze stress degraded samples of EDA injection. Stress degradation were carried out under same condition as specified for bulk drug and analyzed in the same way. The degradation products were well resolved with distinct R_f value. Minor variation was observed in % degradation of bulk drug and formulation (table 4.40).

4.7 SECTION-D

DEGRADATION KINETIC STUDY OF EDARAVONE BY HPTLC METHOD

4.7.1 EXPERIMENTAL

4.7.1.1 Chemicals and Reagents

The chemicals and reagents utilized in this section for degradation kinetic study were same as described in section 4.6.1.1.

4.7.1.2 Equipments and chromatographic conditions

The equipments and chromatographic conditions used in this section for degradation kinetic study were same as described in section 4.6.1.2.

4.7.1.3 Preparation of standard, stock and sample solutions

Standard and stock solutions were prepared in same solvent with same dilutions as described in section 4.6.1.3. For degradation kinetic study EDA solutions were prepared at a concentration of 1mg/ml with variable strength of acid (HCl), Base (NaOH) and H₂O₂ for hydrolysis and oxidative degradation and were stressed at variable temperature for variable time for kinetic study. For neutral degradation samples were prepared in double distilled water with the aid of sonication as EDA was partially soluble in water and soluble in boiling water. For photolytic degradation solution was prepared in ACN. Aliquots of 0.5 mL of the sample solutions were withdrawn at different time intervals, placed into a 10 mL

volumetric flask. After neutralization with equivalent strength of NaOH/HCl the volume was made up to the mark with mobile phase. The solutions were filtered through 0.2 mm membrane filter before application. The solutions (concentration $C_0 = 12 \mu\text{g/spot}$) were applied, developed and scanned by chromatographic conditions of the HPTLC method described section 4.6.1.2.

The concentrations of drug remaining were calculated from the formula:

$$\% \text{ Deg} = \frac{\left[\begin{array}{l} \text{(Initial area of untreated stock solution} \\ \text{- reduced area of treated stock solution)} \end{array} \right]}{\text{Actual initial area of untreated stock solution}} \times 100$$

The degradation rate kinetics was determined using linear and nonlinear regression analysis. The rate constant (K_{obs}), half-life ($t_{1/2}$) were also calculated from the slope of lines at each temperature for acid, base, neutral and oxidative degradation processes. In the present study linear and nonlinear fit function from Graphpad Prism Software was used.

4.7.2 RESULTS AND DISCUSSION

The degradation kinetic of EDA was investigated in acid, base, neutral, oxidative and photolytic degradation. Each experiment was done in triplicate at each temperature and time interval. The mean concentration of EDA was calculated for each experiment using $12 \mu\text{g/spot}$. The linear regression analysis was performed for neutral, oxidative and photolytic degradation, while acid and base degradation followed nonlinear regression analysis at the selected temperature and concentration.

4.7.2.1 Kinetics of acid and base degradation

The % degradation of EDA during acid and base hydrolysis was determined by HPTLC method described in section 4.6.1.2. As indicated by reaction constants (table 4.41 and 4.43) non linear regression fits better for acid and base degradation. For both acid and base degradation nonlinear regression analyses was performed for pseudo first order reaction kinetics at selected temperature and concentration and are shown in figure 4.42 and 4.44 respectively. Both acid and base degradation were assumed to follow pseudo first order degradation rate kinetic since the r^2 value is highest for second order process and the

concentration of the stressor was much higher and constant during whole degradation process.

The estimates of K_{obs} and $t_{1/2}$ can be obtained directly by plotting logarithm of observed % Deg versus time data in nonlinear regression analysis using Graphpad Prism Software. The calculated $t_{1/2}$ and E_a for acid and base degradation are presented in table 4.42 and 4.44 and arrhenius plots are shown in figure 4.43 and 4.45 respectively. The magnitude of rate constants indicates that rate of degradation is influenced not only by temperature but also by hydrogen and hydroxide ion concentration.

Table 4.41: Linear and non linear regression equation and r^2 value for zero, first and second order reaction for acid degradation

S. No	Conc. (HCl)	Te mp.	r^2 value for LRA			r^2 value for NLRA		
			Zero Order	First Order	Second Order	Zero Order	First Order	Second Order
1	0.05 N	60	0.8274	0.7765	0.687	0.9567	0.9866	0.9977
		70	0.9309	0.8714	0.7579	0.9735	0.9933	0.9989
		80	0.7758	0.7441	0.6712	0.938	0.9793	0.9958
2	0.1 N	60	0.6364	0.6509	0.6147	0.8803	0.9565	0.9892
		70	0.7245	0.7113	0.6518	0.9152	0.9707	0.9936
		80	0.5053	0.5244	0.5209	0.9087	0.9581	0.9844
3	0.2 N	60	0.6675	0.6745	0.6404	0.8933	0.9569	0.9873
		70	0.447	0.4841	0.4949	0.881	0.9448	0.9793
		80	0.3172	0.38	0.4217	0.8029	0.8941	0.9519

LRA- linear regression analysis, NLRA- nonlinear regression analysis

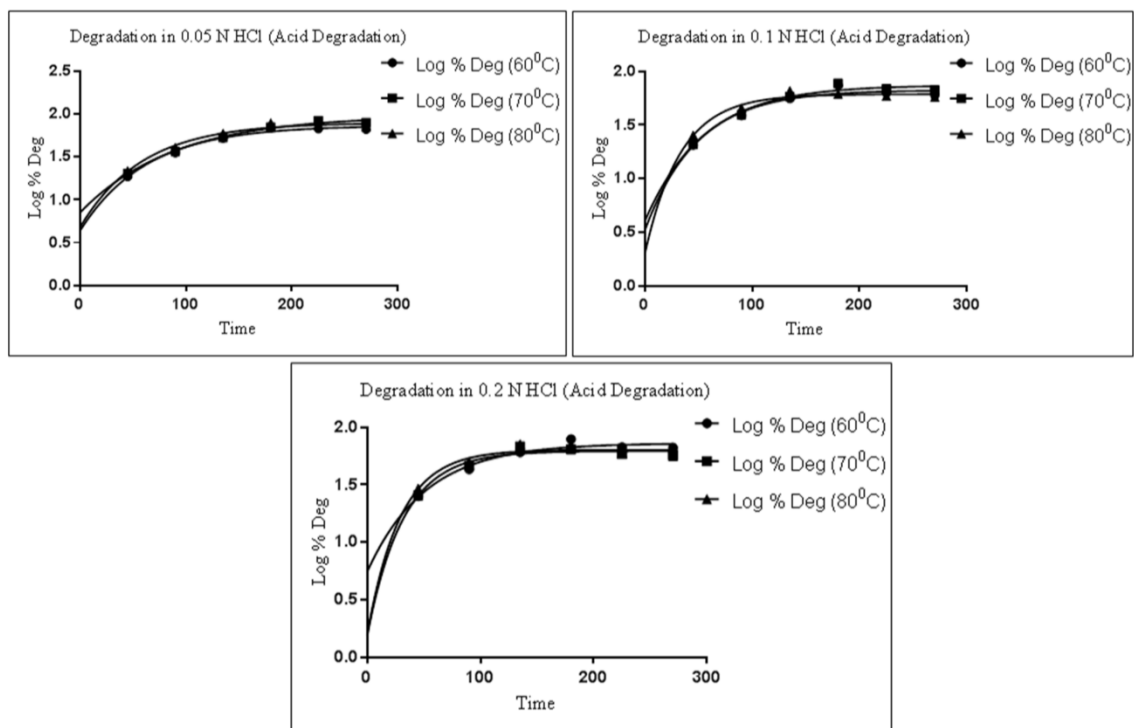


Figure 4.42: Non linear pseudo first order reaction kinetic plots for acid degradation

Table 4.42: Half- life ($t_{1/2}$) and activation energy (E_a) for pseudo first order reaction kinetic of acid degradation

S. No	Conc. (HCl)	Regression Equation	Temp.	$t_{1/2}$ (Hr.)	E_a (kJ/mol)
1	0.05 N	-145*X - 1.414	60	43.49	-1.2056
			70	61.05	
			80	40.72	
2	0.1 N	-955.9*X + 1.138	60	33.76	-7.9478
			70	38.05	
			80	23.05	
3	0.2 N	-1488*X + 2.78	60	35.79	-12.3719
			70	22.01	
			80	20.09	

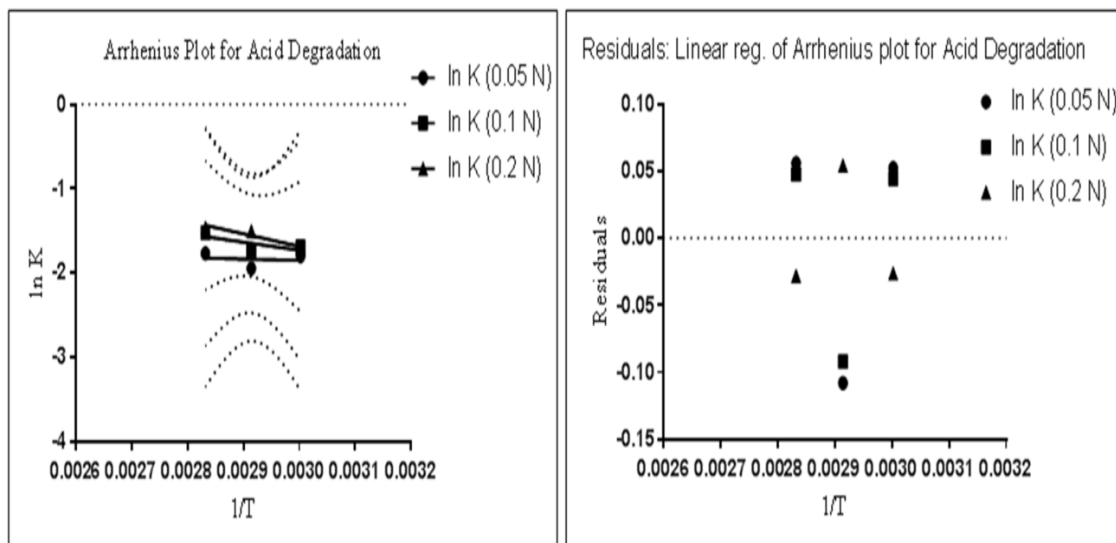


Figure 4.43: Arrhenius plot and residual plot for acid degradation

Table 4.43: Linear and non linear regression equation and r^2 value for zero, first and second order reaction for base degradation

S. No	Conc. (NaOH)	Temp.	r^2 value for LRA			r^2 value for NLRA		
			Zero Order	First Order	Second Order	Zero Order	First Order	Second Order
1	0.2 N	60	0.8781	0.8688	0.858	0.978	0.9815	0.9847
		70	0.8317	0.8242	0.7937	0.9279	0.9604	0.9818
		80	0.6169	0.6352	0.6346	0.8811	0.9308	0.964
2	0.5 N	60	0.7241	0.7206	0.7165	0.9584	0.9635	0.9682
		70	0.7845	0.7761	0.7475	0.9293	0.9618	0.9825
		80	0.5707	0.5926	0.5962	0.8758	0.9277	0.9623
3	0.8 N	60	0.6664	0.6675	0.6679	0.9292	0.9368	0.9439
		70	0.7121	0.714	0.6952	0.9118	0.9523	0.9778
		80	0.4188	0.4636	0.492	0.798	0.8743	0.9289

LRA- linear regression analysis, NLRA- nonlinear regression analysis

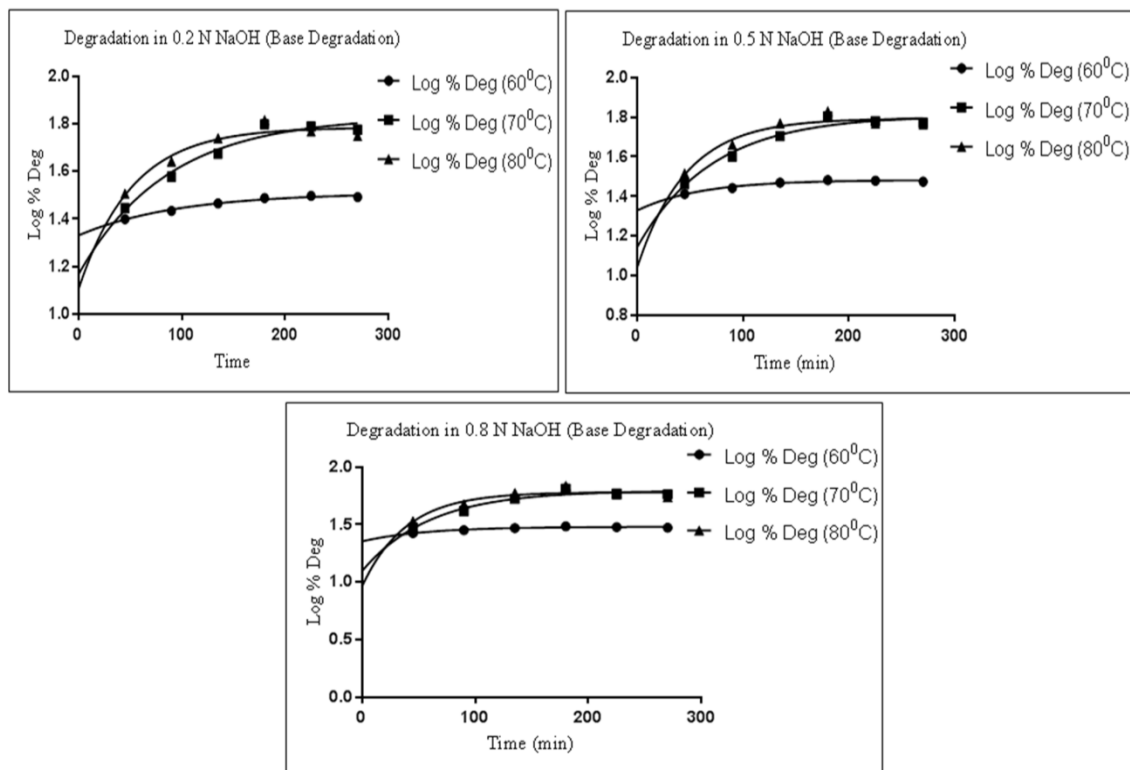


Figure 4.44: Non linear pseudo first order reaction kinetic plots for base degradation

Table 4.44: Half- life ($t_{1/2}$) and activation energy (E_a) for pseudo first order reaction kinetic of base degradation

S. No	Conc. (HCl)	Regression Equation	Temp.	$t_{1/2}$ (Hr.)	E_a (kJ/mol)
1	0.2 N	$-1576 * X + 2.72$	60	66.44	-13.1036
			70	59.76	
			80	35.67	
2	0.5 N	$-635 * X + 0.09073$	60	41.07	-5.2796
			70	48.92	
			80	31.79	
3	0.8 N	$-905.9 * X + 0.94$	60	38.39	-7.5320
			70	41.26	
			80	26.77	

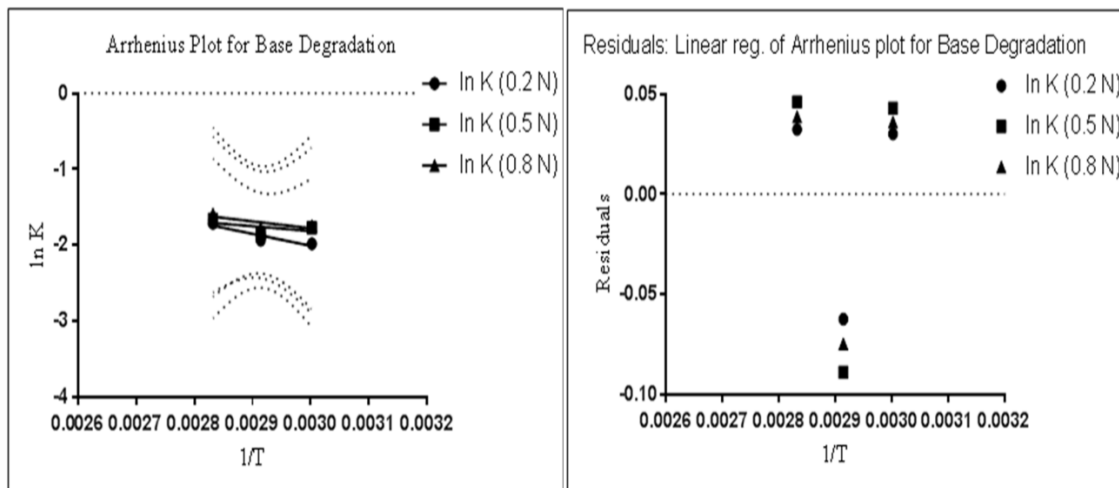


Figure 4.45: Arrhenius plot and residual plot for base degradation

4.7.2.2 Kinetics of neutral, oxidative and photolytic degradation

The disappearance of EDA during neutral, oxidative and photolytic degradation followed apparent zero order reaction kinetic at selected concentration and temperature, as r^2 values were highest for zero order reaction kinetics. The zero order reaction kinetic plots for neutral, oxidative and photolytic degradation are shown in figure 4.46, 4.48 and 4.49 respectively. After studying different parameters that affected the rate of degradation it can be concluded that the rate of degradation is directly proportional to temperature in case of neutral degradation. Rate of degradation increases with the increase in concentration of stressor and time of degradation in oxidative degradation and rate of degradation increases with the increase in time in photolytic degradation. The regression equation and r^2 value for zero, first and second order reaction for these degradation conditions are presented in table 4.45, 4.47 and 4.48 for neutral, oxidative and photolytic degradation respectively. The resulting K_{obs} values were plotted against temperature (in kelvin) to obtain arrhenius plot for neutral degradation. The zero order reaction kinetic plots and arrhenius plot along with residual plots and calculated $t_{1/2}$ and E_a for neutral degradation are presented in figure 4.47 and table 4.46 respectively.

Table 4.45: Regression equation and r^2 value for zero, first and second order reaction for neutral degradation calculated by linear regression analysis

S. No	Te mp.	r^2 Value			Regression Equation		
		Zero Order	First Order	Second Order	Zero Order	First Order	Second Order
1	80	0.9957	0.9948	0.9641	$3.966 * X + 14.26$	$0.05888 * X + 1.228$	$-0.004845 * X + 0.0551$
2	90	0.9931	0.9897	0.951	$4.062 * X + 14.77$	$0.0587 * X + 1.241$	$-0.004711 * X + 0.05354$
3	100	0.995	0.9895	0.9542	$3.942 * X + 17$	$0.05373 * X + 1.287$	$-0.004038 * X + 0.04861$

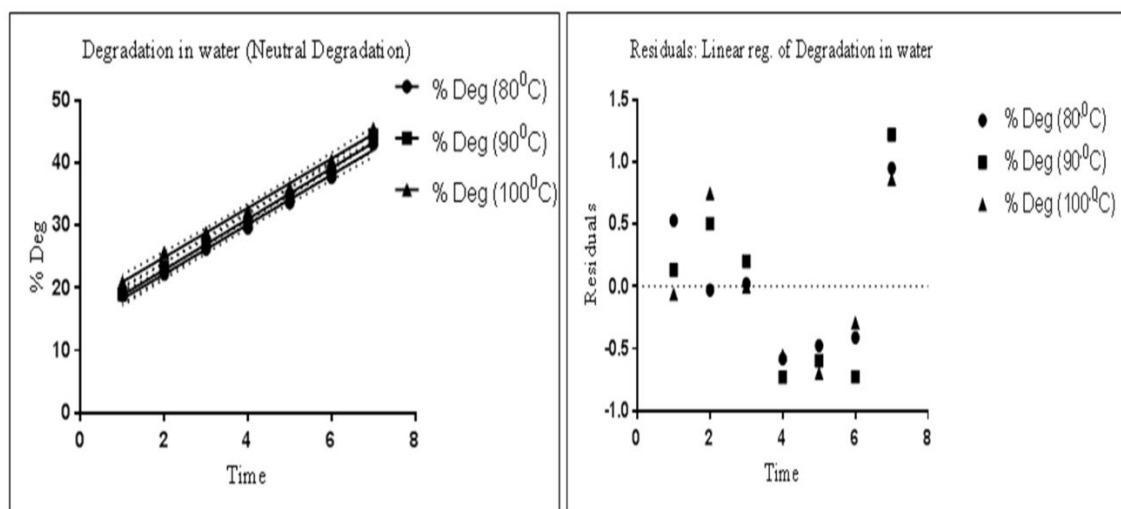


Figure 4.46: Zero order reaction kinetic and residual plots for neutral degradation

Table 4.46: Half- life ($t_{1/2}$) and activation energy (E_a) for zero order reaction kinetic of neutral degradation

S. No	Stressor	Temp.	$t_{1/2}$ (Hr.)	E_a (kJ/mol)
1	Neutral Degradation	80	203.0594	0.379722
		90	198.2802	
		100	197.0606	

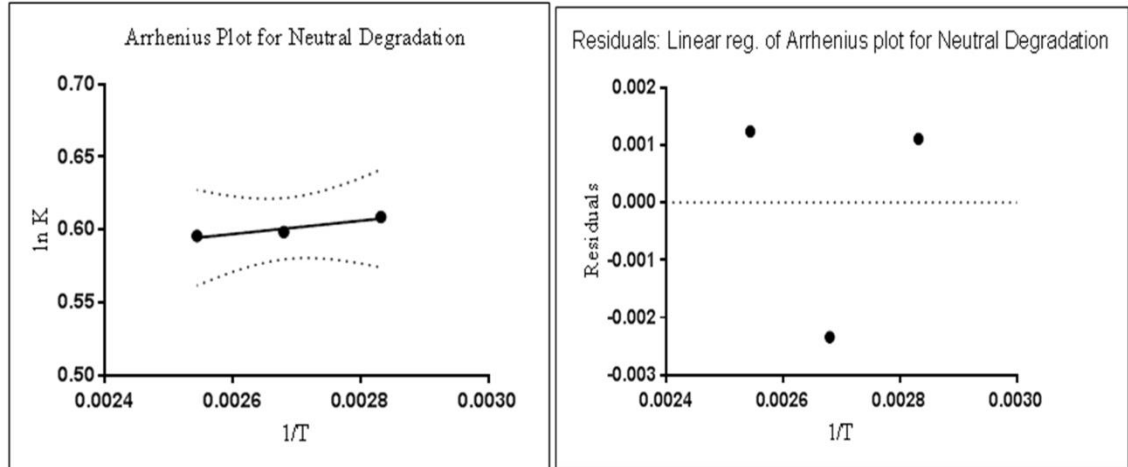


Figure 4.47: Arrhenius plot and residual plot for neutral degradation

Table 4.47: Regression equation and r^2 value for zero, first and second order reaction for oxidative degradation

S. No	Te mp.	r^2 Value			Regression Equation		
		Zero Order	First Order	Second Order	Zero Order	First Order	Second Order
1	6 %	0.9928	0.9829	0.9438	$0.7504 * X + 20.21$	$0.005791 * X + 1.447$	$-0.0002525 * X + 0.03212$
2	3 %	0.9933	0.9889	0.935	$0.7915 * X + 11.72$	$0.006903 * X + 1.329$	$-0.0003505 * X + 0.04053$

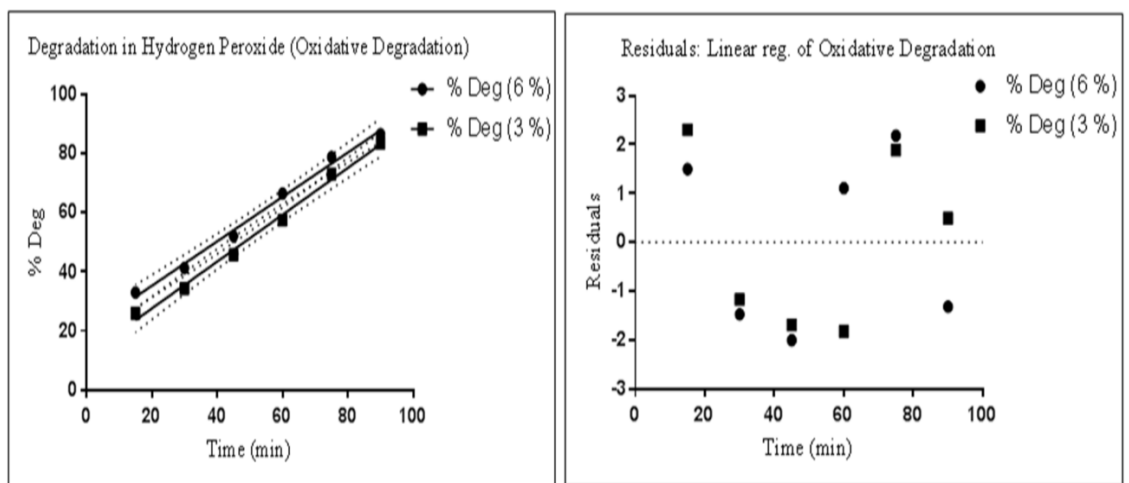


Figure 4.48: Zero order reaction kinetic and residual plots for oxidative degradation

Table 4.48: Regression equation and r^2 value for zero, first and second order reaction for photolytic degradation

S. No	r^2 value			Regression Equation		
	Zero Order	First Order	Second Order	Zero Order	First Order	Second Order
1	0.9809	0.9065	0.7675	$2.989 * X - 6.279$	$0.04659 * X + 0.8422$	$-0.004678 * X + 0.1038$

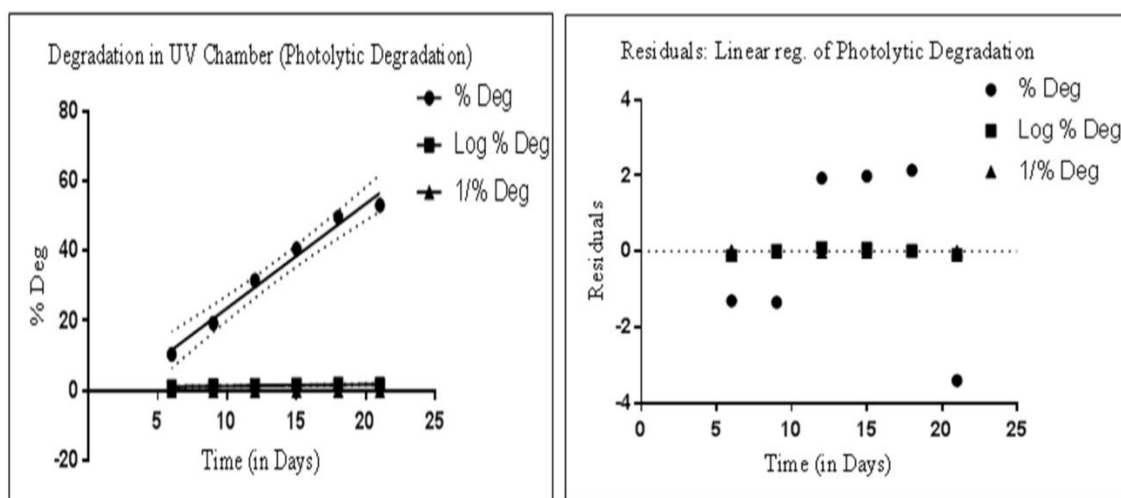


Figure 4.49: Zero order reaction kinetic and residual plots for photolytic degradation

4.8 SECTION-E

ISOLATION AND CHARACTERIZATION OF MAJOR DEGRADATION PRODUCTS OF EDARAVONE

4.8.1 EXPERIMENTAL

4.8.1.1 Chemicals and reagents

The EDA bulk drug was purchased from Sigma Aldrich Co. St. Louis USA. Analytical grade petroleum ether (pet. ether), ethyl acetate, methanol (MeOH), acetone and dichloromethane (DCM) were procured from Spectrochem Pvt. Ltd., Mumbai India. Silica

gel-G for TLC and column chromatography (60-120 mesh, 0.12-0.25 mm) was procured from Spectrochem Pvt. Ltd., Mumbai, India. Other chemicals and reagents utilized in present section were same as described in section 4.4.1.1 and 4.6.1.1.

4.8.1.2 Equipments and Chromatographic Conditions

Column chromatography was performed in glass column of 45cm X 3cm (length X diameter). The preparative TLC was performed on 20 cm X 20 cm (length X diameter) glass plate and 20 cm X 20 cm (length X diameter) twin trough glass chamber. Other equipment's and chromatographic conditions used to check % degradation and purity of isolated degradation products were same as described in section 4.4.1.2.

4.8.1.3 Preparation of Stock, Sample and Buffer solutions

Stock, sample and buffer solutions were prepared in same way with similar dilutions as described in section 4.4.1.3.

4.8.1.4 Isolation and Characterization of Degradation Products (DPs)

EDA was unstable when exposed to acid, base, neutral, oxidative, photolytic, dry heat induced and thermal-humidity induced degradation conditions. During degradation kinetic study it was observed that in acid and base degradation the peak area of EDA increases after some time and temperature of degradation and followed non-linear kinetic, hence was not chosen for isolation. During dry heat degradation it was observed that peak area of DP-7 and DP-4 increases with increase in time of degradation, hence was chosen for isolation. LC-MS/MS spectral study was conducted to determine the mass of the unknown degradants and literature survey revealed that no structural information of these unknown degradants with mass numbers (521, and 332) is available. Hence two major DPs (DP-4 and DP-7) were selected for isolation and characterization from dry heat induced degradation condition. DP-7 was formed during acid, base, neutral, photolytic and dry heat induced degradation and was formed in higher percentage as compared to other DPs (based on HPLC peak area). DP-4 was also formed under dry heat induced degradation and was second major DP formed after DP-7, hence was isolated.

The stress condition producing optimum yields of DPs were chosen based on the degradation profile and kinetic studies using same chromatographic conditions and column. The % degradation and purity of isolated DPs were analyzed by HPLC.

4.8.1.4.1 DP-7 (*Rt*-16.36)

Degradant enrichment

The appropriate quantities of the DPs were prepared for structure elucidation. For enrichment of DP-7 about 1 g of EDA bulk drug was spread on petri dish in 1mm thickness and kept in hot air oven at controlled temperature of 80⁰C for 30 days. About 800 mg of drug remains after 30 days. The % degradation was checked by HPLC and given in table 4.49.

Isolation and purification

DP-7 was isolated by column chromatography and was further purified by recrystallization using hot pet. ether.

Column chromatography

The sample containing approximately 50.5 % (table 4.49) of DP-7 was subjected to silica gel column chromatography. The HPLC chromatogram is shown in figure 4.50. Isolation was carried out using wet column chromatography. To prepare the wet column 500 g of silica gel was mixed with pet. ether to form homogenous slurry with stirring to remove air bubbles and then poured into a glass column.

The sample for loading, on the column was prepared by dissolving 0.5 g of the enriched degradant in 50 mL acetone containing 0.001% methanol. 1.5 g of silica was added to the solution, mixed thoroughly by stirring and the excess of solvent was removed by rotary evaporator under reduced pressure to ensure uniform distribution of sample over silica. The silica became free flowing which was then carefully loaded on to the wet column layer bed. The top of the column was covered with cotton. 0.5 g of sample was fractioned at a time.

For elution gradient mixture of pet ether and ethyl acetate was used as mobile phase. The column was first eluted with pet ether alone and then the polarity was increased by 5 % increments of ethyl acetate till 30%. Each time fractions of 50 mL were collected and concentrated by rotary evaporator. For each eluent system, approximately one liter volumes were used and were monitored by TLC. The positions of different spots were observed under UV-light. TLC showing similar fractions with same R_f value were mixed and concentrated to dryness using a rotary evaporator.

DP-7 elutes as first component, the purity of DP-7 was checked on TLC using pet. ether and ethyl acetate (80:20 v/v) as mobile phase. The fractions were further monitored by HPLC.

Recrystallization

The crude residue obtained after column chromatography were further purified by recrystallization using hot pet ether.

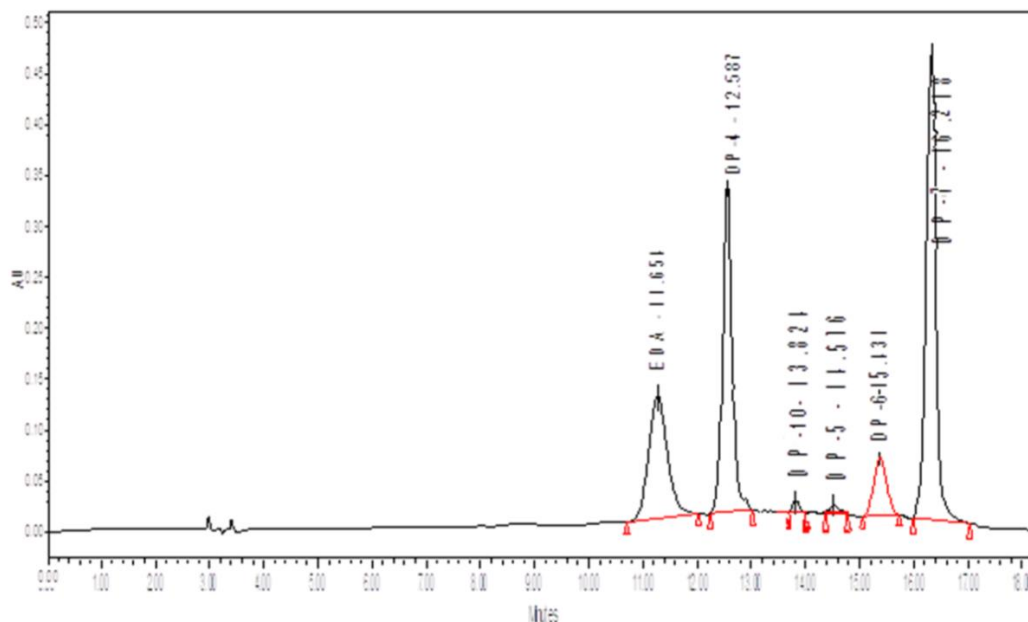


Figure 4.50: HPLC chromatogram of enriched degradant

Table 4.49: Percentage of degradants in sample after degradant enrichment

S. No	Name	Retention Time	% Area
1	EDA	11.65	20.45
2	DP-4	12.58	16.43
3	DP-10	13.82	1.56
4	DP-5	14.57	1.04
5	DP-6	15.43	10.14
6	DP-7	16.27	50.47

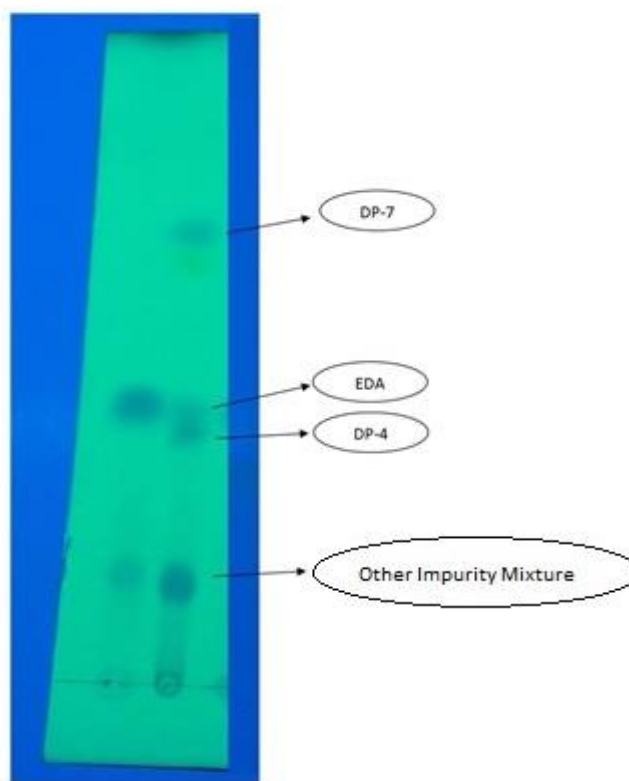


Figure 51: TLC showing positions of EDA, DP-7 and DP-4

4.8.1.4.2 DP-4 (*R_t* 12.5)

Degradant enrichment

Same sample as described above for DP-7 that contains approximately 16.5 % of DP-4 was used for isolation of DP-4.

Isolation and purification

Column chromatography

Same sample and column was used for isolation of DP-4 as described above. DP-4 elutes as 4th component, the elution of which was confirmed and monitored by TLC. DP-4 elutes along with other component so was found as mixture and had approximately 50% purity. The fractions showing similar TLC profile with similar *R_f* values were collected and concentrated to dryness. The crude residue obtained during isolation of DP-7 was further purified by column chromatography.

For loading the crude residue obtained above was processed in similar way as described above in section 4.8.1.4.1. The mobile phase for elution was same but the gradient was modified and polarity was increased more gradually as mixture was obtained. The column was first eluted with pet ether: ethyl acetate (90:10). The polarity was then gradually increased by 2 % increments of ethyl acetate. The purity of DP-4 was checked by TLC and further confirmed by HPLC, which showed 90 % HPLC purity.

Preparative TLC

DP-4 was further purified by preparative TLC. The preparative plates were prepared in same way as described in section 3.6.1.4.1. 20 mg of sample was dissolved in methanol and applied over preparative TLC plates. The plates were developed in pre-saturated 20 X 20 cm twin trough glass chamber using mobile phase pet. Ether, ethyl acetate in the ratio of 85:15. DP-4 was observed as dark purple band. The purple bands were scraped, mixed and extracted with ethyl acetate (3-4 times). The organic layers were combined and was evaporated to dryness over rotary evaporator under reduced pressure.

Recrystallization

The residue obtained after preparative TLC was recrystallized by dichloromethane.

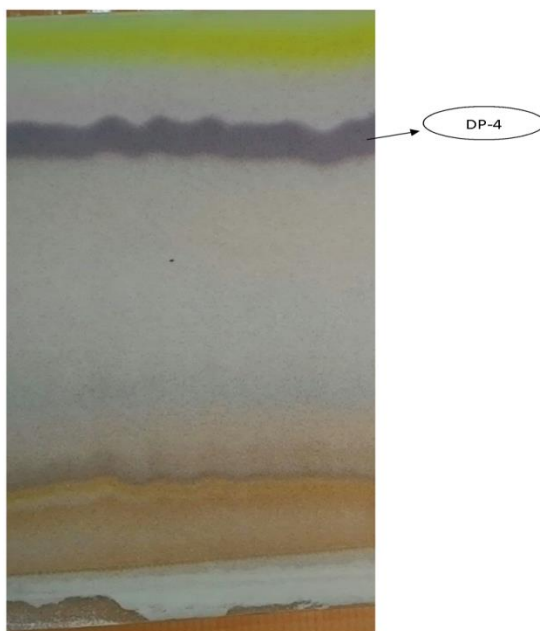


Figure 4.52: TLC showing position of DP-4

4.8.1.5 Structure elucidation of isolated DPs

The structures of DP-7 and DP-4 were proposed using spectroscopic methods FT-IR, LC-MS/MS and NMR.

4.8.2 RESULTS AND DISCUSSION

4.8.2.1 Isolation and Purification of DPs

4.8.2.1 DP-7 (*Rt*-16.36)

The analytical chromatogram of crude and purified DP is given in figure 4.53. The HPLC purity of recrystallized DP-7 was 99.7%. The peak purity study of isolated DP-7 is shown in table 4.50 and figure 4.54.

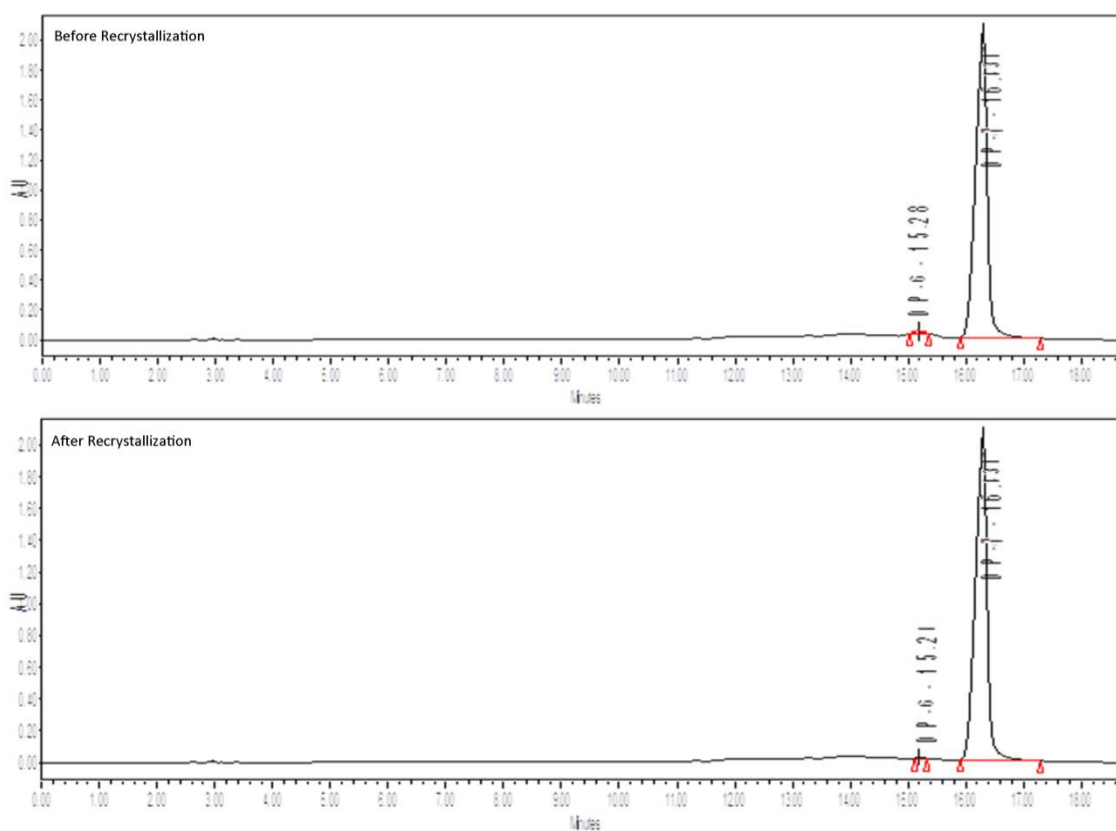


Figure 4.53: Analytical Chromatogram of DP-7 before and after recrystallization

Table 4.50: Peak purity study of isolated DP-7 and DP-4

S. No.	Peaks	Rt	Peak purity Angle	Peak purity Threshold
1.	DP-7	16.43	0.950	0.965
2.	DP-4	12.63	0.698	0.895

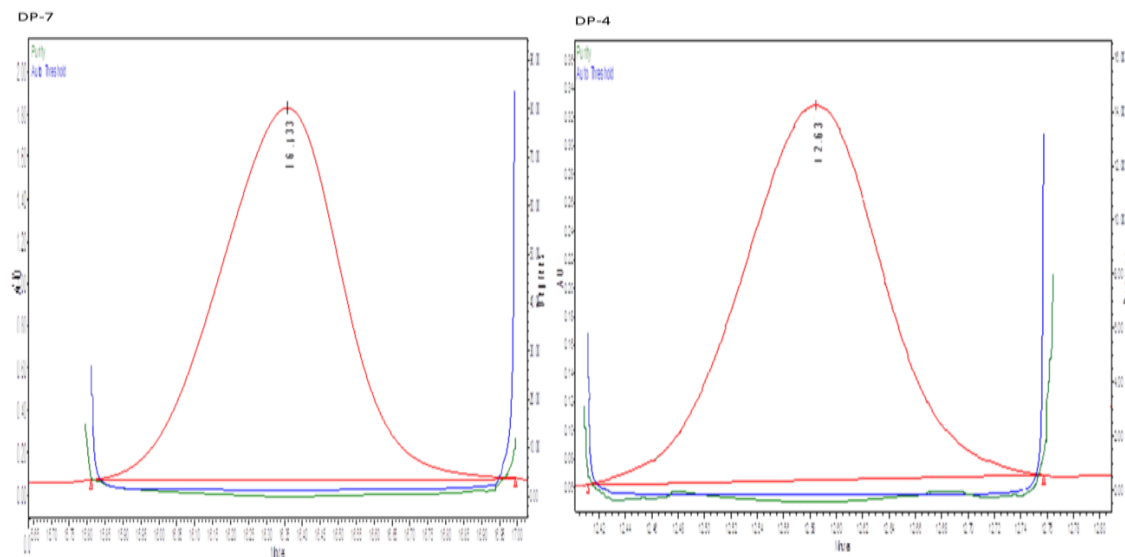


Figure 4.54: Peak purity plot of DP-7 and DP-4

4.8.2.2 DP-4 (R_t -12.5)

The analytical chromatogram of crude and purified DP-4 is given in figure 4.55. The HPLC purity of recrystallized DP-4 was 99.2%. The peak purity study of isolated DP-4 is shown in table 4.50 and figure 4.54.

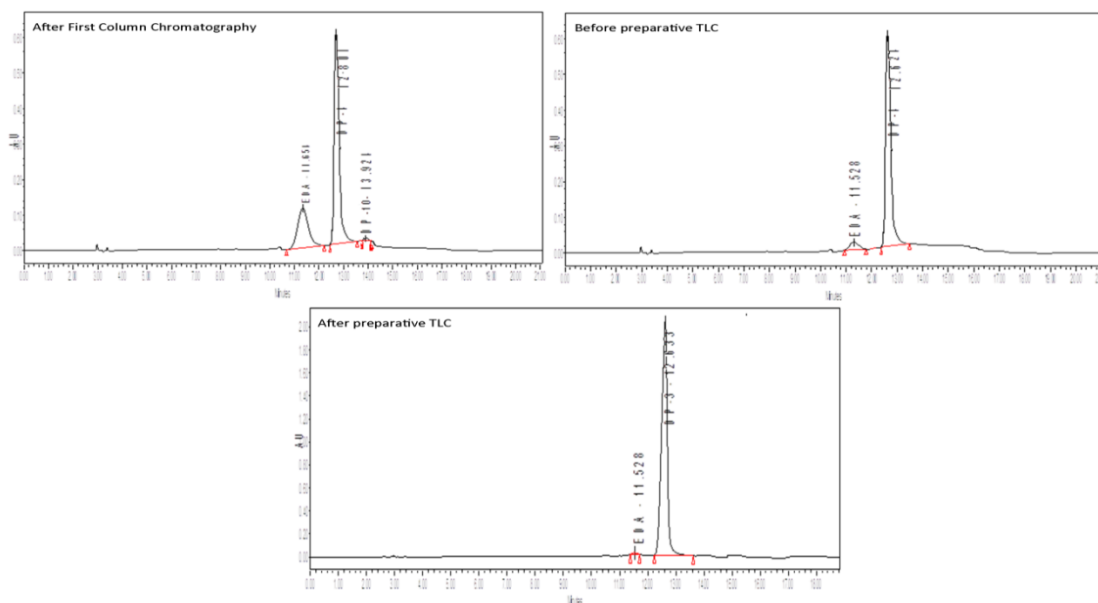


Figure 4.55: Analytical chromatogram of DP-4 a) after first column chromatography b) before preparative TLC c) after preparative TLC

4.8.2.2 Structural characterization of DPs

4.8.2.2.1 Characterization of DP-7

MS/MS Spectra

To determine molecular mass, EDA and isolated DP-7 were subjected to LC-MS/MS in positive ion mode and the plots are shown in figure 4.56 and 4.57. The molecular weight (MW) of DP-7 is 520 which is 346 amu more as compared to the EDA which has MW 174. The proposed fragmentation pattern of EDA and DP-7 are illustrated in figure 4.58.

MS/MS of EDA (m/z 175): The ESI-MS/MS spectrum of EDA showed $[M+H]^+$ ion at 175 in positive mode and $[M-H]^-$ ion at 173 in negative mode. The spectrum showed abundant product ions at m/z 147 due to the loss of carbonyl group which further fragment to give most abundant product ions at m/z 133 due to the loss of methyl group.

MS/MS of DP-7 (m/z 521): The ESI-MS/MS spectrum of the ion at m/z 521 showed most abundant product ions at m/z 348 which further fragment to give product ions at m/z 175 and 178. m/z 175 correspond to EDA while m/z 178 may be due to hydroxy derivative of EDA.

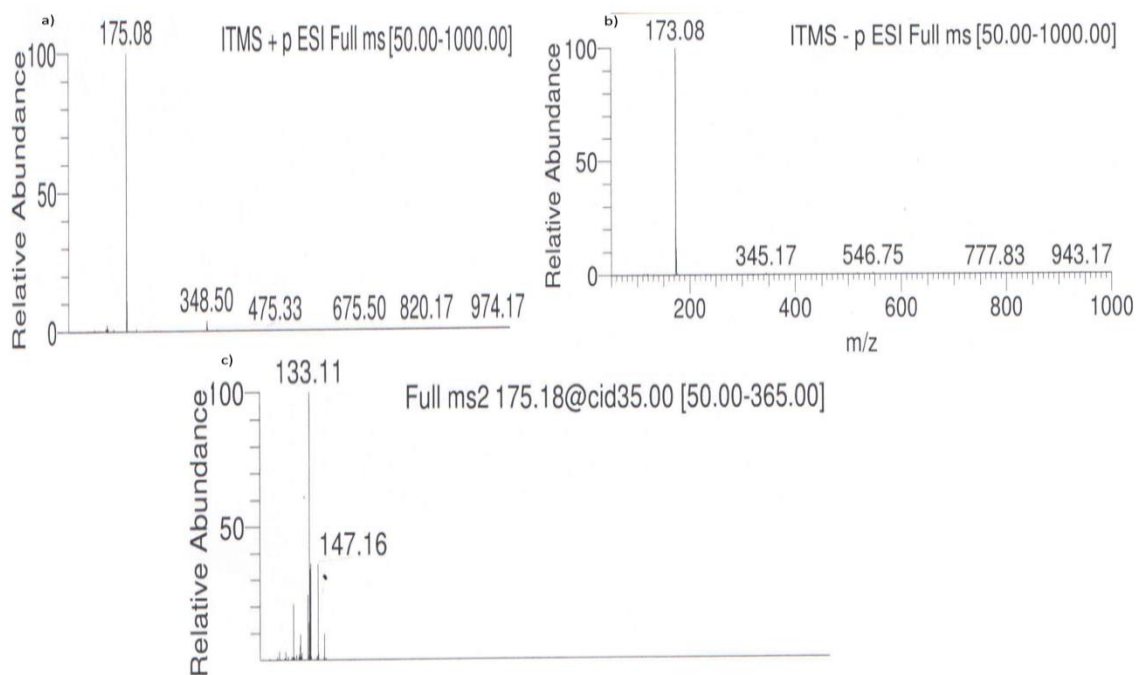


Figure 4.56: ESI-MS/MS Spectra of EDA Standard

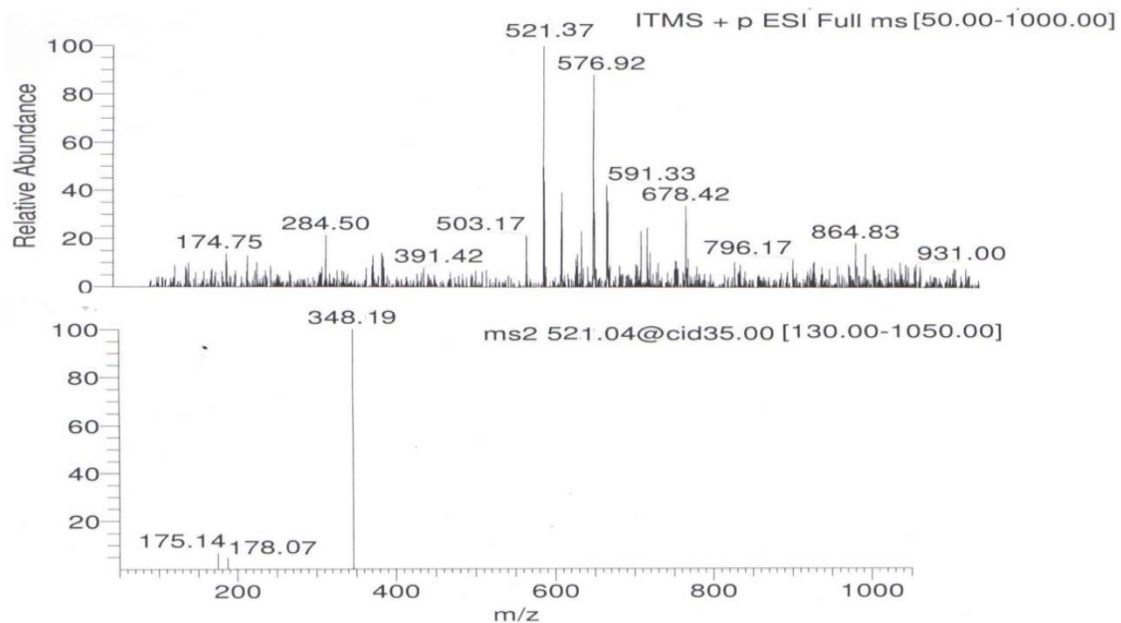


Figure 4.57: ESI-MS/MS Spectra of DP-7

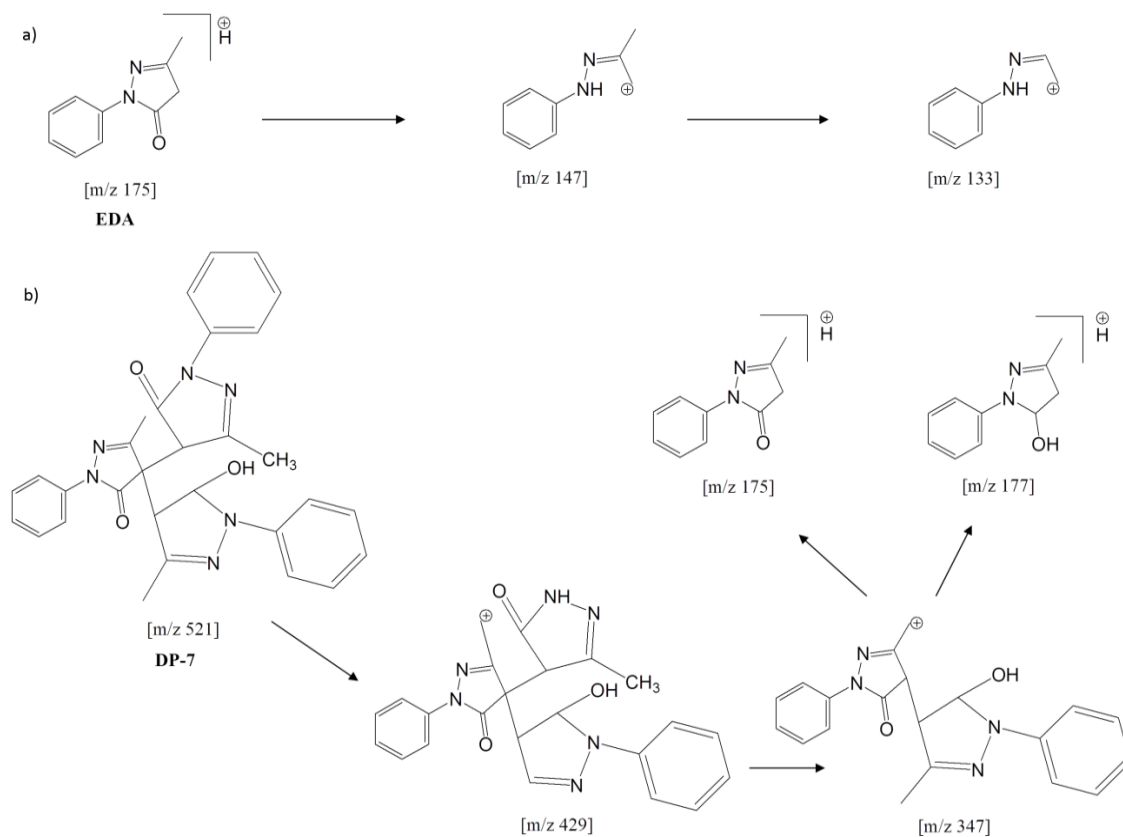


Figure 4.58: Proposed fragmentation pathway of EDA and DP-7

IR Spectra

In IR spectra it was observed that the carbonyl peak at 1797 cm^{-1} in EDA standard was shifted to 1720 cm^{-1} in DP-7. The amide peaks at 1597 and 1579 cm^{-1} in EDA standard were observed at 1620 and 1595 cm^{-1} in DP-7. Stretching vibration at 3608 cm^{-1} may be due to $-\text{OH}$ group in DP-7. The IR spectral assignment for EDA, DP-7 and DP-4 is presented in table 4.51. The IR Spectra of EDA standard, and DP-7 are illustrated in figure 4.59 and 4.60 respectively.

Table 4.51: IR Spectral assignments for EDA Standard, DP-7 and DP-4.

Standard (EDA)		DP-7		DP-4	
Wave No (cm^{-1})	Assignments	Wave No (cm^{-1})	Assignments	Wave No (cm^{-1})	Assignments
1797.66	Stretching – CO	1720.50	Stretching – CO	1797.66	disappeared
1597.06	Stretching -	1620.21	Stretching -	1591.27	Stretching
1579.70	CONH	1595.13	CONH	1579.70	-CONH
Not observed		3608.81	Stretching - OH	3604.96	Stretching - OH
	Not observed			3869.20	Stretching
				3838.38	-NH ₂
	Not observed			3728.40	Stretching -N-

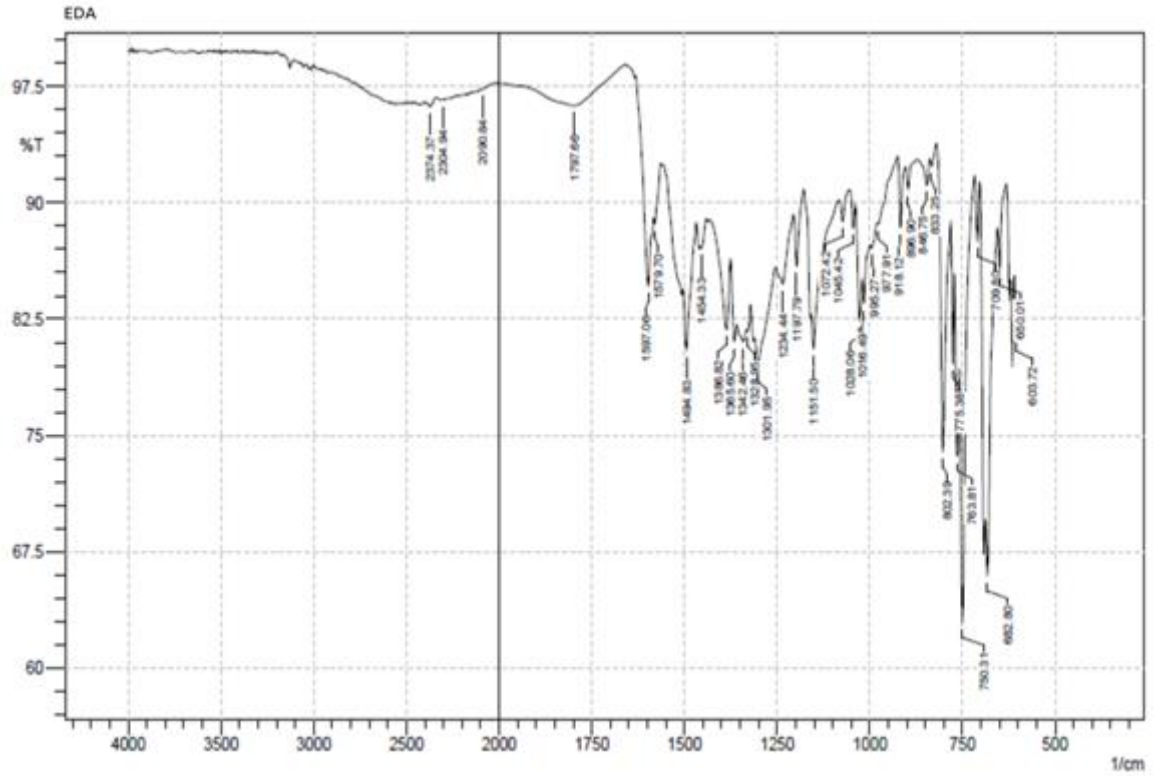


Figure 4.59: IR spectra of EDA Standard

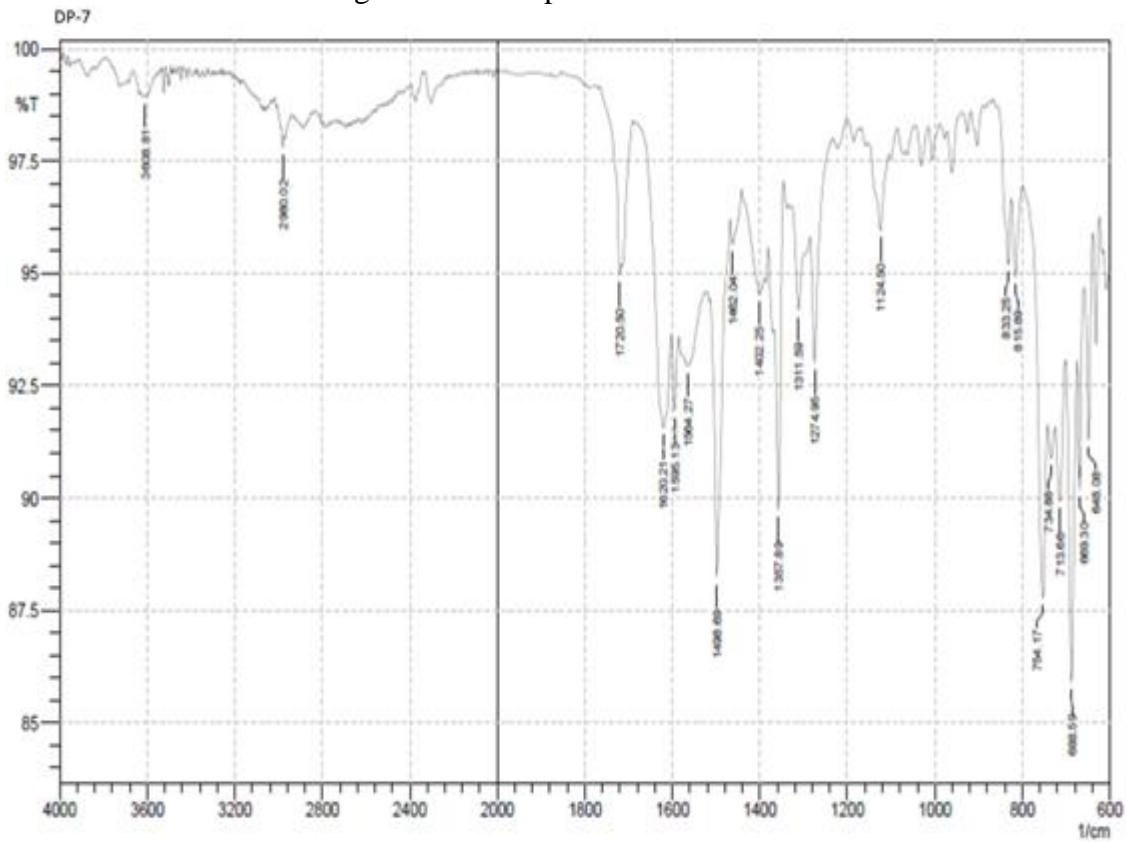


Figure 4.60: IR spectra of DP-7

NMR Spectra

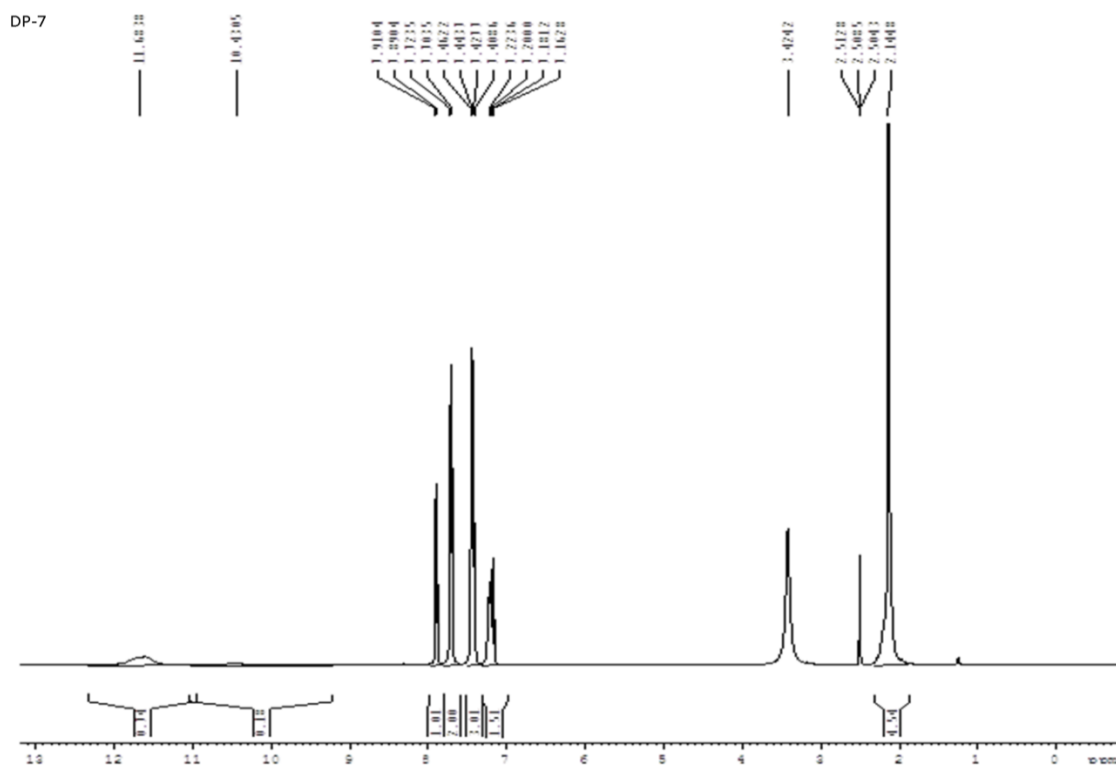
The ^1H spectrum of DP-7 indicates presence of hydroxyl group, which was further confirmed by D_2O exchange. In D_2O spectrum singlet at 3.4 disappears while in EDA standard none of the peaks were disappeared. Heterocyclic and aromatic protons were also observed at 7.91, 7.89, 7.72, 7.70 and 7.46, 7.44, 7.42, 7.40 δ value respectively in DP-7. Solvent peak of DMSO was observed at 2.51, 2.508 and 2.504 ppm in DP-7, the same was observed in EDA standard also.

The ^{13}C NMR spectrum of DP-7 indicates the presence of fourteen different carbon atom while in EDA ten different carbon atoms are present. This may be due to presence of identical carbon atoms since the mass spectrum shows increment in MW by 346 amu. The ^1H and ^{13}C spectral assignments for DP-7 and PDM are illustrated in table 4.52 and 4.53. The ^1H spectra of EDA and DP-7 are shown in figure 4.61 and 4.62. The ^{13}C spectra of EDA and DP-7 are shown in figure 4.63 and 4.64.

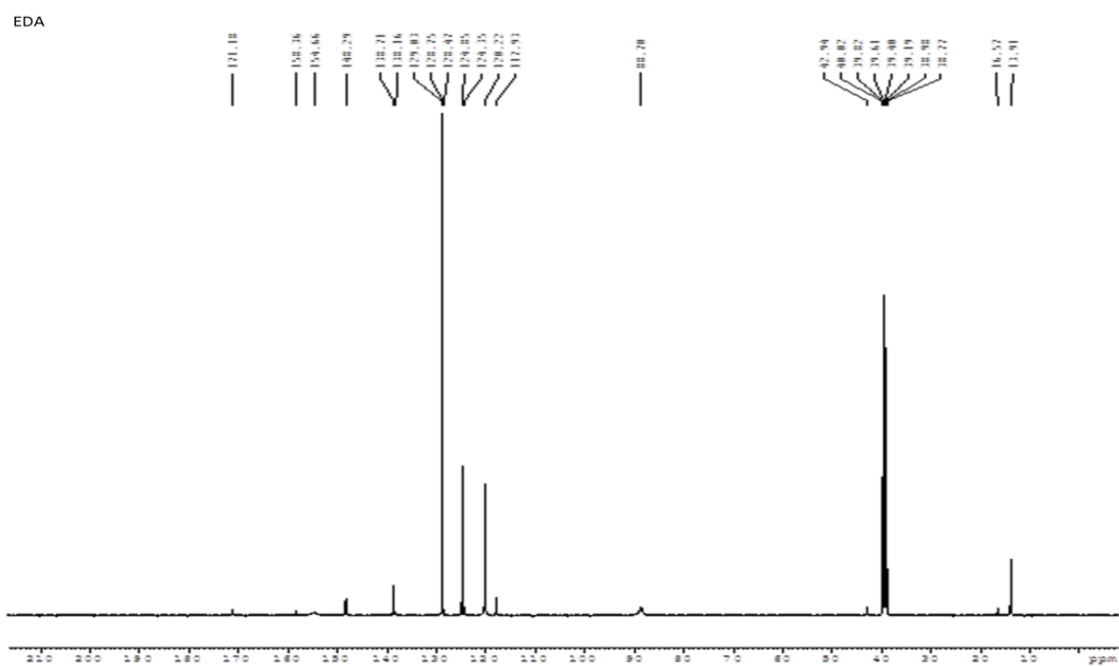
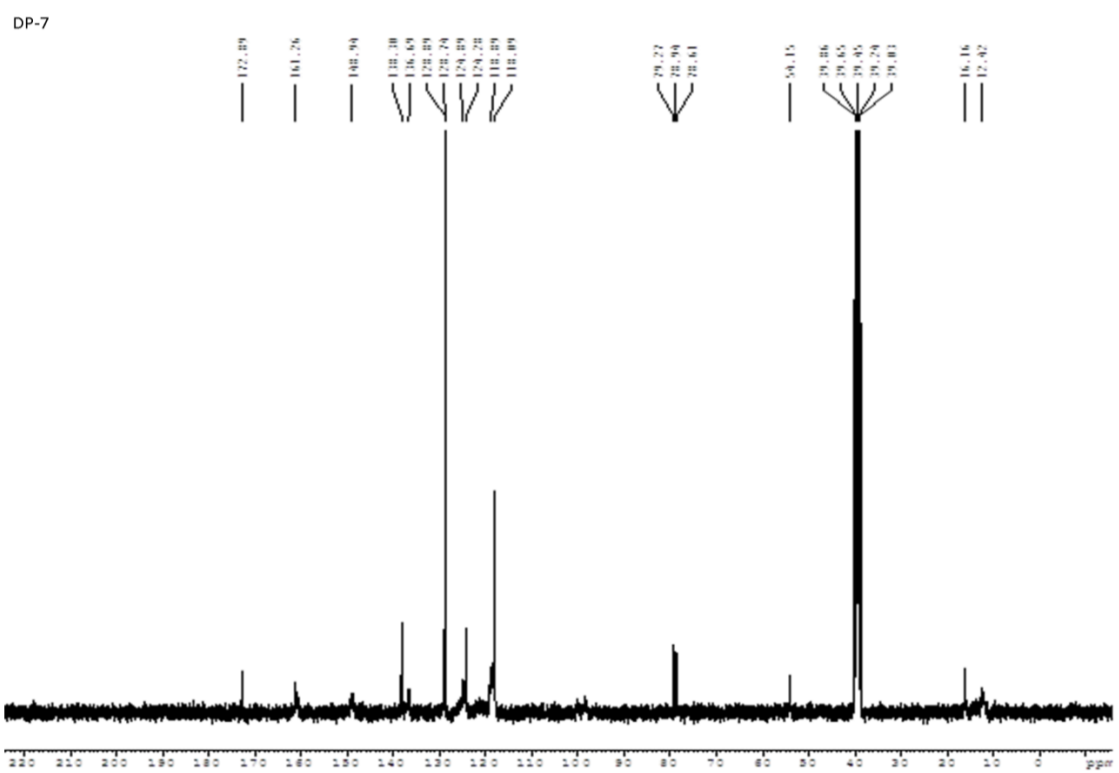
Further in DEPT-135 (figure 4.66) spectra of DP-7 inverted peak of $-\text{CH}_2$ was not observed which indicated the structure does not contain $-\text{CH}_2$ group. While the DEPT-135 (figure 4.65) spectra of EDA indicates the presence of one inverted peak at 43.11 ppm due to presence of one $-\text{CH}_2$. The D_2O spectra of EDA and DP-7 are illustrated in figure 4.67 and 4.68.

Table 4.52: ^1H - NMR Data of EDA standard and DP-7

Standard (EDA)			DP-7		
Position	Chemical Shift (δ , ppm)	Multiplicity	Position	Chemical Shift (δ , ppm)	Multiplicity
1	11.48	s (Broad)	1	11.68	s
3	7.758	d	2	10.43	s (broad)
	7.738				
4	7.444, 7.424, 7.404	t	3	7.91, 7.89, 7.72, 7.70	dd

Figure 4.62: ^1H NMR Spectra of DP-7Table 4.53: ^{13}C - NMR Data of EDA standard and DP-7

Standard (EDA)		DP-7	
Position (Carbon)	Chemical Shift (δ , ppm)	Position	Chemical Shift (δ , ppm)
1	171.18	11	172.89
3	158.36	1	161.26
5	148.29	3,13,23	148.94
8	129.03	25	138.30
7	128.75	5, 15	136.69
9	128.47	29, 27	128.89
5	124.85	9, 7, 19, 17	128.74
10	124.35	8, 18	124.89
2	88.70	6, 10, 16, 20	124.28
4	42.94	28	118.89
		26, 30	118.09
		12	54.15
		22	16.16
		2	12.42

Figure 4.63: ^{13}C NMR Spectra of EDAFigure 4.64: ^{13}C NMR Spectra of DP-7

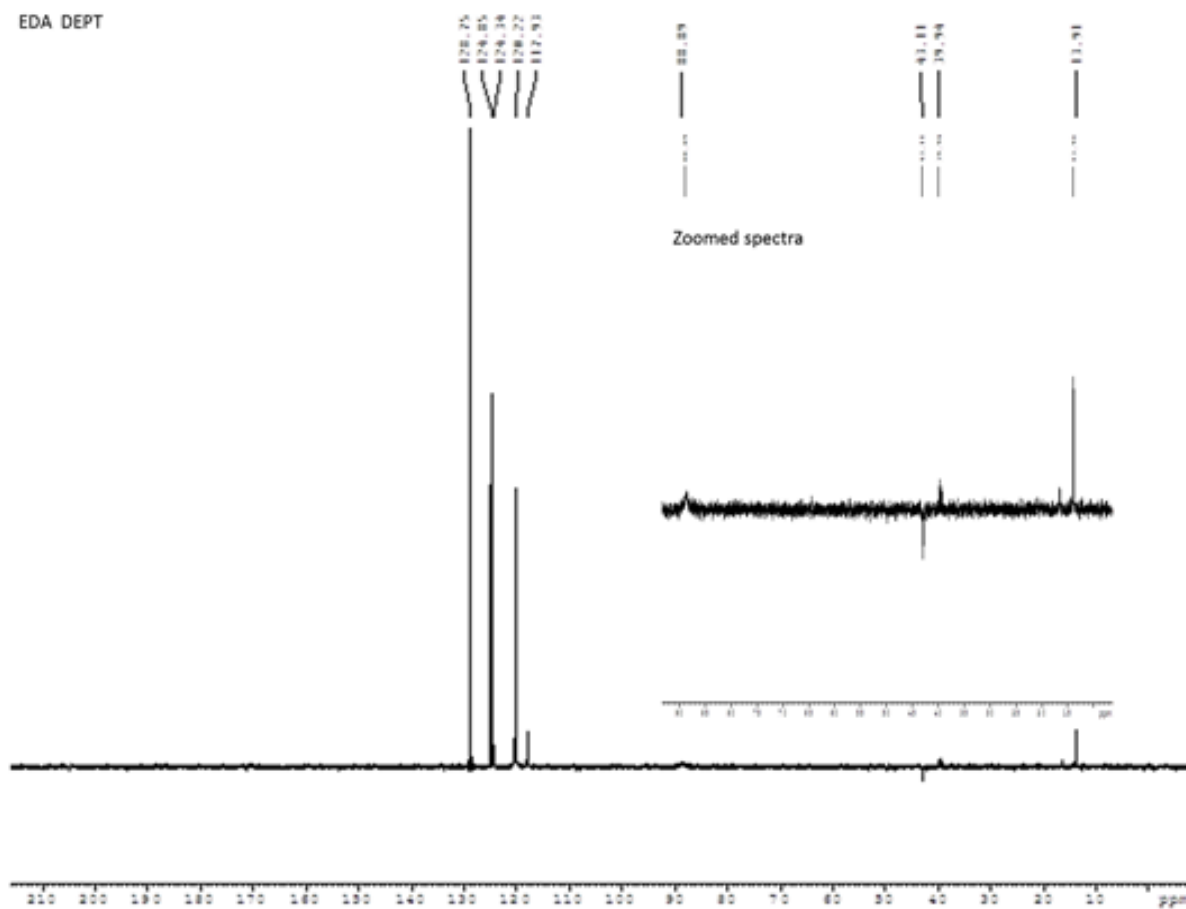


Figure 4.65: DEPT-135 Spectra of EDA

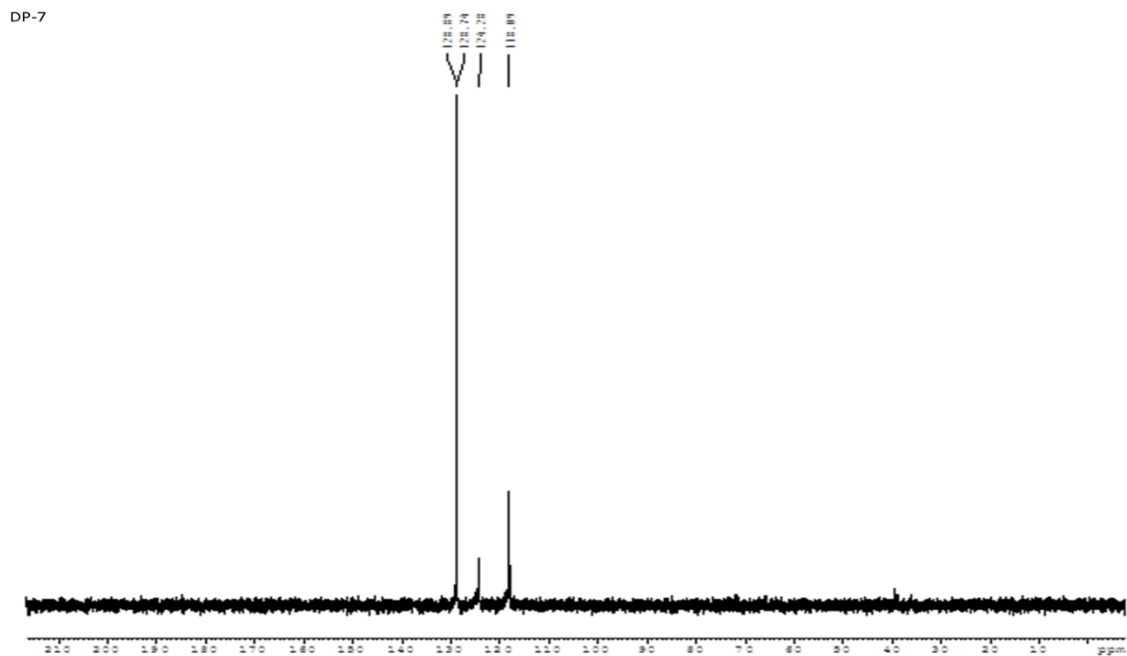
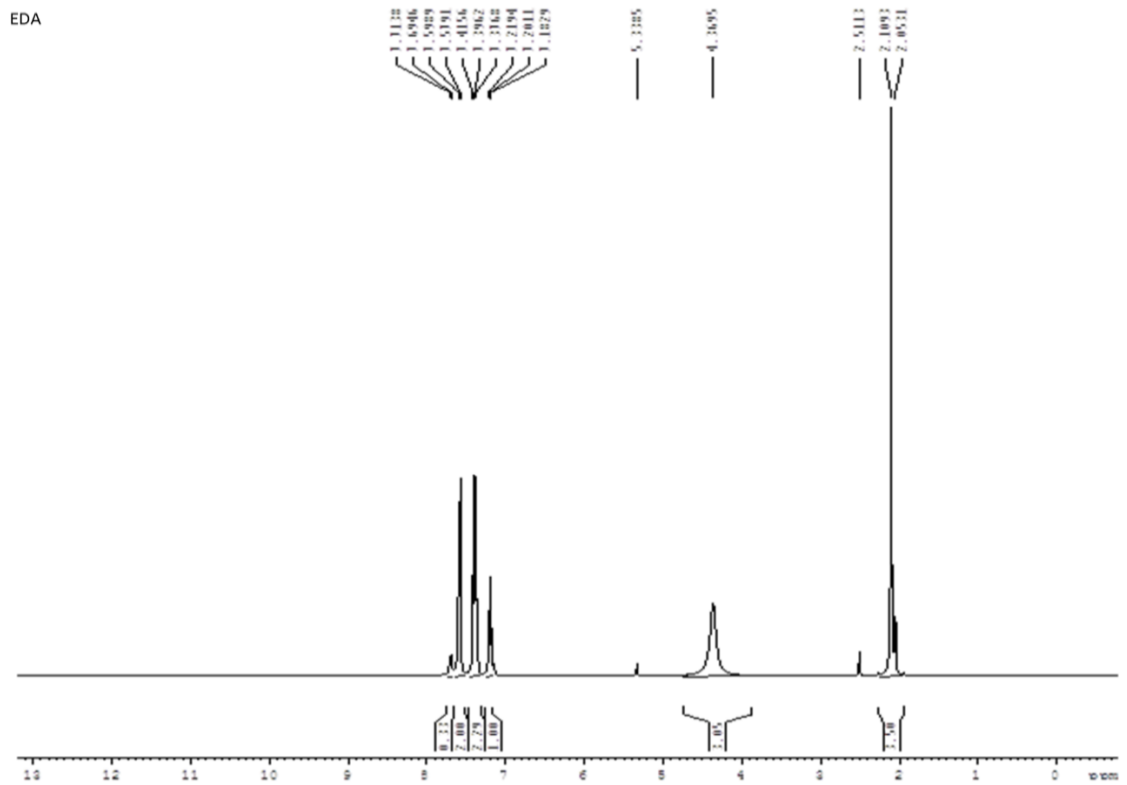
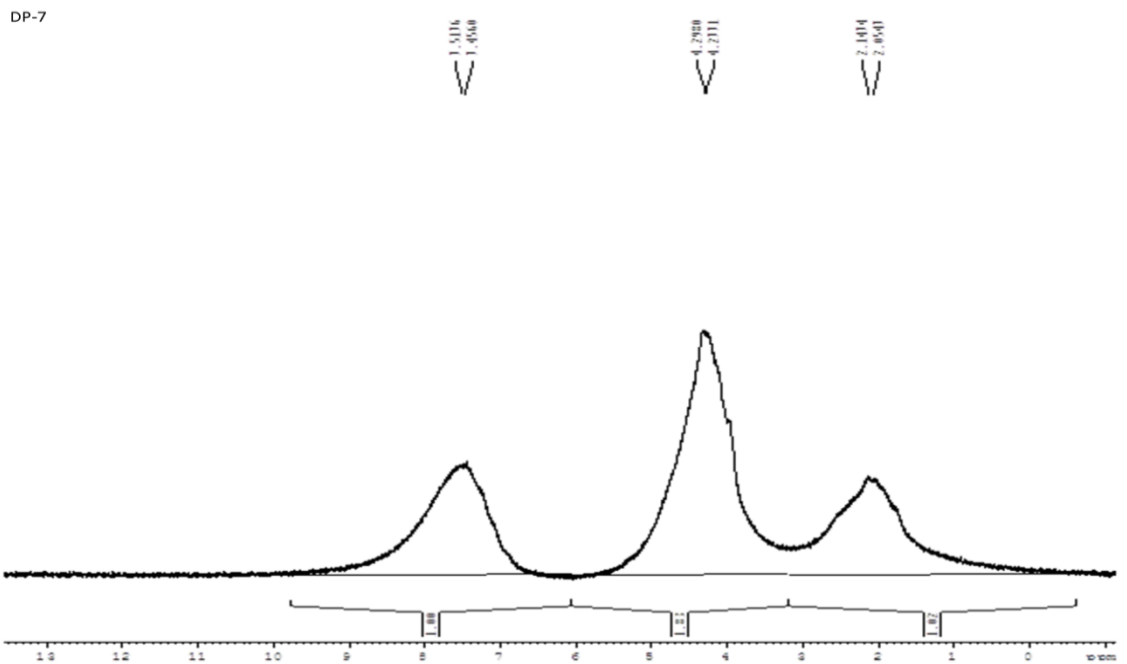


Figure 4.66: DEPT-135 Spectra of DP-7

Figure 4.67: D₂O Spectra of EDAFigure 4.68: D₂O Spectra of DP-7

DSC Thermogram

DSC thermogram of both EDA standard and DP-7 are shown in figure 4.69 and 4.70. The DSC thermogram of EDA shows an endothermic peak at 131 °C indicating its melting temperature. Similarly in DP-7 a sharp endothermic peak was observed at 264.97 °C so it can be concluded that DP-7 melts at this temperature. Furthermore the sharp peak confirms the purity of DP-7.

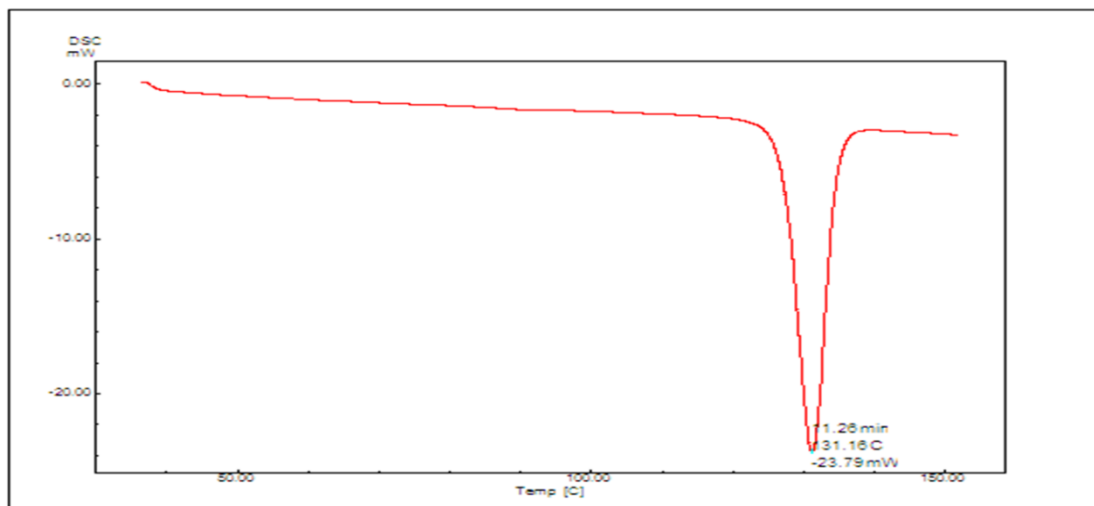


Figure 4.69: DSC thermogram of EDA

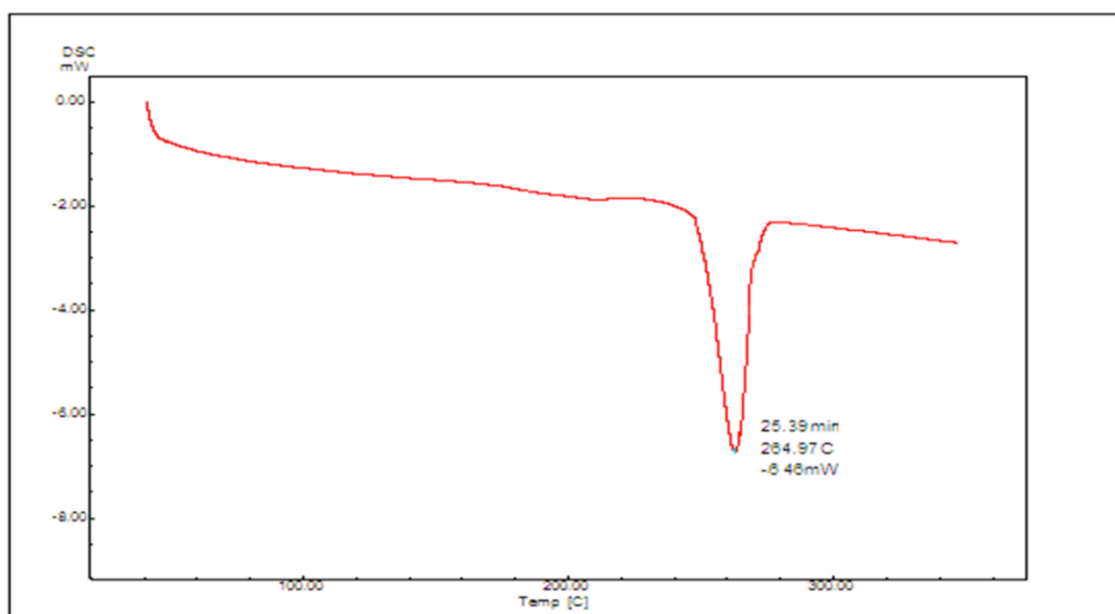


Figure 4.70: DSC thermogram of DP-7

Based on observations retrieved from various spectral data as mentioned and discussed above, DP-7 was confirmed as trimer of EDA in which one of the carbonyl group was replaced with hydroxyl group, chemically named as 4-(4,5-dihydro-3-methyl-5-oxo-1-phenyl-1H-pyrazol-4-yl)-4-(4,5-dihydro-5-hydroxy-3-methyl-1-phenyl-1H-pyrazol-4-yl)-3-methyl-1-phenyl-1H-pyrazol-5(4H)-one. The comparative structures of EDA and DP-7 is shown in figure 71 with their assigned positions used in interpretation.

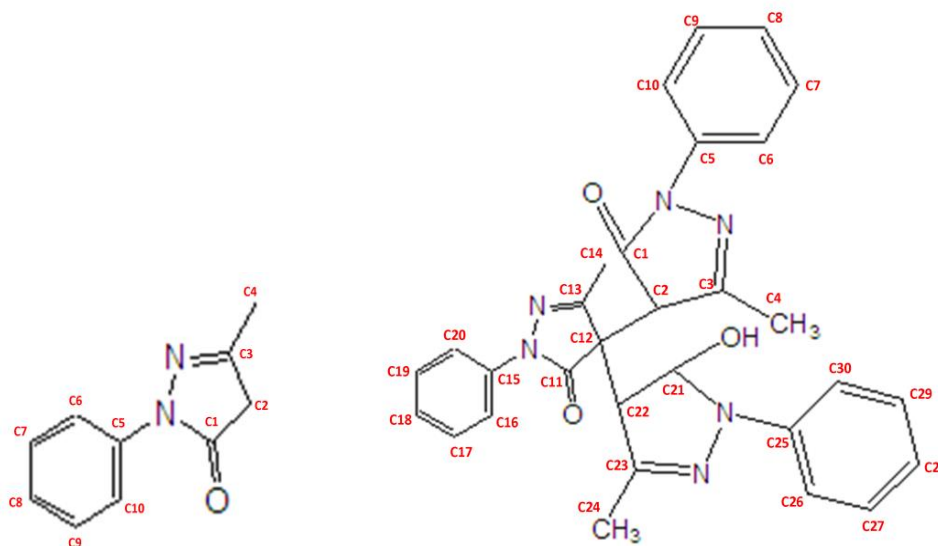


Figure 71: Structure of a) EDA and b) DP-7 with their assigned numbers

4.8.2.2.2 Characterization of DP-4

MS/MS of DP-4 (m/z 332):

The molecular mass of isolated DP-4 was determined by the LC-MS/MS in positive ion mode and is shown in figure 4.72. The molecular weight of DP-4 is 332 which is 158 amu more as compared to the EDA and 14 amu less as compared to dimer of EDA (MW 346). The fragmentation pattern of DP-4 is illustrated in figure 4.73. In the ESI-MS/MS spectrum of $[M+H]^+$ ion of DP-4 the most abundant product ion was observed at m/z 197. The spectrum also include abundant product ions at m/z 239 (238.92) formed by loss of phenyl hydrazine which losses one carbon atom and form product ion at m/z 225. From product ion of m/z 197 further fragmentation takes place to produce product ions at m/z 171 due to the loss of C atom.

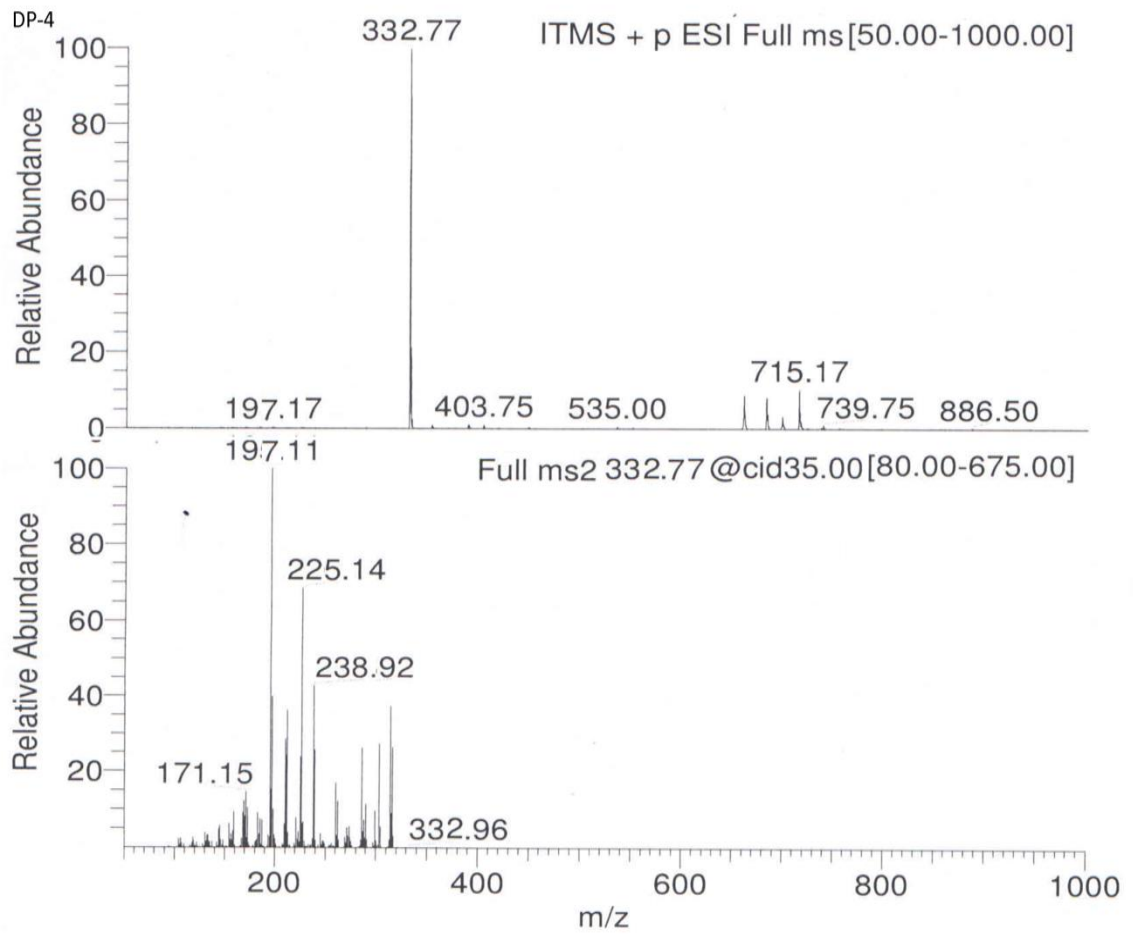


Figure 4.72: ESI-MS/MS spectra of DP-4

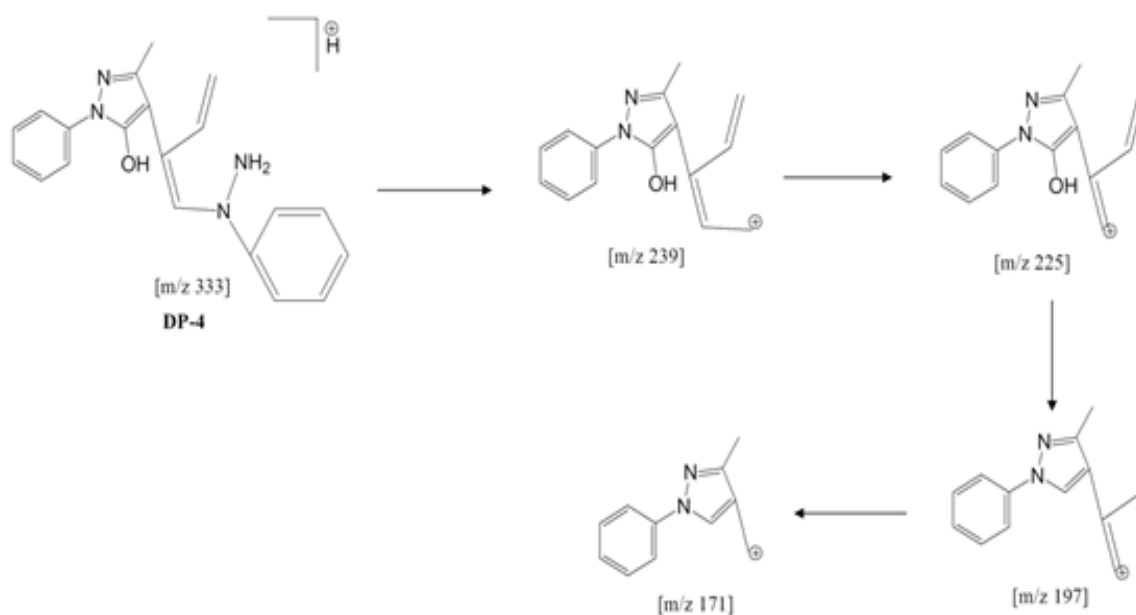


Figure 4.73: Proposed fragmentation pathway of DP-4

IR Spectra

In IR spectra (figure 4.74) it was observed that -CO stretching vibration at 1797.66 cm^{-1} in EDA standard was disappeared which indicates that carbonyl group has either removed or converted into other group. The vibrations at 1591.27 and 1579.70 cm^{-1} and -NH_2 stretching vibration at 3869.20 , 3838.34 indicates the possibility of primary amino group in DP-4. The stretching vibration at 3728.40 indicates the presence -NH group in DP-4. The -OH peak at 3604.96 was also observed in DP-4 while -NH_2 , -NH and -OH stretching vibrations were not observed in EDA standard. The IR spectral assignment for DP-4 is presented in table 4.51.

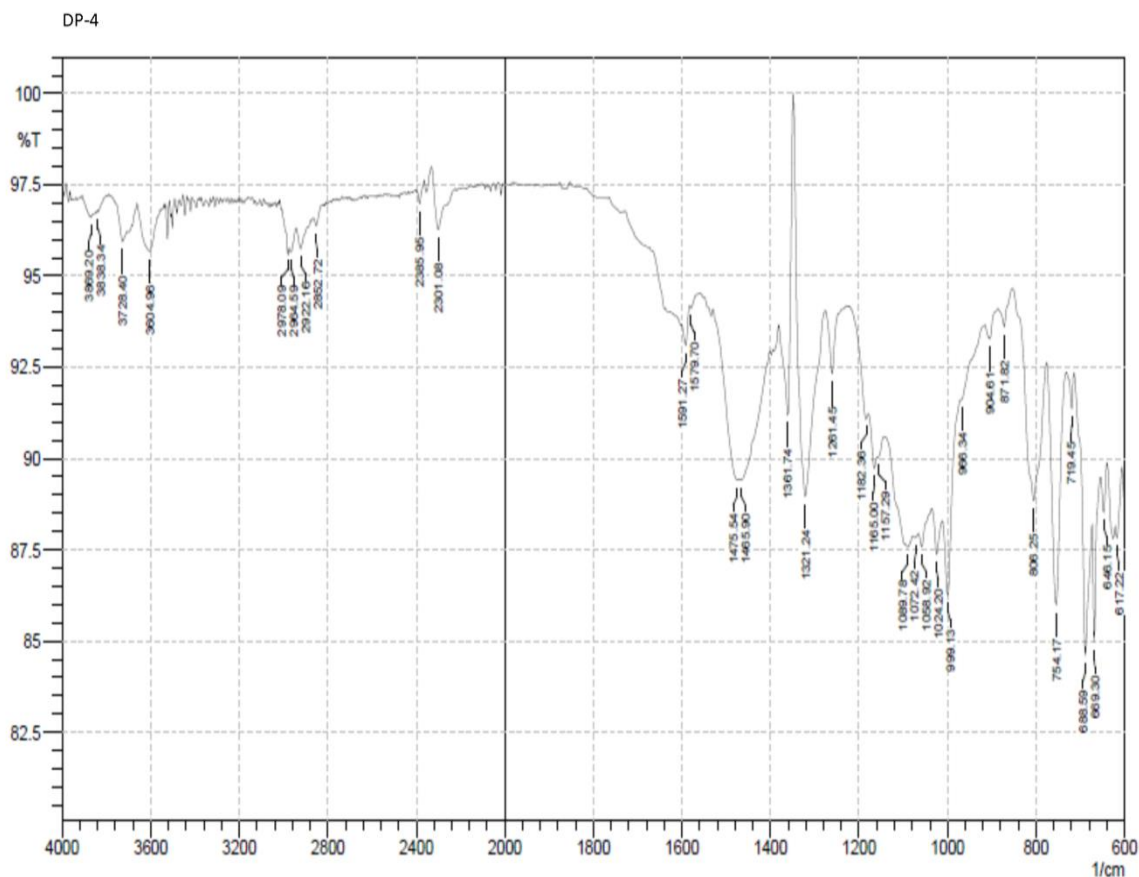


Figure 4.74: IR Spectrum of DP-4

NMR Spectra

The ^1H spectrum of DP-4 indicates presence of hydroxyl group and amino group which was further confirmed by D_2O exchange. In D_2O spectrum singlets at 9.6 and 3.38 were disappeared. Heterocyclic peaks were observed at 8.07, 8.057, 8.053, and 8.03. Other peaks in the region of 7.97 to 7.1 ppm indicate that two aromatic rings possibly benzene ring of EDA were exposed to different environment. The sharp peak at 1.2 indicates the possibility of methyl group. Other peaks in the region of 2.3 to 2.0 indicate the possibility of $-\text{CH}_2$ and $-\text{CH}$ groups.

The ^{13}C NMR spectrum of DP-4 indicates the presence of twenty different carbon atoms. This may be due to breakage of second heterocyclic ring that has exposed aromatic ring (benzene) in different environment since the mass spectrum shows increment in MW by

158 amu that is 14 amu less than MW of dimer. The ^1H and ^{13}C spectral assignments for DP-4 are illustrated in table 4.54. The ^1H and ^{13}C spectra of DP-4 are shown in figure 4.75 and 4.76.

Further in DEPT-135 (figure 4.77) spectra of DP-4 one inverted peak of $-\text{CH}_2$ was observed at 29.01 ppm which indicated the structure contain only one $-\text{CH}_2$ group. The D_2O spectrum of DP-4 is shown in figure 4.78.

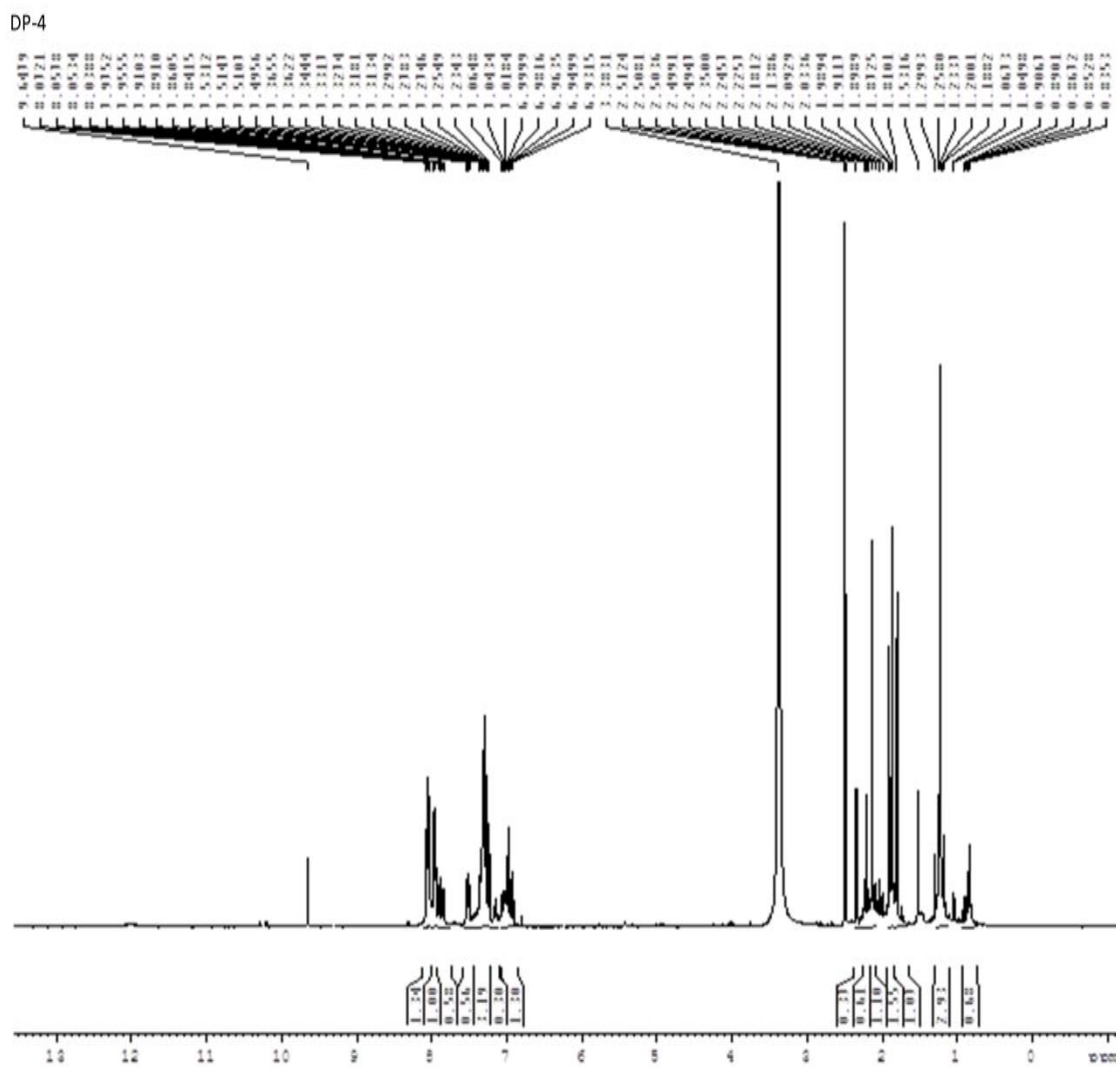


Figure 4.75: ^1H NMR Spectra of DP-4

Table 4.54: ^1H and ^{13}C NMR Spectral assignments of DP-4

Position	^1H		^{13}C	
	Chemical (δ , ppm)	Shift	Position	Chemical Shift (δ , ppm)
6,10	7.97, 7.95		1	162.92
7,9	7.91, 7.89		3	151.74
8	7.86, 7.84		5	150.59
19, 17, 18, 20, 16	7.55, 7.53, 7.510 7.49	7.514,	15	140.62
12	2.3		12	129.11
13	2.24		7,9	128.55
4	2.1		17, 19	128.28
-NH ₂	9.6		8	128.20
-OH	3.38			
			18	119.74
			6, 10	117.53
			16, 20	117.20
			18	117.03
			14	116.83
			11	31.26
			2	28.98
			12	22.08
			13	15.58
			14	15.25

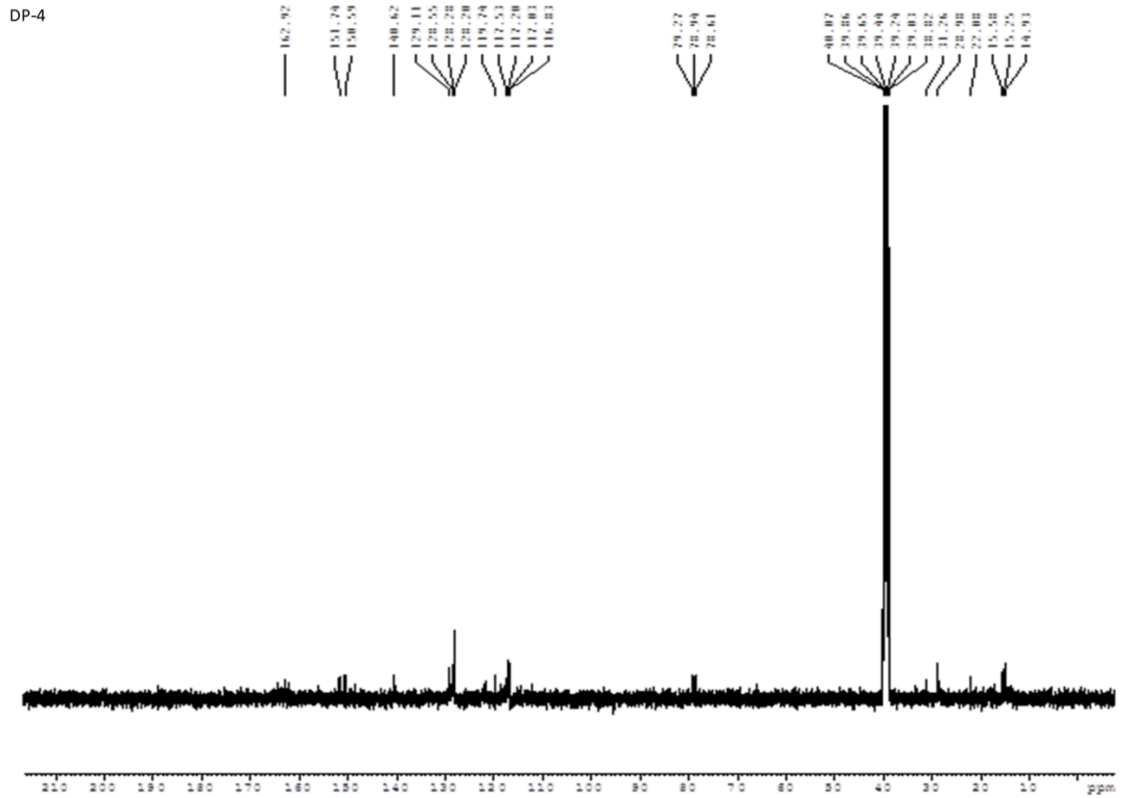
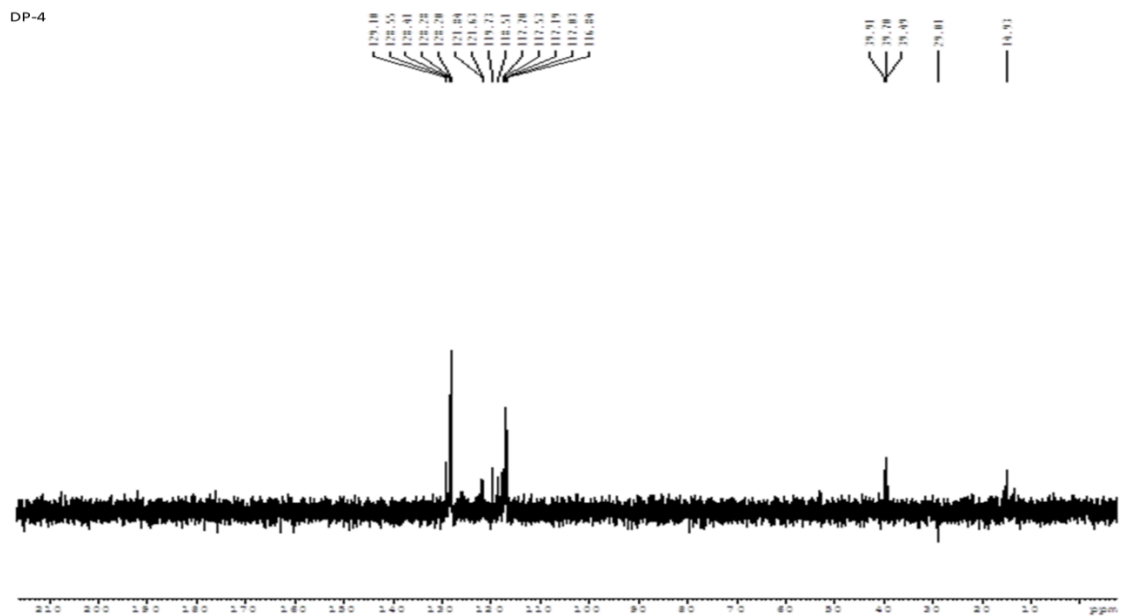
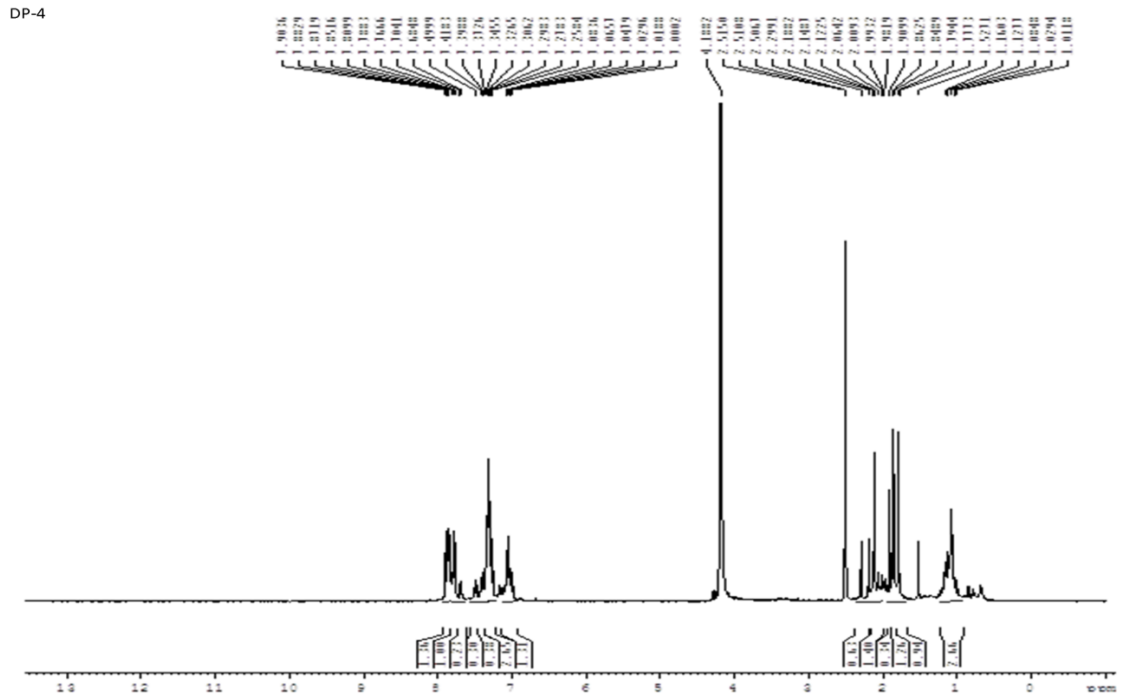
Figure 4.76: ^{13}C NMR Spectra of DP-4

Figure 4.77: DEPT Spectra of DP-4

Figure 4.78: D₂O Spectra of DP-4

DSC Thermogram

DSC thermogram of DP-4 is shown in figure 4.79 that showed an exothermic peak at 216.27 °C which indicates that the compound undergo some chemical conversion and needs to be explored further by other thermal methods.

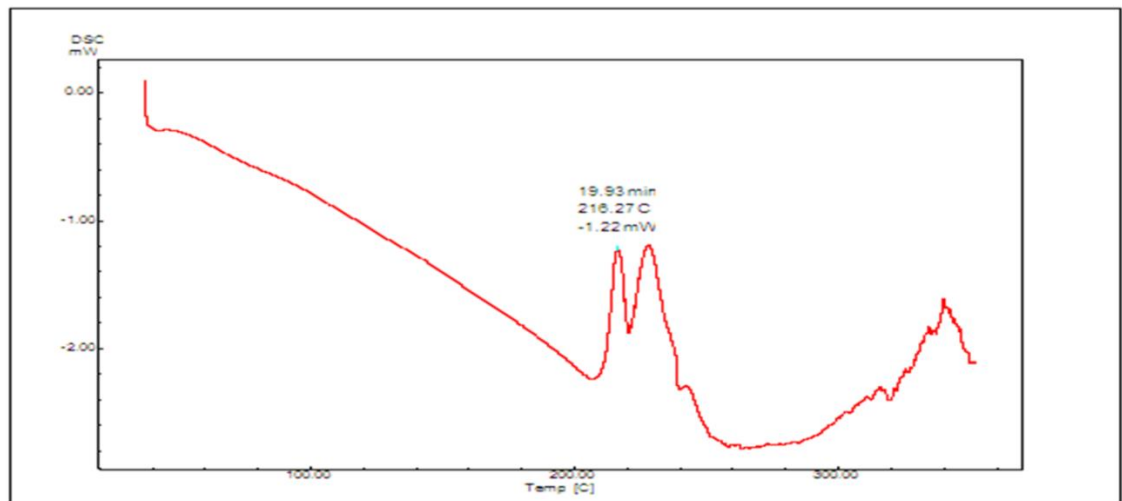


Figure 4.79: DSC thermogram of DP-4

Based on observations retrieved from various spectral data as mentioned and discussed above, DP-4 was assigned a structure, chemically named as 3-hydroxy-dihydro-thiazolo(1-(2-methyl-buta-1,3dienyl)-1-phenylhydrazine)5-one. The structure of DP-4 is shown in figure 4.80 with their assigned positions used in interpretation.

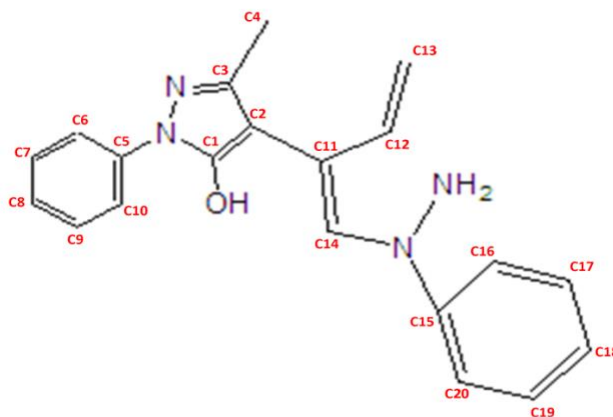


Figure 4.80: Structure of DP-4 with their assigned numbers

4.9 SECTION-F

IMPURITY PROFILING AND DEGRADATION STUDY OF EDARAVONE

4.9.1 EXPERIMENTAL

4.9.1.1 Chemicals and Reagents

Chemicals and reagents used in present section were same as described in section 3.4.1.1 and 4.4.1.1.

4.9.1.2 Equipments and Chromatographic Conditions

The equipments and chromatographic conditions utilized for impurity profiling and degradation study were same as described in section 3.4.1.2 and 4.4.1.2.

For LC-MS/MS analysis EDA degradation samples were subjected to similar chromatographic conditions as mentioned in section 4.4.1.2. The m/z values were determined in both positive and negative ESI mode and were compared to the molecular weights (MW) of the known process related impurities and degradation products (DPs) reported in literature. The fragmentation patterns were also investigated. Based on the fragmentation pattern and MW presence of known process related impurity and DPs were

confirmed and also, structures were proposed for the unknowns and the fragmentation pathways were outlined based on the results.

4.9.1.3 Preparation of Stock, Sample and Buffer solutions

Stock, sample and buffer solutions were prepared in same way with similar dilutions as described in section 4.4.1.3.

4.9.2 RESULTS AND DISCUSSION

Six impurities of EDA were reported in Pharmacodia (30) and are shown in figure 4.81. One of the DP, DP-6 which has MW 518 was identified as EDA IM-F. Other DPs did not matched with the MW of reported impurities and were characterized. The structures and MW of reported impurities are illustrated in figure 4.81.

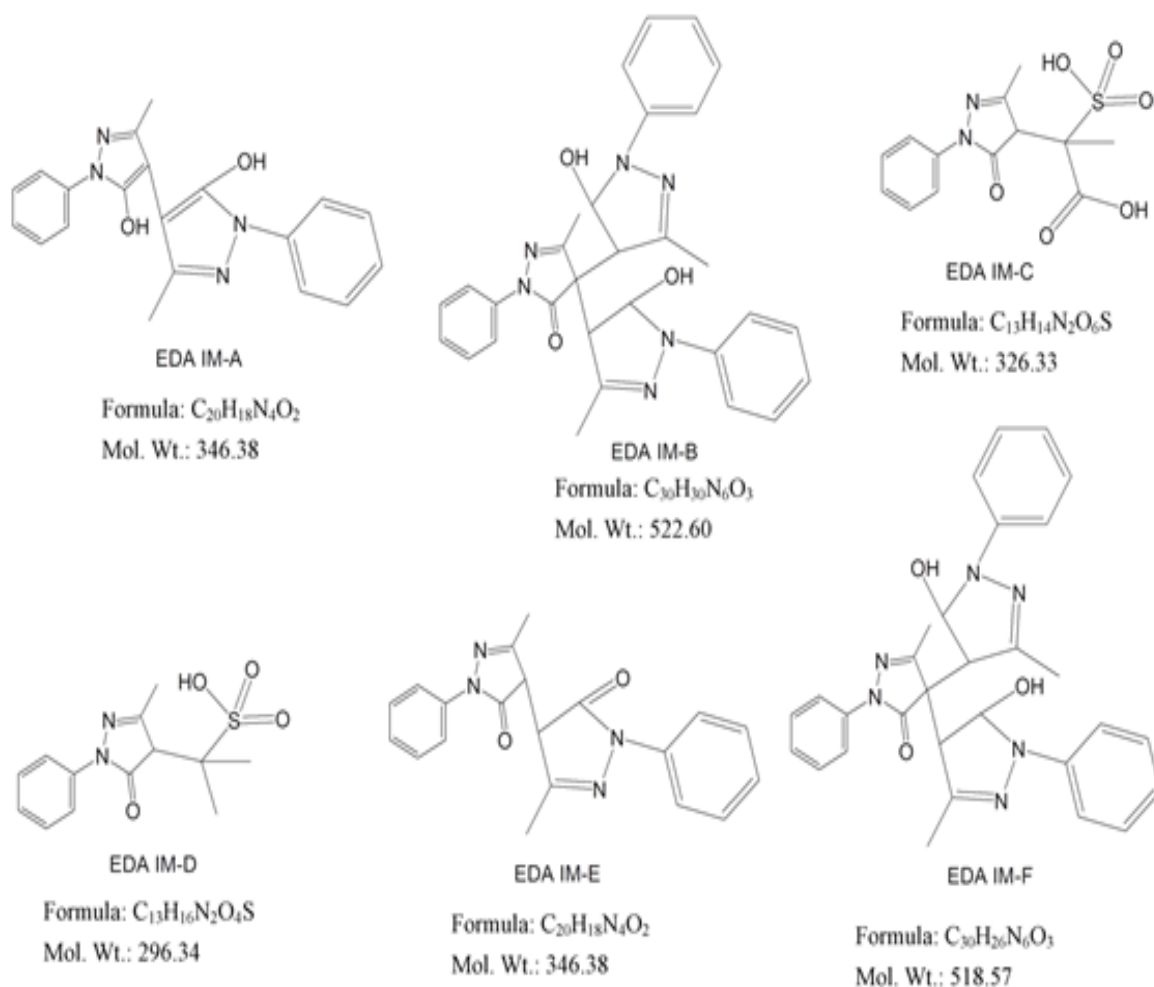


Figure 4.81: Molecular structure of EDA Impurities

4.9.2.1 LC-PDA Study

The stress degradation of EDA showed the formation of various degradation products (DPs) in LC-PDA and are summarized in table 4.55. Total 10 DPs were observed in LC-PDA. The peak purity studies revealed that some peaks were not pure in LC-PDA when mixture of degradants was injected, while the peaks were pure in individual injections of degradants. Further, the LC-MS/MS study of individual degradants revealed that the peaks had same retention time but different masses.

Table 4.55: Summary of forced degradation of EDA analysed by LC-PDA

Stressor Type	Stressor Conc.	Time	DPs Formed with Rt	% Deg (API)*	% Deg (Formulation)*
Acid degradation	0.05N HCl at 70 ⁰ C	180 min	DP-3(7.19), DP-5(14.25), DP-6(15.35), DP-7(15.96) DP-1(6.09),	70.87	69.99
Base degradation	0.2N NaOH at 70 ⁰ C	180 min	DP-9(13.29), DP-10(13.94), DP-6(15.38), DP-7(16.24) DP-8(9.66),	63.51	63.00
Neutral degradation	100 ⁰ C	7 hr	DP-6(15.36), DP-7(16.16) DP-10(13.89),	46.54	45.31
Oxidative degradation	6% H ₂ O ₂ at RT	45 min	DP-2(6.55), DP-5(14.35), DP-10(13.90)	52.07	51.80
Photolytic degradation	5382 LUX and 144UW/cm ²	21 days	DP-6(15.34), DP-7(16.16)	44.27	44.01
Dry Heat	80 ^o C	21	DP-4(12.57),	67.42	20.41 (for 72 Hr)

induced degradation		days	DP-10(13.90), DP-5(14.35) DP-6(15.32), DP-7(16.36)		
Thermal Humidity induced degradation	40 ° C 70 ± 5% RH	21 days	DP-8(9.54), DP-4(12.59) DP-6(15.42), DP-7(16.18)	37.59	37.04

4.9.2.2 LC-MS/MS study and characterization of DPs

The LC-PDA analysis showed total 10 DPs while 13 different masses were observed in LC-MS/MS, hence the nomenclature of DPs showing different masses were modified during explanation to avoid confusion. The modified nomenclature of DPs used for interpretation is shown in table 4.56. According to the fragmentation pattern and m/z values, the structures and fragmentation pathways for EDA and DPs were proposed.

Table 4.56: Modified nomenclature of DPs in LC-MS/MS study

Stressor Type	DPs nomenclature with Rt (LC-PDA)	Modified nomenclature of DPs in LC-MS/MS
Base Hydrolysis	DP-10(13.91)	No change
Neutral Hydrolysis	DP-10(13.89)	DP-11
Oxidation	DP-10(13.94)	DP-12
Dry Heat	DP-10 (12.82)	DP-13

EDA (m/z 175)

MS/MS and proposed fragmentation pathway of EDA standard is explained in section 4.8.2.2.1 and ESI-MS/MS spectra is provided in figure 4.56 and proposed fragmentation pathway is shown in figure 4.58.

DP-1 (m/z 203) and DP-9 (m/z 255)

Both DP-1 and DP-9 were formed during base degradation. The positive ion ESI-MS of DP-1 showed abundant $[M-H]^+$ ion at m/z 203 which was formed from DP-9 that has m/z 255 by loss of pyrozole-3-one with 82 amu. The spectrum of DP-9 showed most abundant peak at 203 that correspond to DP-1 while spectrum of DP-1 showed most abundant peak at m/z 175 corresponding to EDA which further fragment to give product ion at m/z 133. The spectrum of DP-1 also includes product ion at m/z 185. ESI-MS/MS spectra of DP-1 and DP-5 is provided in figure 4.82 and 4.83, the proposed fragmentation pathway is shown in figure 4.84.

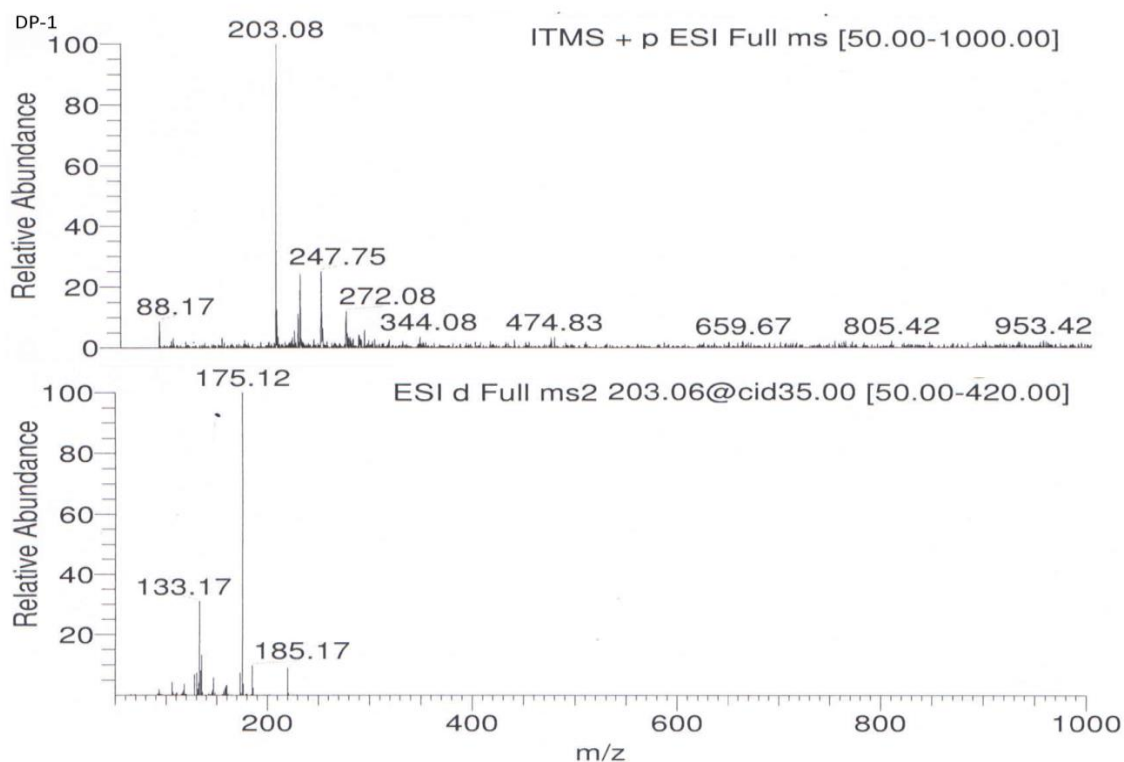


Figure 4.82: ESI-MS/MS spectra of DP-1

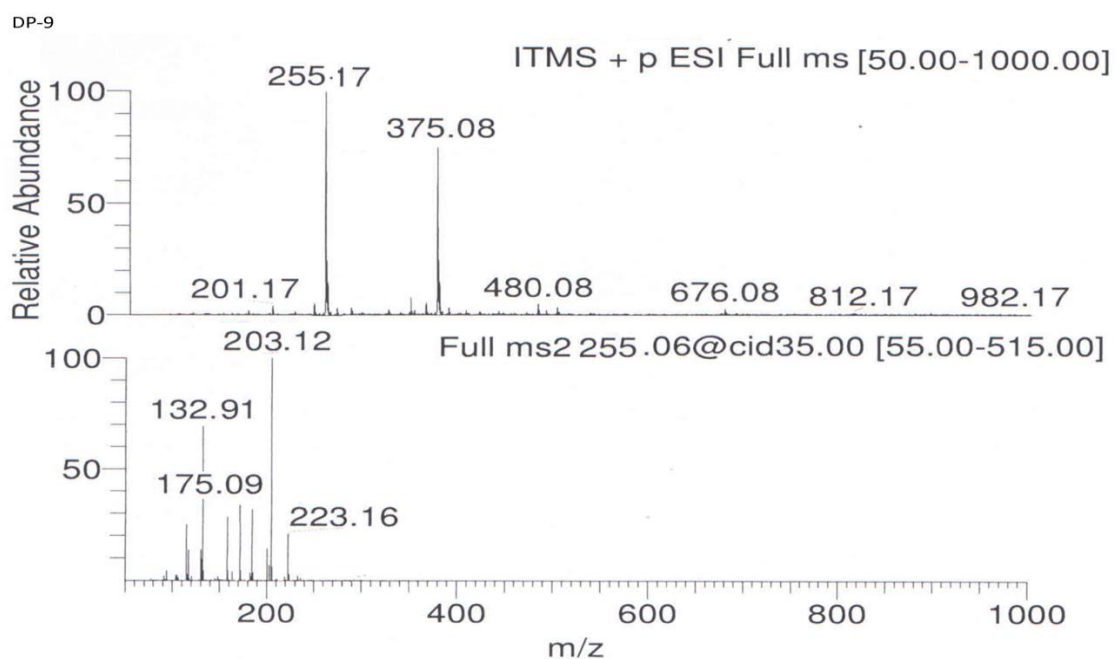


Figure 4.83: ESI-MS/MS spectra of DP-9

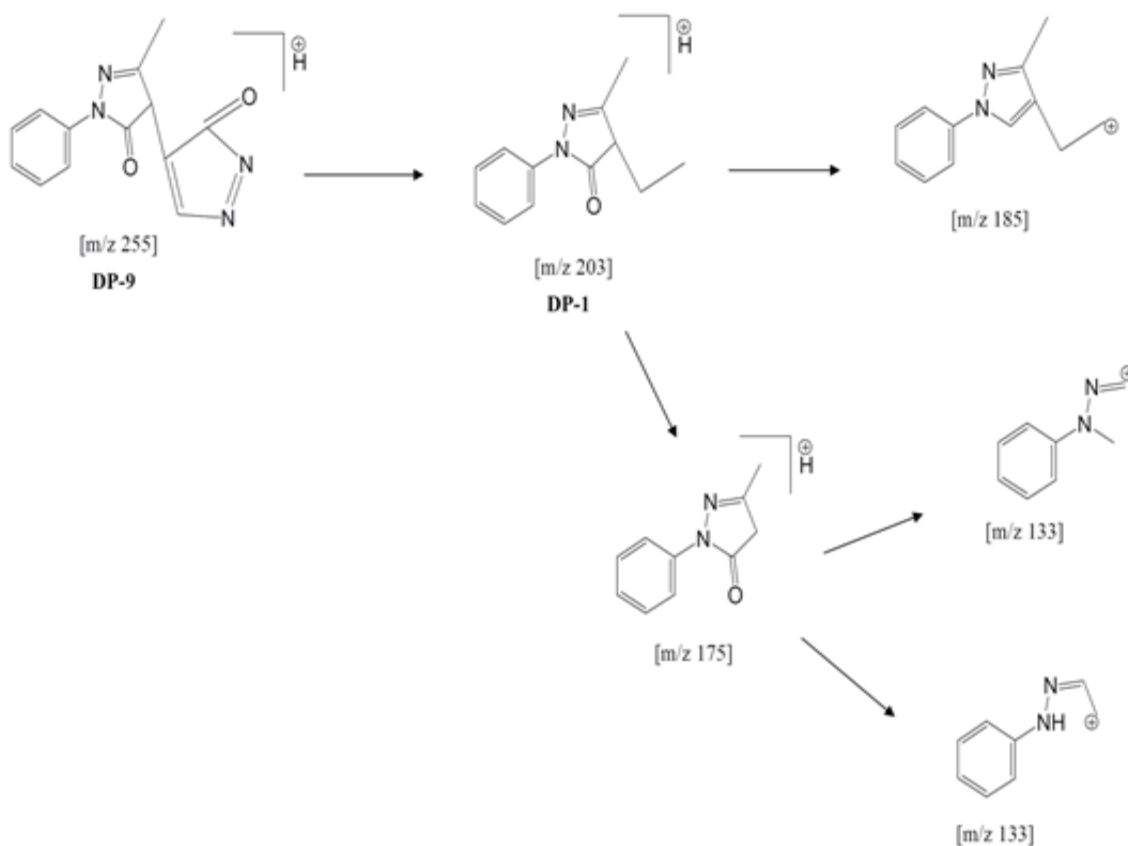


Figure 4.84: Proposed fragmentation pathway of DP-1 and DP-9

DP-2 (m/z 191)

The positive ion ESI-MS/MS (figure 4.85) spectrum of DP-2 showed abundant $[M+H]^+$ ion at m/z 191. The spectrum showed most abundant product ions at m/z 173 that correspond EDA. The proposed fragmentation pathway of DP-2 is shown in figure 4.86.

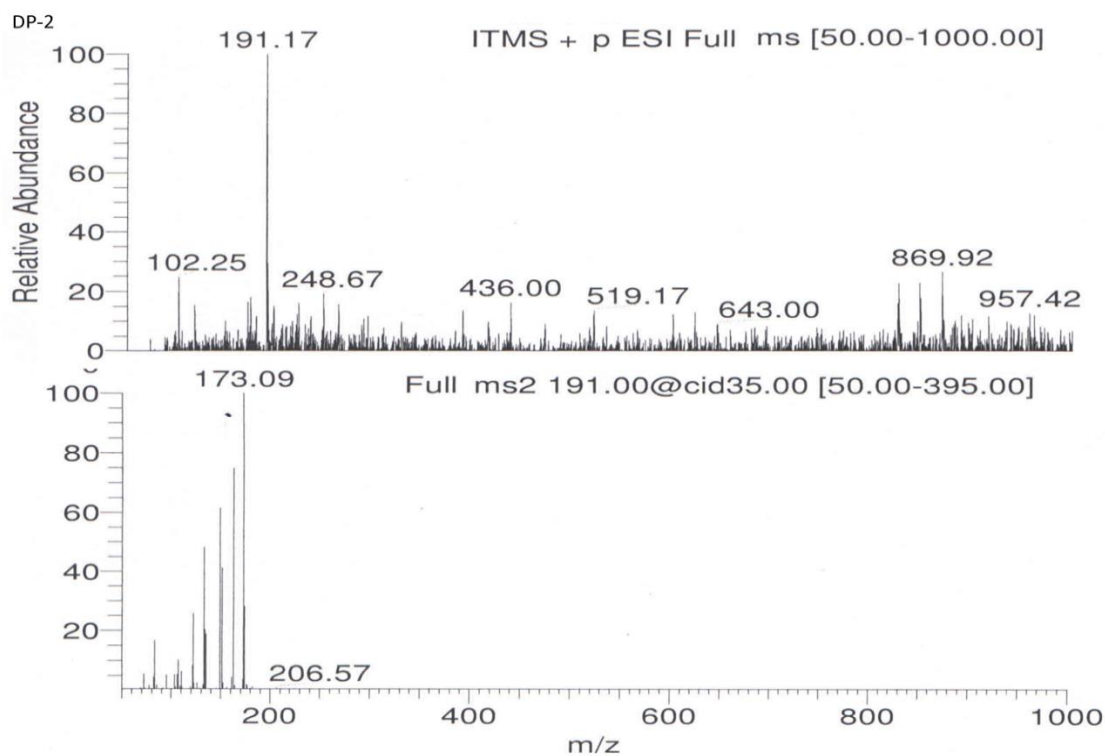


Figure 4.85: ESI-MS/MS spectra of DP-2

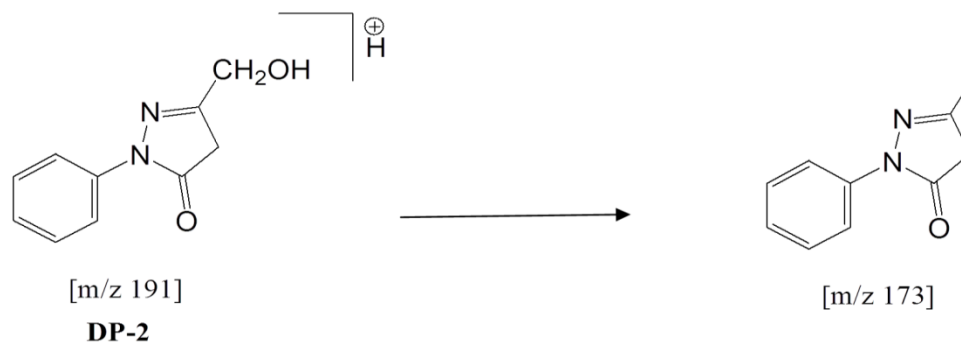


Figure 4.86: Proposed fragmentation pathway of DP-2

DP-3 (m/z 219)

The positive ion ESI-MS/MS (figure 4.87) spectrum of DP-3 showed abundant $[M+H]^+$ ion at m/z 219 (218.95). The spectrum showed abundant product ions at m/z 201 formed by loss of oxygen. The proposed fragmentation pathway of DP-3 is shown in figure 4.88.

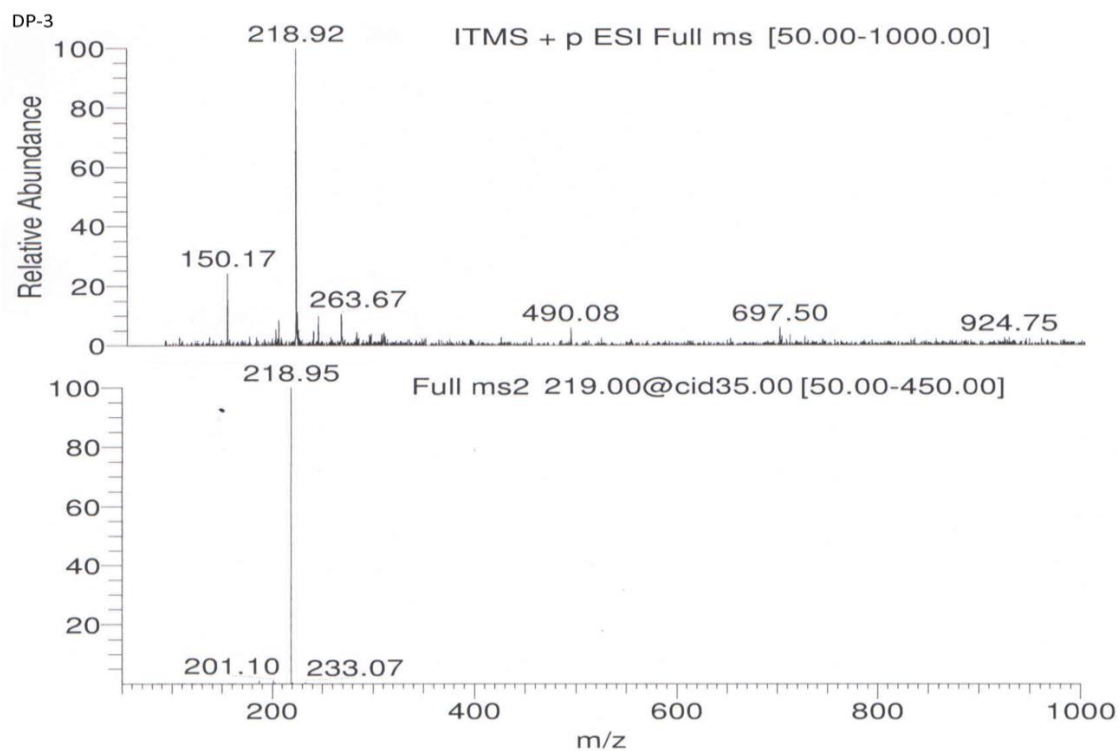


Figure 4.87: ESI-MS/MS spectra of DP-3

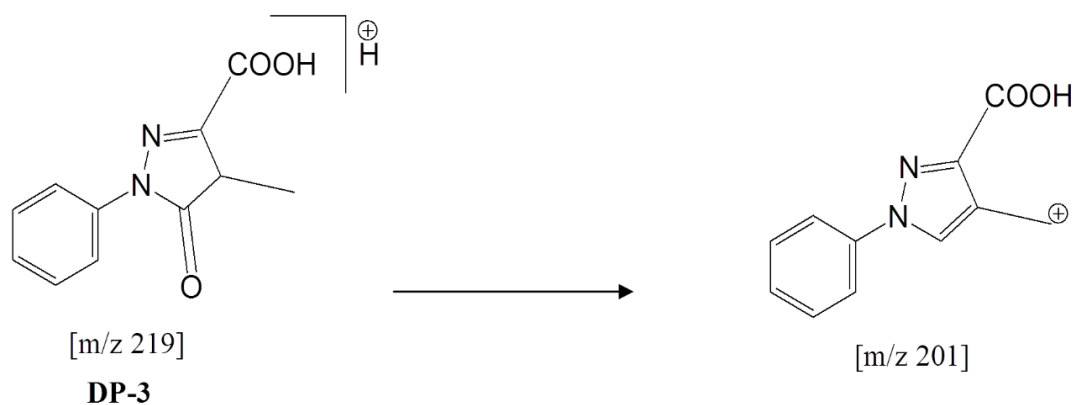


Figure 4.88: Proposed fragmentation pathway of DP-3

DP-4 (m/z 332)

ESI-MS/MS and proposed fragmentation pathway of DP-4 is explained in section 4.8.2.2.2 and figure 4.73. The ESI-MS/MS spectrum is provided in figure 4.72.

DP-5 (m/z 361)

The positive ion ESI-MS/MS (figure 4.89) of DP-5 showed abundant $[M+H]^+$ ion at m/z 361. The spectrum showed most abundant product ions at m/z 175 that correspond to EDA. The spectrum also showed abundant product ion at m/z of 343 (342.94) formed by loss of $-OH$. From m/z 343 breakage of dimeric linkage takes place that produces product ions of m/z 187 and 175. The proposed fragmentation pathway is described in figure 4.90.

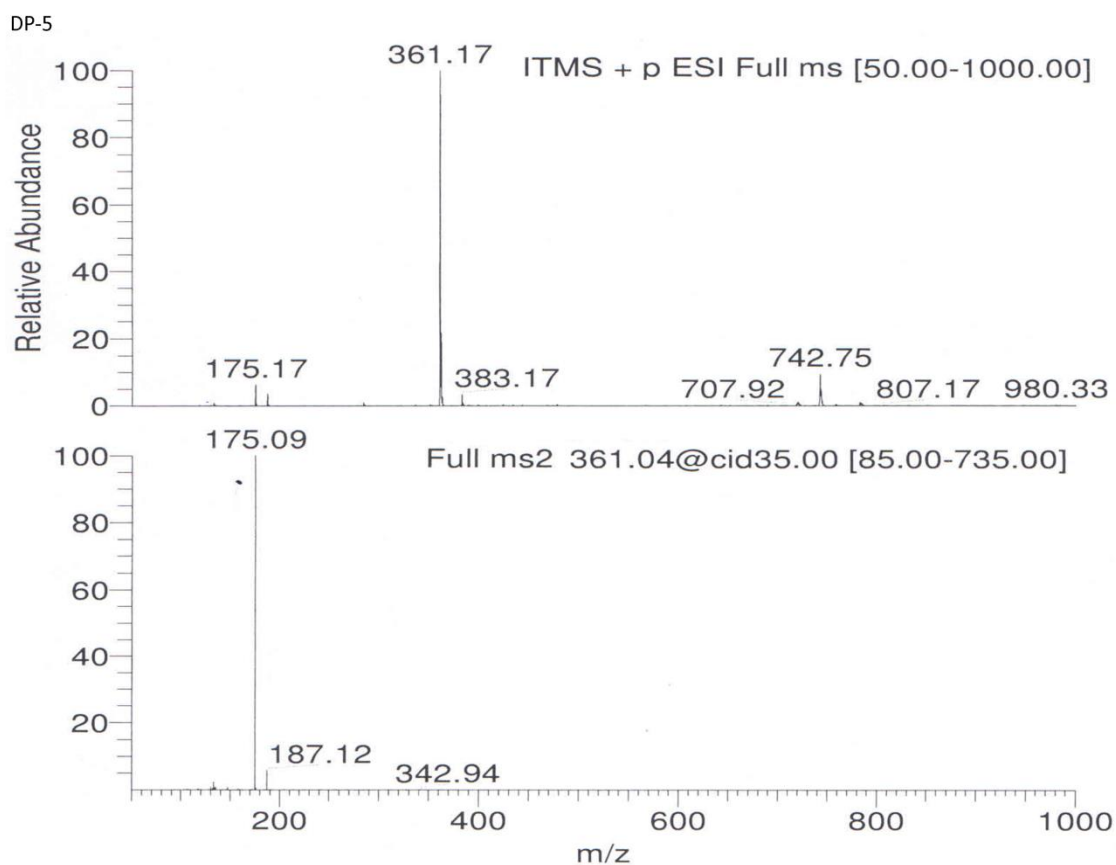


Figure 4.89: ESI-MS/MS spectra of DP-5

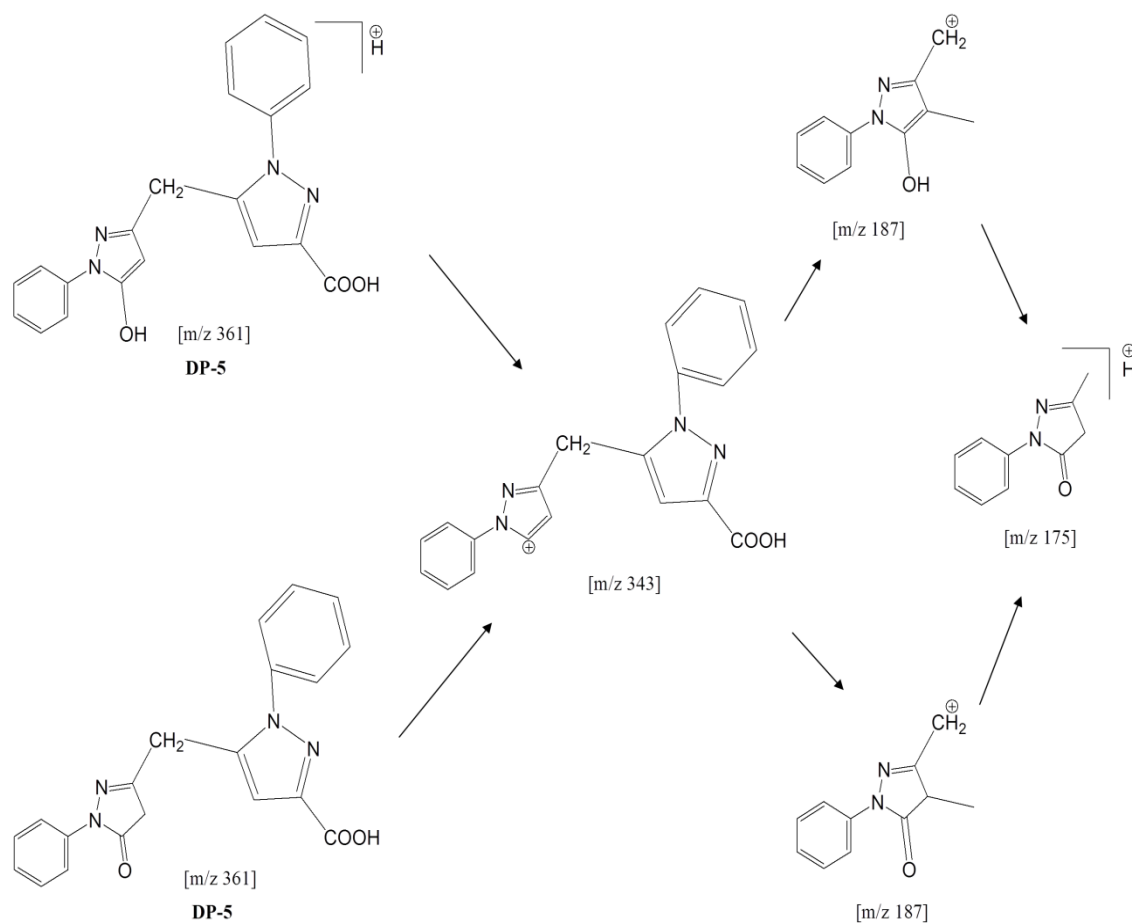


Figure 4.90: Proposed fragmentation pathway of DP-5

DP-6 (m/z 519)

The positive ion ESI-MS/MS (figure 4.91) of DP-6 showed abundant $[M+H]^+$ ion at m/z 519. The MW of the parent ion confirms the proposed structure for EDA IM-F (table 4.57), which is one of the impurity of EDA reported in pharmacodia (30). The spectrum showed the most abundant product ion at m/z of 345. The spectrum also showed product ion at m/z 427 formed by loss of one heterocyclic ring of DP-6. The product ion at m/z 175 corresponds to EDA. The proposed fragmentation pathway of DP-6 is given in figure 4.92.

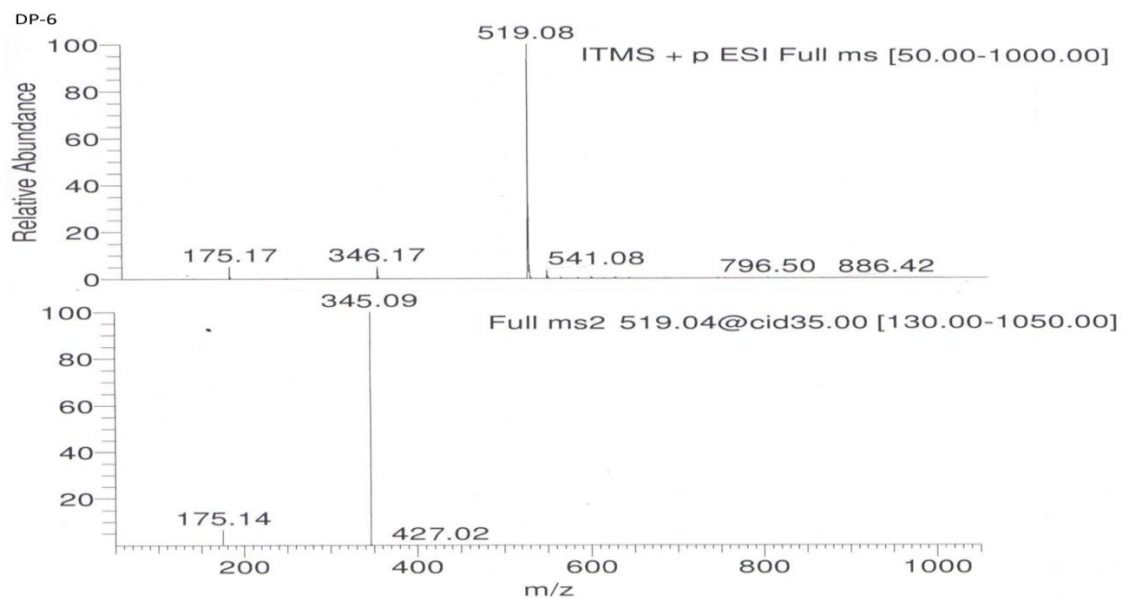


Figure 4.91: ESI-MS/MS spectra of DP-6

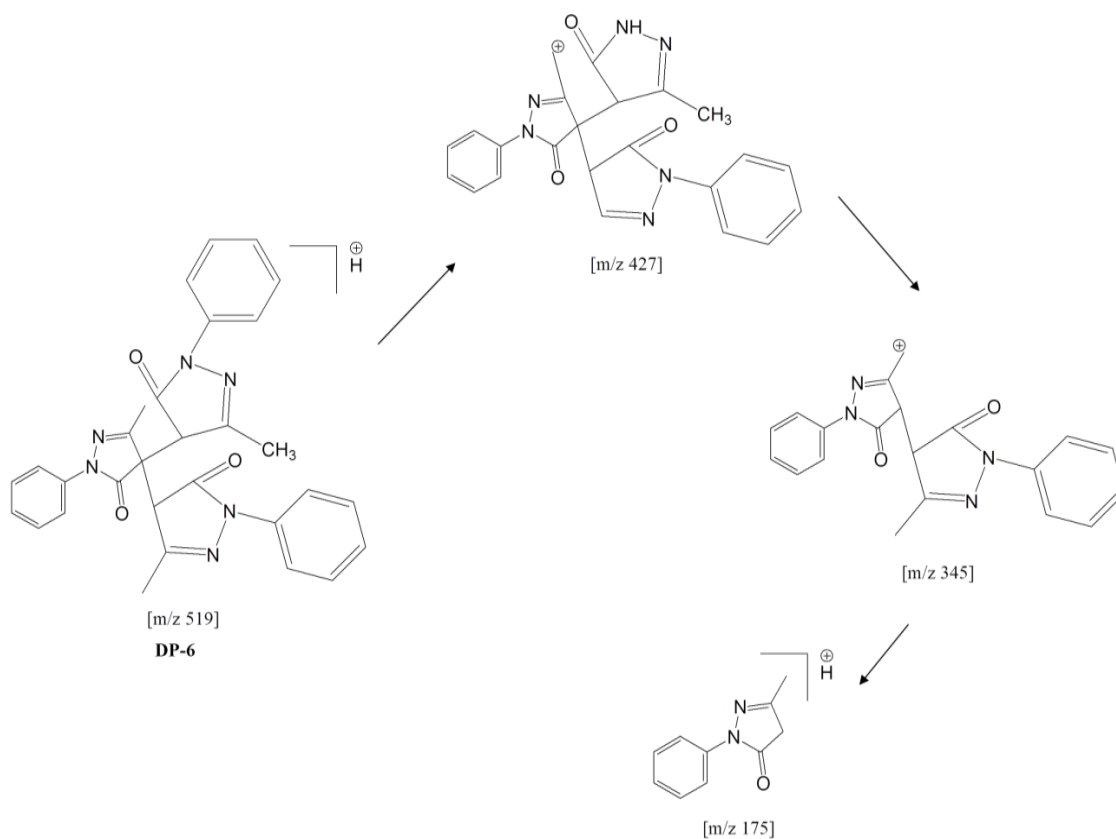


Figure 4.92: Proposed fragmentation pathway of DP-6

DP-7 (m/z 521)

MS/MS and proposed fragmentation pathway of DP-7 is explained in section 4.8.2.2.1 and figure 4.58. The ESI-MS/MS spectra is provided in figure 4.57.

DP-8 (m/z 245) and DP-11 (284)

Both DP-8 and DP-11 were formed during neutral degradation. The MS was taken in both positive and negative mode for DP-8. The positive ion ESI-MS (figure 4.93) spectrum of DP-8 showed abundant $[M+H]^+$ ion at m/z 245 while the negative ion ESI-MS spectrum showed abundant $[M-H]^-$ ion at m/z 243, that did not show protonated ions.

DP-8 was formed from DP-11 that showed abundant $[M+H]^+$ ion at m/z 284. DP-11 fragments (figure 4.94) and gives product ion with m/z 245 i. e. DP-8 and m/z 269. There is possibility of formation of two structures with same MW and are shown in proposed fragmentation pathway in figure 4.95.

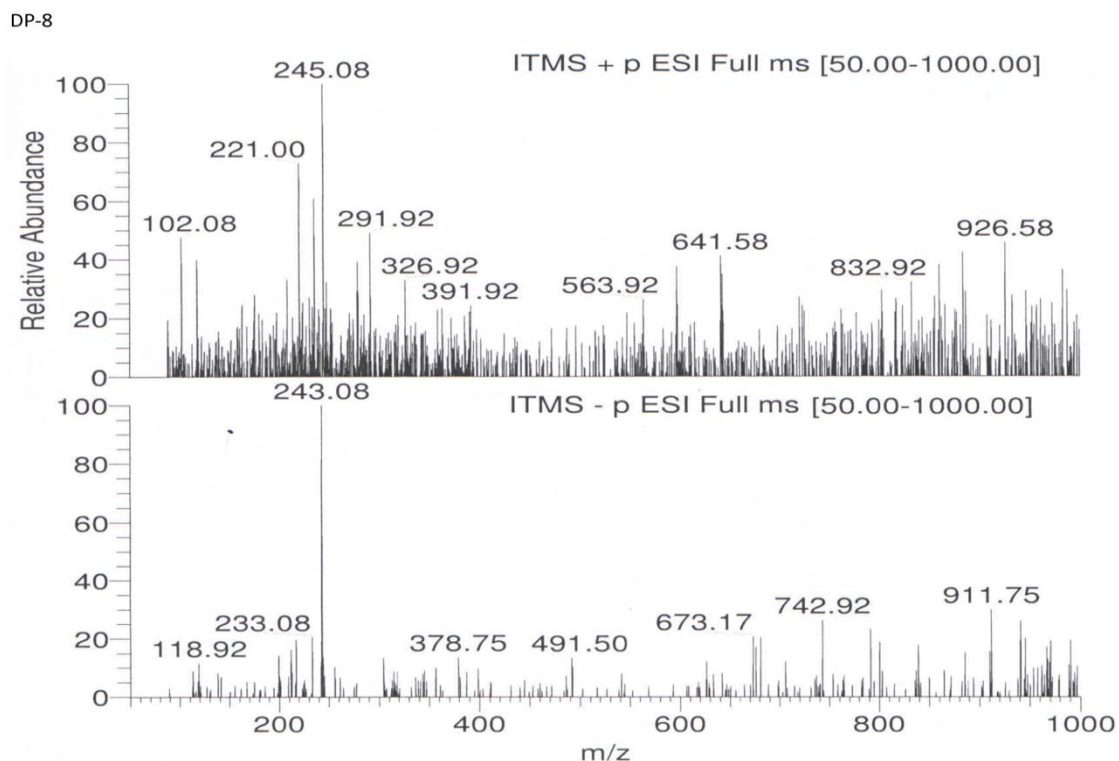


Figure 4.93: ESI-MS/MS spectra of DP-8

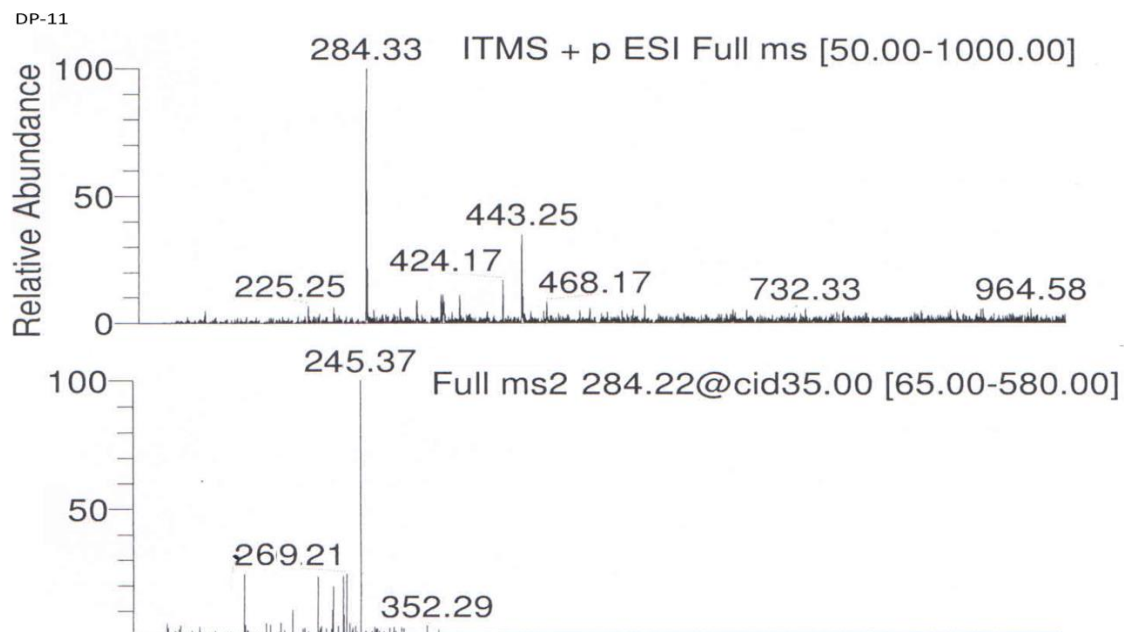


Figure 4.94: ESI-MS/MS spectra of DP-11

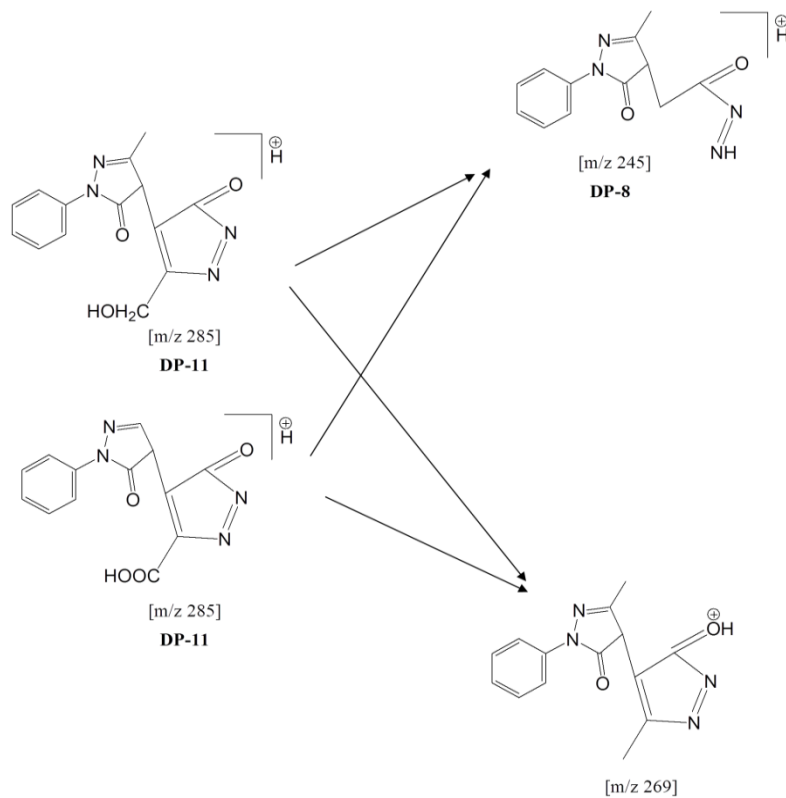


Figure 4.95: Proposed fragmentation pathway of DP-8 and DP-11

DP-10 (m/z 377)

The positive ion ESI-MS/MS (figure 4.96) of DP-10 showed abundant $[M+H]^+$ ion at m/z 377. The ESI-MS/MS spectrum of $[M+H]^+$ ion of DP-10 showed most abundant product ions at m/z 361. The spectrum also showed product ion at m/z 345.

DP-13 (m/z 535)

The positive ion ESI-MS/MS (figure 4.97) of DP-13 showed abundant $[M+H]^+$ ion at m/z 535 and $[M-H]^-$ ion at m/z 533 in negative mode. The ESI-MS/MS spectrum of $[M+H]^+$ ion of DP-13 showed most abundant product ions at m/z 361. The spectrum also showed product ion at m/z 377 that correspond to DP-10 and at m/z 345. The proposed fragmentation pathway of DP-10 and DP-13 are shown in figure 4.98.

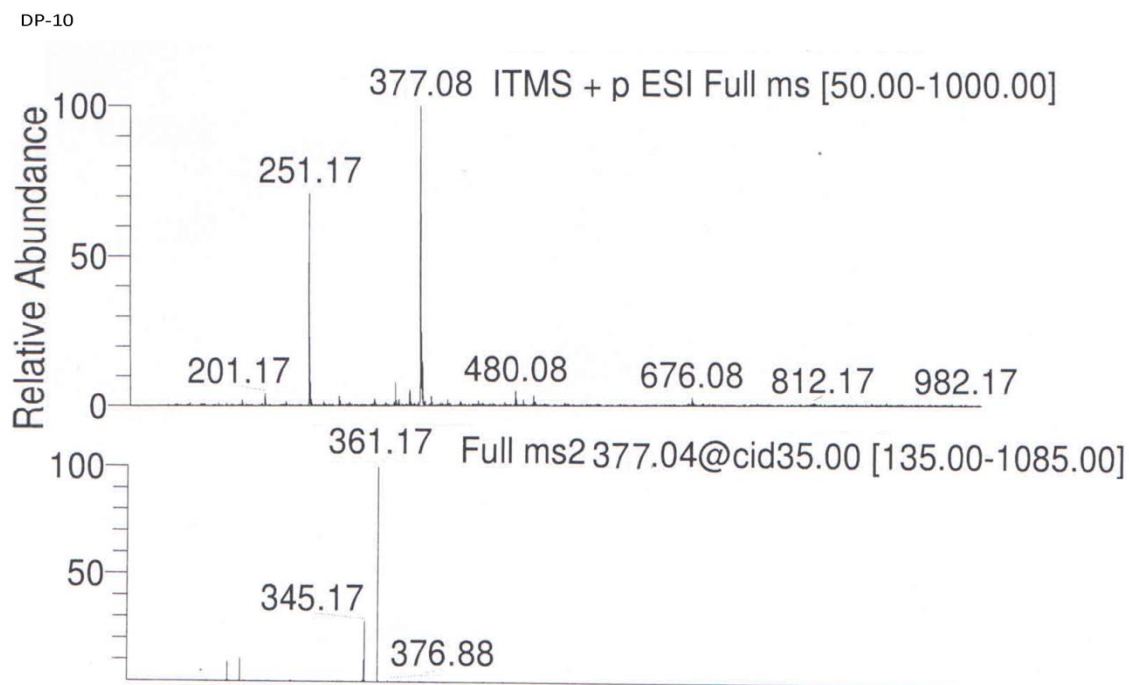


Figure 4.96: ESI-MS/MS spectra of DP-10

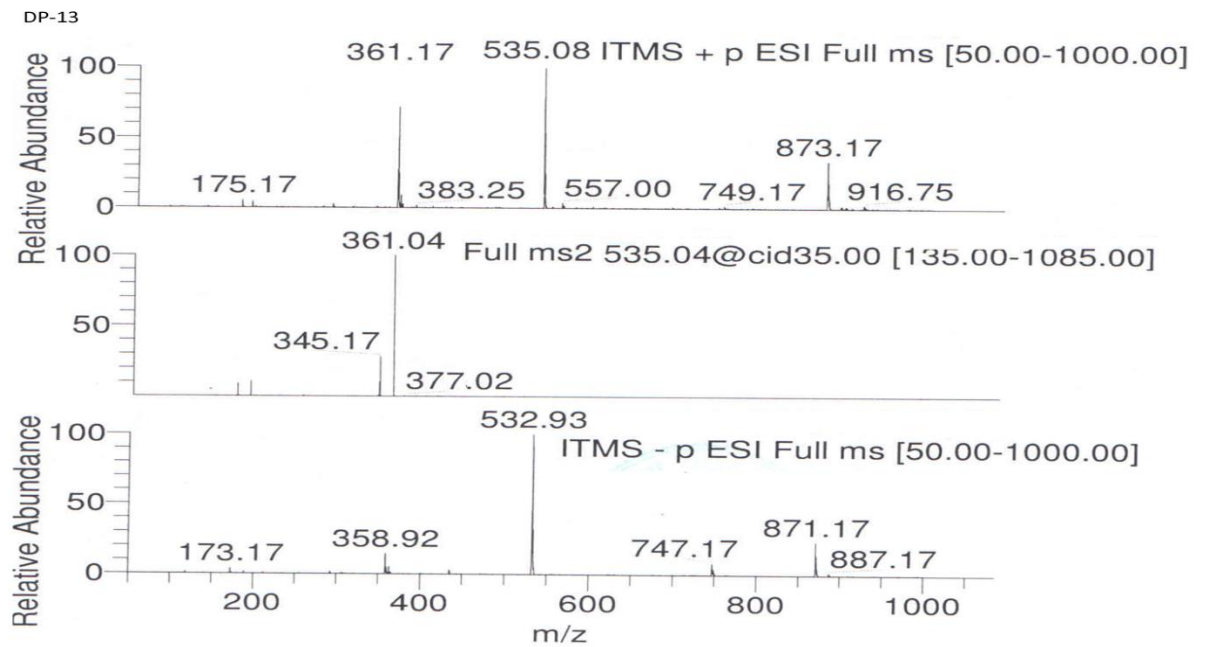


Figure 4.97: ESI-MS/MS spectra of DP-13

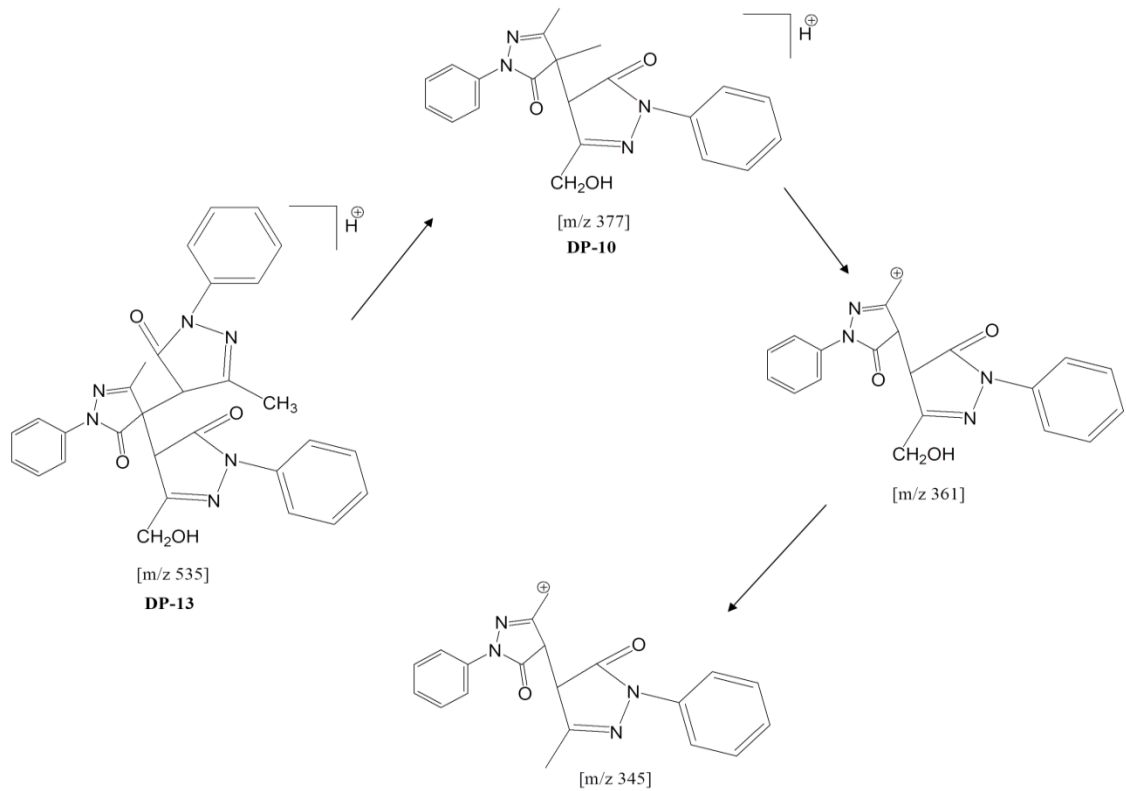


Figure 4.98: Proposed fragmentation pathway of DP-10 and DP-13

DP-12 (m/z 565)

The positive ion ESI-MS/MS (figure 4.99) of DP-12 showed abundant $[M+H]^+$ ion at m/z 565. The spectrum showed abundant product ions at m/z 389 (388.96) and 201 formed by breakage of trimeric bond producing dimer and monomer. Further both dimer and trimer can fragment to form product ion at m/z 175 corresponding to EDA which was most abundant product ion. The proposed fragmentation pathway of DP-12 is shown in figure 4.100.

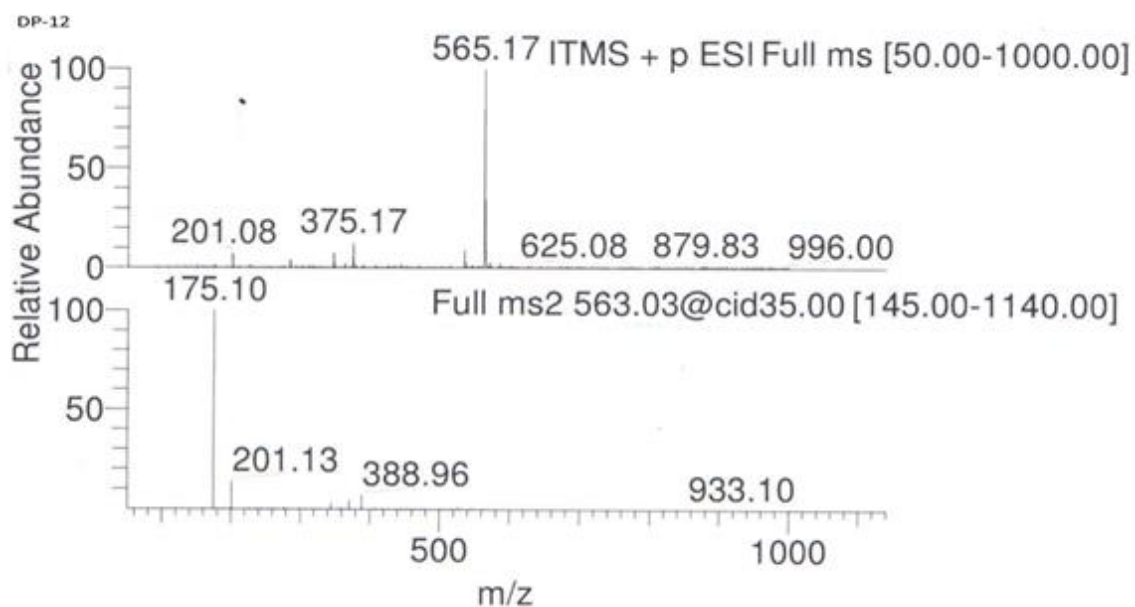


Figure 4.99: ESI-MS/MS spectra of DP-12

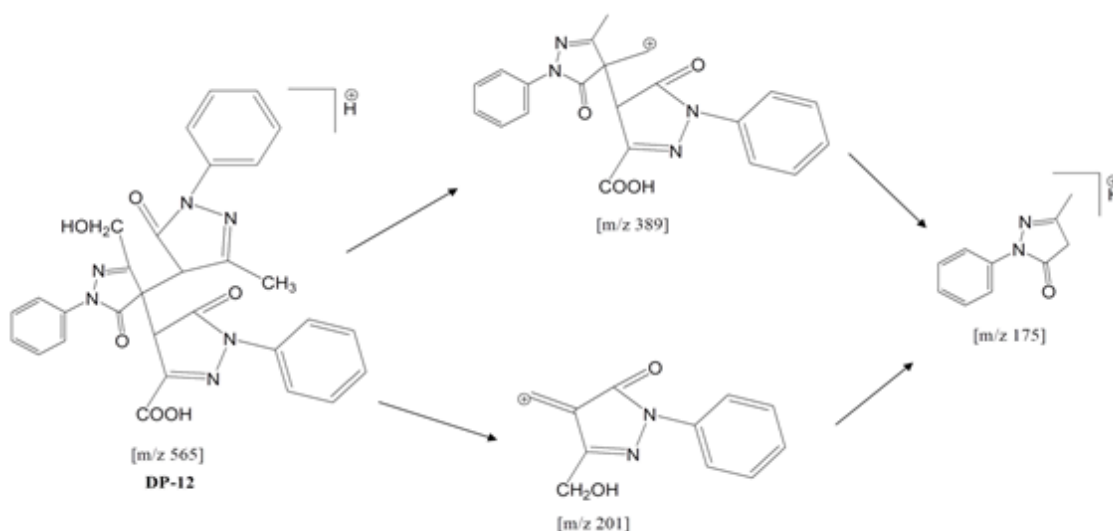
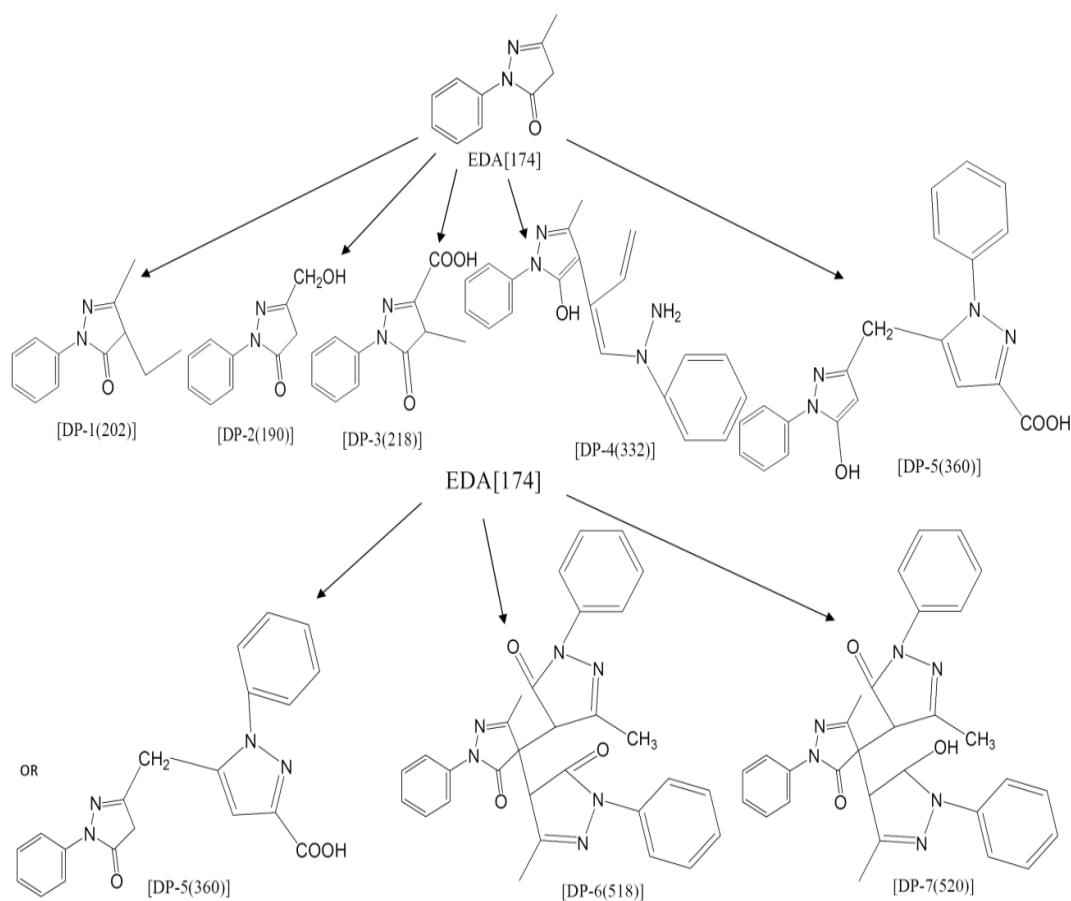


Figure 4.100: Proposed fragmentation pathway of DP-12

Finally based on above observations and interpretation, schematic flow chart of EDA degradation showing formation of all degradants was prepared and is shown in figure 4.101. Chemical structures of EDA and all the related compounds already reported or unknown along with their origin, degradation route, R_t and observed m/z values for major fragments are shown in table 4.57.

It is clear from the table that EDA contain 13 impurities which may be inherent (process related) or degradation related. Out of total 13 impurities observed during impurity profiling and degradation study of EDA, 12 were unknown. Out of 12 unknown impurities two of them were isolated and characterized by IR, LC-MS/MS and NMR spectral studies. Other DPs were characterized by LC-MS/MS study and their structures and fragmentation pathways were proposed.



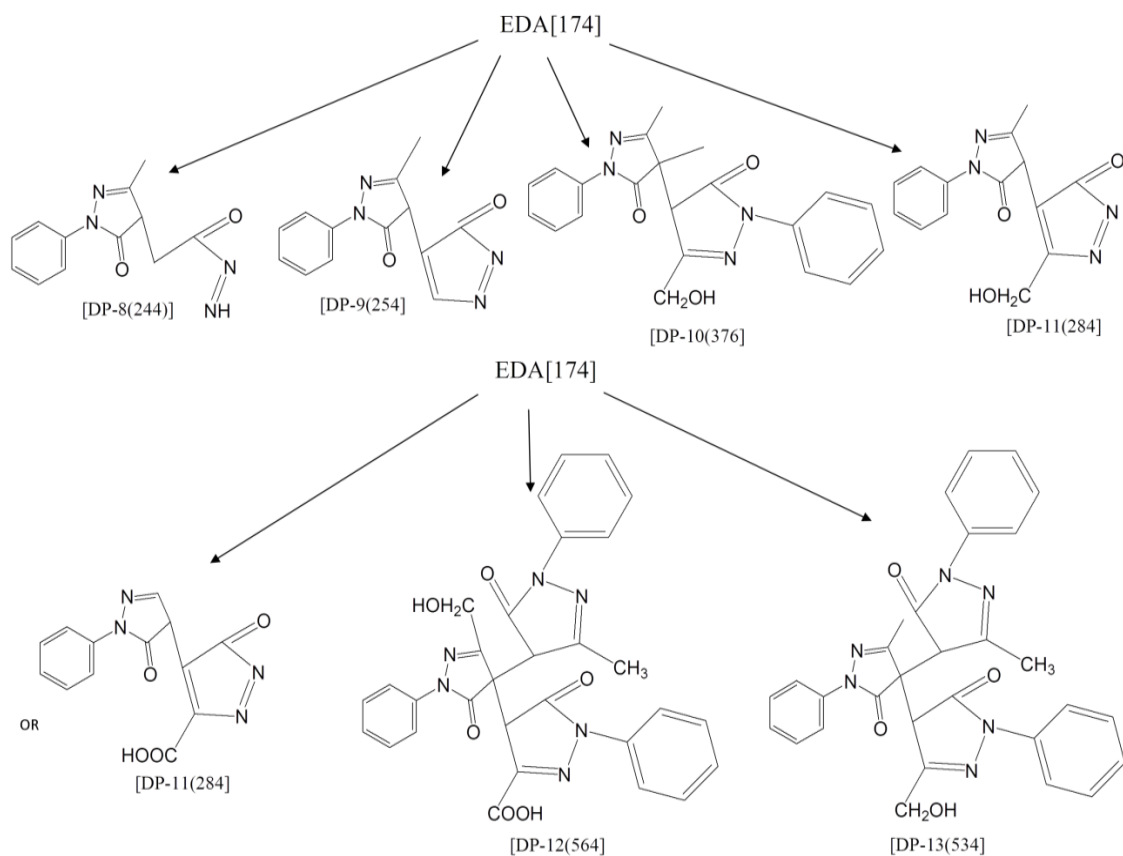
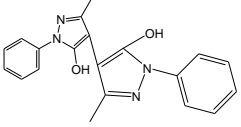
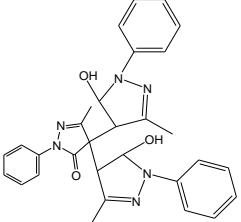
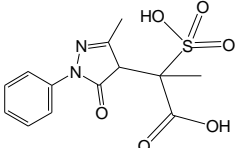
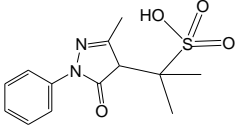
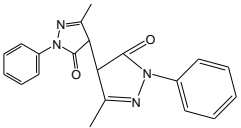
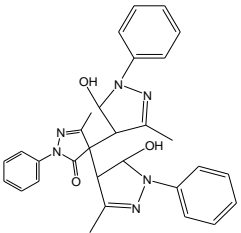
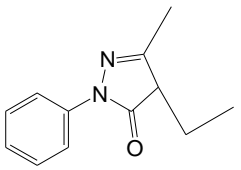
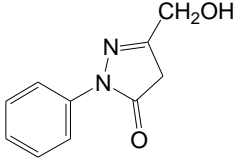
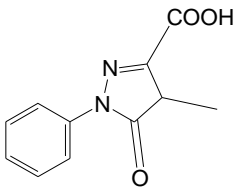
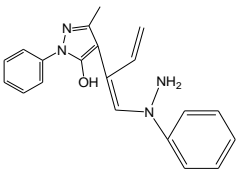
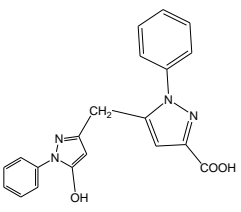
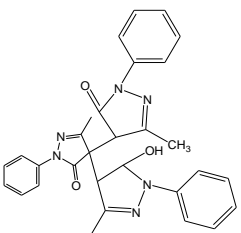


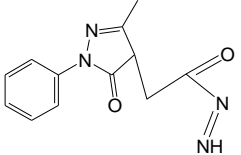
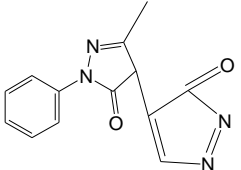
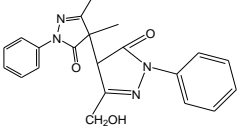
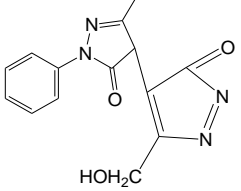
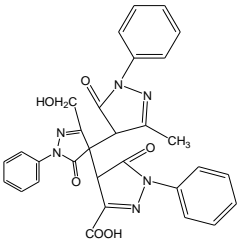
Figure 4.101: A schematic representation of EDA degradation with proposed structures and molecular weights of DPs

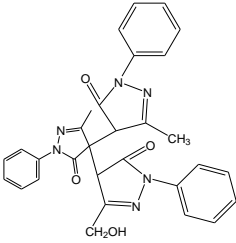
Table 4.57: Chemical structures of EDA and related compounds, their origin, degradation route, Rt and observed m/z values for major fragments.

Analyte	Structure	Molecular formula molecular weight Fragments (m/z)	Origin	Degradation route	RT (LC-PDA)
EDA		$C_{10}H_{10}N_2O$ 174.20 (147.16, 133.11)	API	--	11.54

EDA IM-A		$C_{18}H_{18}N_4O_2$ 346.38	Not specified	--	--
EDA IM-B		$C_{30}H_{30}N_6O_3$ 522.60	Not specified	--	--
EDA IM-C		$C_{13}H_{14}N_2O_6S$ 326.33	Not specified	--	--
EDA IM-D		$C_{13}H_{16}N_2O_4S$ 296.34	Not specified	--	--
EDA IM-E		$C_{20}H_{18}N_4O_2$ 346.38	Not specified	--	--
EDA IM-F DP-6		$C_{30}H_{26}N_6O_3$ 518.57 (427.02, 345.09, 175.14)	Not specified	Acid, oxidative, photolytic and dry heat induced degradation	15.32
DP-1		$C_{12}H_{14}N_2O$ 202.25 (185.17, 175.12, 133.17)	Degradation product (unk)	Base degradation	5.97

DP-2		$C_{10}H_{10}N_2O_2$ 190.20 (206.57, 173.09)	Degradation product (unk)	Oxidative degradation	6.55
DP-3		$C_{11}H_{10}N_2O_3$ 218.07 (233.07, 218.95, 201.10)	Degradation product (unk)	Acid degradation	7.10
DP-4		$C_{20}H_{20}N_4O$ 332.40 (238.92, 225.14, 197.11, 171.15)	Degradation product (unk)	Dry heat induced degradation	12.58
DP-5		$C_{20}H_{16}N_4O_3$ 360.37 (342.94, 187.12, 175.09)	Degradation product (unk)	Acid, oxidative, Photolytic and dry heat induced Degradation	14.35
DP-7		$C_{30}H_{28}N_6O_3$ 520.58 (348.19, 178.07, 175.14)	Degradation product (unk)	Neutral, dry heat induced and photolytic degradation	16.36

DP-8		$C_{12}H_{12}N_4O_2$ 244.25	Degradation product (unk)	Neutral degradation	9.66
DP-9		$C_{13}H_{10}N_4O_2$ 254.24 (223.16, 203.12, 132.91, 175.09)	Degradation product (unk)	Base degradation	13.54
DP-10		$C_{21}H_{20}N_4O_3$ 376.15 (361.17, 346.17)	Degradation product (unk)	Base degradation	14.35
DP-11		$C_{13}H_8N_4O_4$ OR $C_{14}H_{12}N_4O_3$ 284.23 (269.21)	Degradation product (unk)	Neutral degradation	14.35
DP-12		$C_{30}H_{24}N_6O_6$ 564.18 (388.96, 201.13, 175.10)	Degradation product (unk)	Oxidative Degradation	14.35

DP-13		$C_{30}H_{26}N_6O_4$ 534.57 (375.02, 361.04, 345.17)	Degradation product (unk)	Dry heat induced degradation	14.35
-------	---	---	------------------------------	------------------------------------	-------

4.10 CONCLUSION

Impurity profiling and degradation study of Edaravone was carried out systematically with LC-PDA detection and LC-MS/MS analysis. Total 10 impurities including degradation related and process related or inherent impurities were observed in LC-PDA while 13 impurities were observed in LC/MS-MS. Two Major degradation products (based on HPLC peak area) formed from dry heat induced degradation condition were isolated and successfully characterized by IR, Mass and NMR spectral studies. The chemical names of isolated degradation product at Rt 16.36 is 4-(4,5-dihydro-3-methyl-5-oxo-1-phenyl-1H-pyrazol-4-yl)-4-(4,5-dihydro-5-hydroxy-3-methyl-1-phenyl-1H-pyrazol-4-yl)-3-methyl-1-phenyl-1H-pyrazol-5(4H)-one and at Rt 12.5 is 3-hydroxy-dihydro-thiazolo(1-(2-methyl-but-1,3dienyl)-1-phenylhydrazine)5-one. The structures and degradation pathway of other 10 unknown degradation products were proposed on the basis of LC-MS/MS analysis. Since Edaravone was susceptible to almost all stress degradation condition degradation kinetic study was carried out for acid, base, neutral, oxidative and photolytic degradation by RP-HPLC and HPTLC method. Acid and base degradation followed non linear pseudo first order kinetic while neutral, oxidative and photolytic degradation followed linear zero order reaction kinetic. A QbD based stability indicating RP-HPLC and HPTLC method for identification and quantification of degradation products and its inherent and/or process related impurities were developed and validated as per ICH Q2(R1) guideline. Both the methods are simple, sensitive, accurate and fast which is applicable for the assay of drug substance and estimation of impurities and degradation products of Edaravone.

4.11 REFERENCES

1. Watanabe T, Morita I, Nishi H, Murota S. Preventive effect of MCI-186 on 15-HPETE induced vascular endothelial cell injury in vitro. *Prostaglandins, Leukotrienes and Essential Fatty Acids*. 1988;33(1):81-7.
2. Yoshida H, Yanai H, Namiki Y, Fukatsu Sasaki K, Furutani N, Tada N. Neuroprotective effects of edaravone: a novel free radical scavenger in cerebrovascular injury. *CNS drug reviews*. 2006;12(1):9-20.
3. Kikuchi K, Kawahara K, Miyagi N, Uchikado H, Kuramoto T, Morimoto Y, et al. Edaravone: A new therapeutic approach for the treatment of acute stroke. *Medical hypotheses*. 2010;75(6):583-5.
4. Kikuchi K, Kawahara K, Tancharoen S, Matsuda F, Morimoto Y, Ito T, et al. The free radical scavenger edaravone rescues rats from cerebral infarction by attenuating the release of high-mobility group box-1 in neuronal cells. *Journal of Pharmacology and Experimental Therapeutics*. 2009;329(3):865-74.
5. Kikuchi K, Miura N, Kawahara K, Murai Y, Morioka M, Lapchak PA, et al. Edaravone (Radicut), a free radical scavenger, is a potentially useful addition to thrombolytic therapy in patients with acute ischemic stroke (Review). *Biomedical reports*. 2013;1(1):7-12.
6. Tanaka E, Niiyama S, Sato S, Yamada A, Higashi H. Arachidonic acid metabolites contribute to the irreversible depolarization induced by in vitro ischemia. *Journal of neurophysiology*. 2003;90(5):3213-23.
7. Kikuchi K, Kawahara K, Uchikado H, Miyagi N, Kuramoto T, Miyagi T, et al. Potential of edaravone for neuroprotection in neurologic diseases that do not involve cerebral infarction (Review). *Experimental and therapeutic medicine*. 2011;2(5):771-5.
8. Kikuchi K, Miura N, Morimoto Y, Ito T, Tancharoen S, Miyata K, et al. Beneficial effects of the free radical scavenger edaravone (Radicut) in neurologic diseases. *Journal of Neurology and Neurophysiology*. 2012;S1;2155-2162.
9. Kikuchi K, Uchikado H, Miyagi N, Morimoto Y, Ito T, Tancharoen S, et al. Beyond neurological disease: New targets for edaravone (Review). *International journal of molecular medicine*. 2011;28(6):899.
10. Tsujita K, Shimomura H, Kawano H, Hokamaki J, Fukuda M, Yamashita T, et al. Effects of edaravone on reperfusion injury in patients with acute myocardial infarction. *The American journal of cardiology*. 2004;94(4):481-4.
11. Stephens J, Blazynski C. Rare disease landscape: will the blockbuster model be replaced? *Expert Opinion on Orphan Drugs*. 2014;2(8):797-806.
12. Abe K, Itoyama Y, Sobue G, Tsuji S, Aoki M, Doyu M, et al. Confirmatory double-blind, parallel-group, placebo-controlled study of efficacy and safety of edaravone (MCI-

- 186) in amyotrophic lateral sclerosis patients. *Amyotrophic Lateral Sclerosis and Frontotemporal Degeneration*. 2014;15(7-8):610-7.
13. Antoniu SA. Fresh from the designation pipeline: orphan drugs designated in the European Union. *Expert Opinion on Orphan Drugs*. 2015;3(6):719-25.
14. Kikuchi K, Tancharoen S, Murai Y, Tanaka E. Future Optimal Dosing Regimens for Thrombolysis in Acute Stroke. *Biochememistry and Analytical Biochememistry* 2016;5(244):2161-1009.10002.
15. Watanabe T, Yuki S, Egawa M, Nishi H. Protective effects of MCI-186 on cerebral ischemia: possible involvement of free radical scavenging and antioxidant actions. *Journal of Pharmacology and Experimental Therapeutics*. 1994;268(3):1597-604.
16. Yamamoto T, Yuki S, Watanabe T, Mitsuka M, Saito K, Kogure K. Delayed neuronal death prevented by inhibition of increased hydroxyl radical formation in a transient cerebral ischemia. *Brain research*. 1997;762(1):240-2.
17. Lapchak PA, Araujo DM. Development of the Nitron-Based Spin Trap Agent NXY-059 to Treat Acute Ischemic Stroke. *CNS drug reviews*. 2003;9(3):253-62.
18. Hoehn B, Yenari M, Sapolsky R, Steinberg G. Glutathione peroxidase overexpression inhibits cytochrome C release and proapoptotic mediators to protect neurons from experimental stroke. *Stroke*. 2003;34(10):2489-94.
19. Okatani Y, Wakatsuki A, Kaneda C. Melatonin increases activities of glutathione peroxidase and superoxide dismutase in fetal rat brain. *Journal of pineal research*. 2000;28(2):89-96.
20. Lapchak PA, Zivin JA. The lipophilic multifunctional antioxidant edaravone (radicut) improves behavior following embolic strokes in rabbits: a combination therapy study with tissue plasminogen activator. *Experimental neurology*. 2009;215(1):95-100.
21. Patel BK, Raj HA, Jain VC. Simultaneous estimation of edaravone and citicoline sodium by ratio derivative spectroscopic method in synthetic mixture. *Pharma Science Monitor*. 2014;1(5):2.
22. Liao P, Yan Z-Y, Xu Z-J, Sun X. A novel fluorescent assay for edaravone with aqueous functional CdSe quantum dots. *Spectrochimica Acta Part A: Molecular and Biomolecular Spectroscopy*. 2009;72(5):1066-70.
23. Fanse SK, Rajput SJ. Development and Validation of a simple UV spectrophotometric and isocratic RP-HPLC method for estimation of Edaravone in bulk and its injection formulation. *Indo American Journal of Pharmaceutical Research*. 2015;5(1):584-92.
24. Zhao Zhen Zhen, Dang Xiao Wei, Zhao Yun Li, Jin Qing Ping, Yu Zhogao. Determination of Edaravone and its related substances by RP-HPLC. *Journal of shenyang pharmaceutical University*. 2012;29(5):359-363.

25. Gandhimathi M, Kumar MS, Baghla R, Ravi T. RP-HPTLC method for the in vitro estimation of edaravone in human plasma. *Indian Journal of Pharmaceutical Sciences*. 2010;72(2):276-282.
26. Tang Dq, Bian Tt, Zheng Xx, Li Y, Wu Xw, Li Yj, et al. LC-MS/MS methods for the determination of edaravone and/or taurine in rat plasma and its application to a pharmacokinetic study. *Biomedical Chromatography*. 2014;28(9):1173-82.
27. Xu Zhenyu. Analysis on impurity profile of Edaravone injection. *China Licensed Pharmacist* 2014;8:009.
28. Yao Z, Hang T, Wang Y, Cai M, Huang Z. Analysis of Related Substances in Edaravone by LC-MS. *Progress in Pharmaceutical Sciences*. 2010;9:009.
29. Borges RS, Queiroz AN, Mendes AP, Araújo SC, França L, Franco E, et al. Density functional theory (DFT) study of edaravone derivatives as antioxidants. *International journal of molecular sciences*. 2012;13(6):7594-606.
30. www.pharmacodia.com (accessed on may 2016)